Task-Invariant Control and Pre-clinical Validation of Partial Assist Exoskeletons

by

Nikhil Vishwas Divekar

A dissertation submitted in partial fulfillment
of the requirements for the degree of
Doctor of Philosophy
(Robotics)
in the University of Michigan
2023

Doctoral Committee:

Associate Professor Robert D. Gregg, Chair
Associate Professor Chandramouli Krishnan
Assistant Professor Talia Y. Moore
Associate Professor Elliot J. Rouse

Nikhil Vishwas Divekar
ndivekar@umich.edu
ORCID iD: 0000-0002-8683-4828

I dedicate this dissertation to Krishna.

ACKNOWLEDGMENTS

I want to express my sincerest appreciation to my advisor, Dr. Robert Gregg, for his guidance, encouragement, and patience throughout my PhD study. During my time at the University of Texas at Dallas and the University of Michigan, he offered me timely guidance, unwavering support, and allowed me to explore the research domain with freedom and at my own pace. I am extremely fortunate to have had the opportunity to work with him. I will always remain in awe of his tremendous work ethic and incredible writing and editing skills which magically transformed many of my written works! Moreover, I cannot thank him enough for being understanding and supportive during the tough phases which I am sure every PhD student goes through.

I would also like to thank my committee members, Dr. Elliot Rouse, Dr. Chandramouli Krishnan, and Dr. Talia Moore for their invaluable inputs. By virtue of coursework and meaningful discussions with my examiners during my proposal and final defense, this dissertation achieved a much higher level than what I had originally envisioned.

I am fortunate for the collaboration with Alicia (Foster) Baxter, MS, CPO—Certified Prosthetist Orthotist, during the later phases of the PhD. Thank you so much Alicia for all the clinical insights, orthotic design and manufacture, and crucially your on-site help during the experiments on our participants with impairments. These experiments would not have been possible without your theoretical and practical expertise.

Over the course of my PhD I completed two embedded Masters (at UT Dallas and U of M). I was fortunate to have distinguished professors to teach me the tricks of the trade in dynamics, control, and optimization (Dr. Mark Spong, Dr. Robert Gregg, Dr. Reza Moheimani, Dr. Wooram Park, Dr. Ram Vasudevan); machine learning and vision systems (Dr. Clayton Scott, Dr. Matthew Roberson); robotics (Dr. Peter Gaskell); biomedical engineering (Dr. Elliot Rouse, Dr. Seth Hays, Dr. Joseph Pancrazio, Dr. Xudong Fan); experimental and statistical design (Dr. Allison Case); and professional communication (Dr. Mario Romero-Ortega). I thank them all from the bottom of my heart for empowering me with the advanced knowledge and skills that I was able to utilize in my PhD.

I want to thank Shihao Cheng, Toby Elery, Kyle Embry, Jonathan Horn, Japman Gill, Emily Keller, Yeves Nazon, Mark Yeatman, Hanqi Zhu, and all other former and current labmates in the Locomotor Control Systems Laboratory (Locolab). It has been a great honor and pleasure for me to work and study with them. Thanks to Gray Thomas, Avani Yerva, Erica Santos, Hannah

Frame, Sara Borboa, Kayla Shepodd, Cally Soh, Jack Doan, Calvin Stence, Kevin Best, Emma Reznick, Jose Perez, Susan Zhao, and Katharine Walters for your immeasurable assistance and discussions on mechanical design, control, programming, and experiments. A special thanks to Jianping Lin, Saurav Kumar, Vamsi Peddinti, Edgar Bolivar, Christopher Nesler, and Ge Lv for being truly amazing colleagues and friends (brothers).

I am grateful for the support of Andrew Rhodes, Denise Edmund, and all other staff at UT Dallas and U of M. It was a great honor and experience to be part of the fantastic programs at both universities.

I would like to express my deepest thanks to my parents Vidya and Vishwas Divekar; my aunts and uncles—Deepa and Ganesh Divekar, Jyotsna and Anant Deshmukh, Vibha and Vivek Ghanekar, and Hemangi and Vaibhav Ghanekar; and my grandparents—Mandakini and Mahadeo Divekar, and Vandana and Vasant Ghanekar, for their tremendous support and unconditional love throughout my life. I would especially like to thank my wife, Prajkta Divekar, for standing by me in this journey, and my parents-in-law, Smita and Vilas Pimpalkhare, for their trust and support. Not to forget baby Arya and the soon arriving treasure for always keeping things bright, lively, and cheerful around the house. I wouldn't have had any chance to start and complete my PhD without them.

In closing, this research would not have been possible without the financial support of the various fellowships and grants that paid for my tuition and stipend. I highly appreciate the support from the Jonsson Family Bioengineering Fellowship, Rackham Predoctoral Fellowship, and NIH R01 grant.

TABLE OF CONTENTS

LIST OF FIGURES

FIGURE

LIST OF TABLES

TABLE

LIST OF ACRONYMS

PDE: partial differential equation
BWS: body-weight support
EMG: electromyography
vGRF: vertical ground reaction force
DOF: degree of freedom
COM: center of mass
SLIP: Spring-Loaded Inverted Pendulum
OA: osteoarthritis
MS: multiple sclerosis
PPS: post polio syndrome
MSD: musculoskeletal disorder
LBP: low back pain
LL: lifting-lowering
LLC: lifting-lowering-carrying
ADL: activity of daily living
VAF: variance accounted for
IMU: inertial measurement unit
VMO: vastus medialis oblique
VL: vastus lateralis
RF: rectus femoris
BF: biceps femoris
TA: tibialis anterior
GM: gastrocnemius
SOL: soleus
BPM: beats-per-minute
LOA%: level-of-assistance percent
LMM: linear mixed model
MVC: maximum voluntary contraction

ABSTRACT

A transition from powerful, bulky, and stiff jointed exoskeletons for driving the limbs of paralyzed individuals to lightweight, highly backdrivable, partial assist exoskeletons for assisting broad populations with mild to moderate mobility impairments is well underway. However this transition cannot be successfully completed without developing and in-vivo testing controllers that are versatile over multiple activities, clinically intuitive, and easily customizable based on each individual's unique needs. This dissertation is focused on providing solutions to this challenging set of requirements via four aims: 1) improving and later assessing the performance (and limitations) of existing "task-invariant" controllers implemented on various backdrivable exoskeletons, 2) developing a novel bilateral knee controller for broad use cases, 3) performing in-vivo validation of the novel controller in the fatigue causing lifting-lowering-carrying tasks, and 4) exploring the customizability of the novel controller for meeting unique needs in highly impaired cases of post-polio-syndrome (PPS) and multiple sclerosis (MS). Accordingly, this work firstly improved a potential energy shaping (body weight supporting) controller by blending its stance and swing torques in multi-support gait phases, by utilizing the vertical ground reaction force signal from a custom designed foot pressure sensor. Subsequently, this controller and more advanced total energy shaping controllers underwent in-vivo testing focused on assessing muscle effort reductions. However, uncovering of shortcomings in customizability and unhelpful behavior outside the normative kinematics datasets (which these "data-driven" controllers strictly relied on) made them unsuitable for aims 3 and 4. By using physically inspired torque basis functions that were intuitively modified and "task-sensitized" to ultimately behave in a biomimetic fashion for multiple tasks, aim 2 produced a versatile, clinically intuitive, and "task-invariant" bilateral knee controller that achieved good in-silico as well as in-vivo results in pilot testing. Aim 3 utilized this novel controller on a highly backdrivable exoskeleton to achieve holistic, multifaceted (performance, postural, muscular, and perceptual) benefits in lifting-lowering-carrying over multiple terrain in both non-fatigued and highly-fatigued physical states. Finally aim 4 produced a clinician-friendly android app (GUI) that helped customize the novel controller for participants with PPS and MS. Meaningful improvements were found with the exoskeleton in the primary metrics, i.e., reductions in the 5xSTS time and stairs ascent time for the participant with PPS; and improvements in leg clearance and compensatory circumduction for the participant with MS.

CHAPTER 1

Introduction

Millions of individuals worldwide could benefit through supplementation of their diminished muscular strength—a decline that occurs acutely due to physical fatigue in healthy individuals, or more chronically as a symptom of an underlying disease or injury. Additionally, a significant number of individuals could derive benefit by reducing their muscular effort during demanding tasks, in order to increase endurance, safety, and productivity, or mitigate joint pain associated with high muscular forces. This dissertation focuses on providing versatile robot-aided assistance in these broad populations, who retain a considerable amount of voluntary motion. This includes mitigating or preventing fatigue in healthy construction workers, reducing patelo-femoral joint pain in knee osteoarthritis (OA), or restoring mobility in populations with neuromuscular weakness such as multiple sclerosis (MS), post-polio syndrome (PPS), stroke, and sarcopenia.

Until recently, researchers developed lower limb exoskeleton technology to provide *complete* assistance to individuals with neuromuscular *paralysis* (e.g., after spinal cord injury). This motivated exoskeletons with 1) bulky frames and stiff but powerful actuators that hauled the entire weight of the paralyzed individuals, and 2) controllers that drove the user's limbs as per prerecorded joint kinematics. This combination of *task-specific*, kinematic enforcing control schemes and cumbersome exoskeleton hardware proves unsuitable for individuals who retain various levels of voluntary motion. These individuals require synergistic *partial* assistance, via versatile (*task-invariant*) controllers that are informed by live motion feedback and exoskeleton hardware that is lightweight and equipped with low-impedance joints and actuators that minimally hinder remnant voluntary motion.

Over the span of several years, this dissertation showcases a series of improvements in partial-assist exoskeleton hardware (Fig. 1.1) and task-invariant controls technology, that build up to a highly backdrivable (low-impedance), modular, and lightweight bilateral knee exoskeleton, equipped with a versatile, clinically intuitive, and easily customizable controller. Enabled by these latest developments, the dissertation culminates with demonstrating holistic benefits to healthy participants in both non-fatiguing and fatiguing multi-terrain lifting-lowering-carrying tasks, and promising benefits to impaired individuals with PPS and MS.

The following section provides a critical literature review of the state–of–the–art in assistive technologies for common musculoskeleetal disorders (MSDs) of the lower limbs. A brief etiology of the disorders is given, followed by the relevant robotic assistive technologies implemented to assist them, and ultimately any shortcomings of the devices are discussed. The last section of this chapter highlights the contributions of this dissertation in addressing these gaps and provides an outline of the organization of the work.

Figure 1.1: Improvements in exoskeleton hardware. Left: Comex1 second generation knee ankle exoskeleton. Middle: Comex2 second generation knee only exoskeleton. Right: M-Blue modular hip-knee, hip only, and knee only exoskeleton (hip-knee configuration shown).

1.1 State-of-the-art in robotic assistance technology for common musculoskeletal disorders

One in eight adults in the U.S. has a mobility disability according to the CDC [Courtney-Long et al., 2015], which limits social activity [Miller et al., 2001], economic productivity [CDC, 2021], and quality of life [Shafrin et al., 2017]. These disabilities are largely associated with advanced age, stroke, or musculoskeletal disorders [Bureau, 2014; Vos et al., 2012]. Most of these individuals have some voluntary control of their lower limbs, and thus require only partial assistance of lower-limb musculature to overcome weakness during activities of daily living (ADLs). However, no broadly applicable intervention fits this critical need [Grimmer et al., 2019]. Conventional orthoses tend to immobilize rather than actively assist joints, causing side-effects including compensations

[Vistamehr et al., 2014], gait asymmetry [Haight et al., 2015], and overdependence on the brace [Lairamore et al., 2011]. Passive orthoses, canes, and walkers cannot provide positive mechanical work to assist the most challenging activities, such as sit-to-stand and stair ascent. We examine the latest in robotic assistive technologies for common disabilities and MSDs next.

1.1.1 Stroke

Stroke is the second leading cause of acquired disability and has lasting remnant motor deficits even after extensive rehabilitation [Katan and Luft, 2018; Woolley, 2001]. Stroke rehabilitation is closely linked to the field of motor learning [Bejarano et al., 2016], which suggests that task-specific practice is superior to isolated muscle strengthening for enhancing neuroplasticity. However, due to post-stroke deficits at various joints, task-specific practice is inevitably performed with various compensations, which then become habitual in the long-term [Beyaert et al., 2015]. In particular, poststroke deficits at the ankle cause foot drop and reduced push-off power [Kluding et al., 2013; Verma et al., 2012], and deficits at the knee cause a locked knee gait and reduced foot clearance [Woolley, 2001]. A physical therapist is unable to simultaneously assist multiple joints like robot-guided training [van Kammen et al., 2020], but robotic therapies have various drawbacks. Treadmill-based robot-guided training enforces normative joint kinematics resulting in less patient effort, reduced kinematic variability, and practice on an unnatural (treadmill) surface—all factors that greatly reduce learning [Dobkin and Duncan, 2012]. While mobile exoskeletons [Buesing et al., 2015] address the last problem, their reliance on pre-defined joint patterns fails to address the first two problems. Moreover, the focus of robot-aided gait training on walking neglects the common ADLs of stair climbing and sit-to-stand, yet rehabilitation of these tasks can reduce fall risk after stroke [Amira et al., 2015; Jacobs, 2016; Morone et al., 2018]. These challenges can be addressed by backdrivable, task-invariant powered orthoses with modularity to accommodate the heterogeneity of the stroke population. In chapters 2 and 3, we perform preliminary able-bodied validation of a task-invariant controller using our first-gen knee-ankle exoskeleton (Comex 1), as a precursor to future testing on stroke participants.

1.1.2 Low back pain—lifting-lowering-carrying

LL tasks are common in warehouse, construction, and military settings and are highly associated with low-back-pain due to their repetitive nature causing overuse injury [Marilyn Sharp et al., 2006]. The squat lift is recommended to prevent low-back injury, but because it involves lifting and lowering the body's center of mas, it is not as energy efficient as the stoop lift. The knee and ankle produce significantly more torque/power for the squat lift than the stoop lift, which primarily uses the hips and puts more stress on the lower back [Hwang et al., 2009; Antwi-Afari

et al., 2017]. The squat lift is more difficult to maintain due to distal muscle fatigue, causing individuals to eventually transition to the stoop lift [Hsiang et al., 1997; Trafimow et al., 1993]. Currently there is no causal orthotic treatment that prevents poor biomechanics (stooping) due to weak/fatigued lower-limb muscles [Hsiang et al., 1997]. In contrast, rigid back braces reduce lumbar loading during stooping but also restrict voluntary motion [Picchiotti et al., 2019]. Other workplace exoskeletons use a posterior elastic element in the back brace to compliantly assist lumbar extension [Ulrey and Fathallah, 2013; Lamers et al., 2018, 2020], but this can increase the activity of trunk flexor muscles [Theurel and Desbrosses, 2019]. Powered workplace exoskeletons address this problem by using hip actuators to assist trunk extension [Theurel and Desbrosses, 2019]. While these devices can compensate for gravity at the hips [Wei et al., 2020; Huysamen et al., 2018], they cannot assist the distal joints which are critically involved in squatting. Instead these designs may encourage stooping.

Moreover, the real working environment involves not just LL, but lifting-lowering-carrying (LLC) over multi-terrain. The current exoskeleton/controller technologies fall short in fulfilling this versatile need. Ideally, assistive torques at the knee will target the root cause of poor LL biomechanics: weak/fatigued distal joint musculature. With this assistance, we would expect to see less stooping post-fatigue with orthotic assistance. The orthosis should also reduce muscle effort to delay fatigue, allowing proper lifting biomechanics for longer periods to prevent low-back injuries in the workplace. Moreover, since quadriceps are stressed during high demand activities such as stairs and ramp climbing, the ideal orthosis should be versatile enough to provide assistance in multiple tasks. To address these gaps, we first designed a novel bilateral knee controller that facilitates multi-terrain lifting-lowering-carrying (LLC) in chapter 4, and later performed preclinical validation on eight healthy subjects using the M-BLUE bilateral knee modules in both fatiguing and non-fatiguing tasks in chapter 5.

1.1.3 Post-polio syndrome and Multiple sclerosis

Post-polio syndrome (PPS) is a neurological disorder that can affect polio survivors decades after the occurrence of the polio infection [Li Hi Shing et al., 2019]. While the polio vaccine has largely eradicated polio in the US and other parts of the world, an elderly population of polio survivors still remains who are at risk of developing PPS. Recent anti-vaccine sentiments fueled by the covid-19 pandemic may once again make this disease more widespread [Harvard International Review, 2023]. From the perspective of mobility, the polio affected neurons gradually degenerate causing progressive muscle weakness, fatigue, pain and hamper gait performance. PPS patients are often exhausted even after little activity. Walking, rising from a chair and stair climbing are a challenge

as they need balance and co-ordination and aggravate fatigue. PPS symptoms affect functional mobility and lead to a sedentary lifestyle that may cause further complications such as obesity and diabetes, causing social isolation and reduce accessibility for patients. Robotic gait assistance can help alleviate this challenge by supporting affected muscles and reducing strain on the body. However, a recent study [Yu et al., 2020] that tested a custom powered knee exoskeleton on three PPS participants demonstrated much worse scores with the powered device on the 10 meter walk test, and the TUG, compared to a simpler passive brace that prevents knee hyper-extension and allowed the participants to use their affected leg like a stick in a "pole jump" gait. However this gait style puts unnaturally high stresses on the pelvis and is not sustainable.

MS is a complex autoimmune disease that affects the central nervous system, and often leads to impairment of the lower-limb extremities and gait disruptions [Hoang et al., 2014]. Some of the characteristics of MS are muscle weakness, spasticity, lack of balance and coordination, and fatigue to perform activities of daily living. Muscle weakness prevents generation of enough force to support the body in demanding tasks such as sit-stand and stair climbing. Moreover, functional spasticity in an antagonistic muscle can have a further debilitating effect on the weakened agonist during gait. Similar to PPS, high demand activities induce additional fatigue that further impairs gait. An assistive exoskeleton can potentially provide optimal assistance to correct the strength deficits, which can potentially increase gait performance and improve endurance by delaying fatigue. However, a large randomized clinical trial with a commercial bilateral knee exoskeleton (Keeogo) showed negative gait performance results, i.e., participants walked significantly slower with the device [McGibbon et al., 2018, 2023] on the timed up and go (TUG), six minute walk test, and timed stair test. Moreover this commercial device is touted to use traditional actuation with high reflected inertia, i.e., it has relatively stiff joints which may hinder voluntary motion.

As both MS and PPS are progressive diseases, the assistive strategies would need to be modified along with the changing needs of the patient. Additionally MS is peculiar for having "flare ups" and deficits that change location on a short term basis. Moreover, the presentation of deficits in both of these diseases is highly individual specific. As such, adaptability and clinician-friendly customizability of assistance provided by robotic assistance devices is crucial to tailor interventions according to the needs of each patient. A versatile control strategy can thus help to tackle the complex task of customization in robotic gait assistive systems. In chapter 6 we make headway in closing this gap by customizing the controller developed in chapter 4 with the help of a custom android app, and perform preliminary validation in two case studies (PPS and MS) using M-BLUE bilateral knees.

1.1.4 Knee osteoarthritis

Weak lower-limb musculature is a significant contributor to the risk of OA, especially at the knee, which represents over 80% of the total burden of the disease [Vos et al., 2012]. The medial and lateral tibiofemoral joint (TFJ) and patella-femoral joint (PFJ) form the three compartments of the knee (and three potential regions for OA). Several studies support the theory of quadriceps weakness being a significant contributing risk factor towards knee OA progression in all three compartments. In [Amin et al., 2009] , it was found that greater quadriceps muscle strength prevented cartilage loss at the PFJ. Additionally these patients presented with less knee pain compared to controls. A proposed theory is that the medial and lateral quadriceps are uneven in strength and cause misalignment of the PFJ [Amin et al., 2009], which can increase pain during loading. This correlation between quadriceps weakness and knee pain was also found for TFJ OA [O'Reilly et al., 1998]. It is known that the quadriceps act as a shock absorbing mechanism during the gait cycle [de Oliveira Silva et al., 2015]. Weak quadriceps can therefore lead to knee instability and greater loading at the articular surfaces, increasing the risk for TFJ OA progression. There is also growing evidence that hip musculature has influence on the progression of both knee and hip OA. Preliminary findings show decreased hip extension, external rotation and abduction weakness in patients with knee OA compared to healthy adults [Deasy et al., 2016]. A similar correlation between weakened hip muscles and hip OA progression has been found [Amaro et al., 2007]. Importantly, the compensatory mechanisms of unilateral hip OA can lead to contralateral hip OA [Amaro et al., 2007] as well as contralateral knee OA [Shakoor et al., 2003]. Therefore, modular orthoses that can provide assistive torques at the knee and hip joints during daily tasks can compensate for weakness in quadriceps and hip musculature and mitigate the symptoms of knee and possibly hip OA. Instead of assisting musculature, current knee OA orthoses unload the medial or lateral knee joint space through the mechanical structure of the brace. These knee orthoses have shown pain reduction and functional improvement [Pollo et al., 2002] but they do not address pain associated with the patellofemoral joint (PFJ) compartment–most likely because they do not reduce patellofemoral loads caused by the action of the quadriceps. To motivate future work with the latest controller and M-BLUE hardware, we present preliminary results at the end of chapter 6 from a PFJ OA case study performed using a simple quasi-stiffness controller using Comex 2.

1.2 Contributions and organization of the Dissertation

In chapter 2, I improve and assess an existing task-invariant control scheme by implementing a custom foot pressure sensor for Comex 1 and perform preliminary in-vivo validation. My group's prior work [Lv et al., 2018] developed the first version of a partial assistance controller that reduced

the effect of gravity on the wearer's joints by way of a nonlinear controls technique of (potential) *energy shaping*. In effect it provided virtual body weight support (vBWS). Since this assistance scheme transcends the need to be pre-programmed for a particular activity/task, it is fundamentally "task-invariant". However, vBWS does not consider body weight load distribution between the two limbs during double support phases, causing excessive assistance torques by assuming all bodyweight is supported by a single limb (single support). By utilizing the vertical ground reaction force (vGRF) feedback from a custom designed force sensing foot plate, *chapter 2* significantly improves the vBWS controller for double support phases, and investigates its efficacy on a single healthy subject for multiple activities of daily living (ADLs) using Comex 1. Experimental results suggest that vBWS with vGRF is an effective assistance scheme for slow activities such as getting up from a chair and performing a squat.

Chapter 3 presents human subject experiments that were my contributions to collaborative work on more advanced task-invariant controllers—specifically, the multi-task optimized energy shaping controller (M-TOES) which crucially utilizes the vGRF in its optimization scheme [Lin et al., 2022]. M-TOES was tested on 3 healthy subjects for all primary ADLs and achieved promising but subject dependent muscular effort reductions for tasks with slow as well as fast dynamics with Comex 1 (equipped with the custom vGRF sensor I developed). Next, the chapter presents the results of my latest collaboration in the experimental testing (n=8) of an updated version of the M-TOES controller implemented on our latest M-BLUE exoskeleton (knee and hip modules). Good matching between controller and normative torques was achieved with these exoskeleton/controller combinations for all ADLs. However, the vast number of non-intuitive basis functions utilized in the M-TOES controls approach hindered customizability, and possibly explains the lack of consistent muscular effort reductions that were achieved across tasks. These limitations precluded the application of M-TOES for LLC and impaired individuals, and paved the way for the subsequent chapters.

Chapter 4 presents a novel, versatile, clinically intuitive, and easily customizable bilateral knee controller for application to LLC and impaired individuals. Assisting LLC requires specialized torques, high in magnitude, fully exploiting the capabilities of the actuator, and not limited by the need to match the % assistance for each task or relying on a normative dataset. Although the controllers tested in chapter 3 guaranteed stability, they have no guarantee of producing helpful torques especially for the impaired populations who have non-normative kinematics that fall grossly outside the training dataset. The critical dependence on a training dataset is also a drawback of machine learning approaches that aim for task-invariance. In chapter 4 I took a more fundamental approach to controller development. By studying fundamental clinical gait analysis literature and using carefully selected, physically inspired torque basis functions, I developed a task-invariant bilateral knee controller which in addition to achieving good torque matching with

normative data, is also clinically intuitive and readily customizable.

Chapter 5 presents for the very first time, multifaceted (performance, postural, muscular, and perceptual) benefits for multi-terrain LLC during both fatigued and non-fatigued states using the novel controller developed in chapter 4 and the latest M-BLUE bilateral knee modules. While prior studies have demonstrated exoskeleton benefits for isolated (e.g., squatting, or stair climbing) tasks, their controllers are not task-invariant and hence would be impractical in the workplace which exhibits a multitude of terrains in which the exoskeleton is expected to adapt in. Moreover, the experimental designs of prior studies do not assess the exoskeletons' performance during fatigue—which is highly linked with low-back-pain incidence—and thus lack impetus for workplace adoption. Moreover, Chapter 5's results shine a spotlight on "distal" joint assistance for LLC assistance, which is a shift in focus from the "direct" approach used by back only and hip-back braces.

In chapter 6, I firstly develop a clinician-friendly android GUI that allows seamless customization of the intuitive controller parameters developed in chapter 4. Next, after customizing the controller to meet unique participant-specific needs and deficits, we demonstrate meaningful improvements in the primary metrics of PPS and MS patients via two case studies performed with the M-BLUE bilateral knee modules. To motivate future work with the novel controller/exoskeleton combination, chapter 6 additionally presents the pain scale improvements seen in a preliminary experiment on a patelo-femoral OA patient using a simple quasi-stiffness controller implemented on Comex 2.

The major contributions of the dissertation are summarized as follows:

- Chapter 2 details the improvements to a potential energy shaping controller by the development and implementation of a custom-made vGRF sensor for Comex 1. The sensor facilitated correction of the controller torques during multi-support task phases. The improved controller is subsequently validated on a healthy participant on multiple terrain.

- Chapter 3 details the pre-clinical validation of 2 advanced energy shaping controllers on Comex 1 (n=3) and the M-BLUE knee and hip modules (n=8) which paves the way for subsequent controller developments and experiments.

- Chapter 4 details the development of a novel, clinically-intuitive, and easily customizable energy shaping inspired control scheme for partial-assist knee exoskeletons.

- Chapter 5 details the pre-clinical validation of the novel controller developed in chapter 4 for the application of lifting-lowering-carrying in both fatigue and non-fatigue states, and for the first time shows holistic, multifaceted benefits in these tasks.

- Chapter 6 firstly explores the customizability of the novel controller developed in chapter 4 for individuals with lower limb impairments using a clinician-friendly android app. Secondly, it presents case studies on participants with PPS and MS using customized versions of the novel controller developed in chapter 4, achieving promising benefits for both participants. Lastly by presenting preliminary results of a simpler (quasi-stiffness) controller on a knee OA patient using Comex 2, the chapter motivates future testing using the novel controller developed in chapter 4.

CHAPTER 2

A Potential Energy Shaping Controller with Ground Reaction Force Feedback for a Multi-activity Knee-ankle Exoskeleton

The work in this chapter was published in 2020 at the *8th IEEE RAS/EMBS international conference for biomedical robotics and biomechatronics* [Divekar et al., 2020]. Authors: Nikhil V Divekar, Jianping Lin, Christopher Nesler, Sara Borboa, Robert D Gregg.

2.1 Introduction

Every year more than 800,000 Americans are affected by stroke, out of which 200,000 are affected by hemiparesis of the lower limb [Ma et al., 2014]. Post-stroke rehabilitation typically involves gait training [Morone et al., 2017]. The most common, persisting gait deficit is foot-drop [Kluding et al., 2013; Verma et al., 2012], which is associated with weakness in dorsi-flexors and/or co-contraction of plantar-flexors. Foot-drop in turn affects patients' foot clearance ability during swing, and also results in foot slap after heel contact. Another ankle deficit is plantar-flexor weakness during push-off, which is usually associated with more proximal compensation strategies to increase gait speed such as hip extension or increased plantar-flexion of the non-paretic leg. Improving ankle biomechanics is important because gait speed is a determining characteristic of functional tests [Patterson et al., 2010].

Knee biomechanics are also affected in the hemiparetic gait [Woolley, 2001]. Quadriceps weakness more often results in the adoption of a locked-knee gait, i.e., greater than normal extension or even hyper-extension of the knee during stance. This strategy is understandably used to avoid the issue of knee buckling upon heel contact. This compensatory mechanism however reduces gait velocity, and can also increase impact forces on the knee. Hamstring weakness can decrease the amount of foot clearance achieved during swing, resulting in compensatory mechanisms from proximal joints such as hip circumduction of the paretic leg or plantar-flexion of the

unaffected leg, e.g., vaulting.

Robot assisted gait training (RAGT) has potential benefits over traditional, therapist-based rehabilitation [van Kammen et al., 2017]. First, RAGT can drastically increase the number of repetitions. Further, RAGT reduces the burden on the therapists, so more patients can be treated by a single therapist. Another advantage is that assistive joint torques can be applied in a more controlled and potentially customized manner. However, RAGT has not shown better outcomes compared to traditional therapist-based rehabilitation [Dobkin and others, 2003]. The current RAGT schemes enforce fixed joint trajectories on a patient, which may not match with a patient's innate trajectory before the stroke. Further, patient gait trajectories evolve towards a normative trajectory throughout the rehabilitation and re-learning process. Therefore, enforcing a particular trajectory may not be the best strategy to help a patient that may have different levels of impairment across the muscles. The second problem with this strategy is that it introduces patient complacency and greatly diminishes the stimulation and level of difficulty, ultimately reducing learning [Bejarano et al., 2016].

Recently, Goldfarb et al. [Murray et al., 2015] attended to this problem through the design of 1) a mobile exoskeleton (Indego) with backdrivable actuators to allow voluntary joint motion, and 2) a walking controller that does not depend on a pre-defined trajectory. The controller was designed primarily to provide a combination of body-weight compensation and stance stabilization through the hip and knee actuators, but this exoskeleton did not have ankle actuators. Moreover, the field of physical therapy supports the notion that the level of impairment on the hemiparetic side increases from proximal (hip) to distal (ankle), and that distal joint recovery needs to be actively facilitated [Sheila Lennon, 2001]. Further, this study did not consider other activities of daily living (ADLs) that are necessary for regaining independence.

RAGT typically focuses on walking, either on a treadmill or level ground. However, stair climbing is an equally important ADL, and improvements gained in walking ability do not necessarily transfer to stair climbing [Morone et al., 2018]. This requires a different set of biomechanics and higher quadriceps and ankle involvement. Moreover, falling on stairs poses a disproportionately higher risk of severe injury or death in older adults [Jacobs, 2016]. Sit-to-stand is another activity that is typically neglected in RAGT. Subjects greatly bias their weight to the non-paretic side when performing sit to stand, thereby increasing its loading [Amira et al., 2015; Marigold and Eng, 2006]. In fact, a lack of rehabilitation in sit-to-stand contributes to the increased fall risk in the post-stroke population [Amira et al., 2015]. Training ADLs with RAGT requires a mobile, backdrivable exoskeleton with a task-invariant controller that allows the patient to practice their preferred joint kinematics with proper torque assistance. Although progress has been made in the design of backdrivable exoskeletons [Zhu et al., 2017; Lv et al., 2018; Wang et al., 2018; Zhu et al., 2019], their control strategies still tend to be task specific.

To address these gaps, our prior work [Lv and Gregg, 2018; Lv et al., 2018] developed a task-invariant exoskeleton control strategy that assists the user's voluntary movements with energetic control objectives rather than kinematic objectives. This work implemented a control technique called potential energy shaping in a unilateral knee-ankle exoskeleton (Comex 1) to reduce the perceived gravity of the user. The control strategy leverages the exoskeleton's backdrivable, torque-controlled actuators, which comprise a high-torque motor with a low-ratio transmission (24:1). This design minimizes the backdrive torques (around 3 Nm) while being capable of output torques up to 60 Nm [Zhu et al., 2017], which is sufficient for rehabilitation of the primary ADLs post-stroke [Hidler et al., 2007; Ng and Hui-Chan, 2012]. However, the potential energy shaping approach in [Lv and Gregg, 2018; Lv et al., 2018] relies on a model that assumes the stance leg is fully loaded with the weight of the user, resulting in excessive plantar-flexor torques as weight transfers from the assisted leg to the contralateral leg during double support. This excessive plantar-flexion can aggravate the foot-drop problem later in swing, during both walking and stair climbing. For sit to stand, the controller provides double the required torque, as body weight should be equally shared between the two legs. During sitting, excessive ankle and knee torques are applied as most of the weight is supported by the seat. These limitations must be overcome before this control approach can serve patient populations.

In this study, we improve the potential energy shaping control method in Comex 1 using ground reaction force (GRF) feedback to taper the torque control output for any activity involving multiple supports. We demonstrate feasibility with a single healthy subject performing a variety of tasks (walking, stair climbing, sit-to-stand, and stand-to-sit), resulting in reduced muscular effort when assisted by the exoskeleton. In Section 2.2.1 we briefly describe the dynamic model and control law of [Lv and Gregg, 2018], which is improved with a GRF-based torque output tapering strategy. Section 2.2.2 describes the exoskeleton and custom foot force sensor used to implement the control strategy. Section 2.2.3 presents the methodology for the human subject experiment, which compares muscle activation between bare, passive, and active modes. Section 2.3 first uses prerecorded human subjects data for level-ground walking to show the tapered torque outputs better match normative joint torques compared to the original control strategy. We then validate the foot sensor by comparing its measurements with a portable force plate. Moreover, the control strategy is implemented in the exoskeleton for experiments with a single healthy subject performing ADLs. We conclude the study with a discussion of the results in Section 2.4 and closing remarks in Section 2.5.

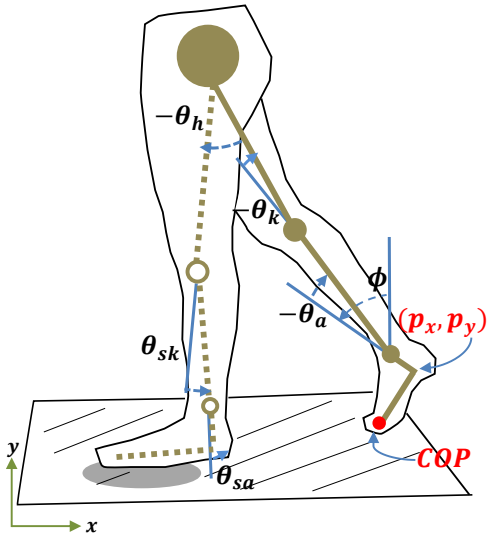

Figure 2.1: Kinematic model of the human body. COP denotes the Center of Pressure. The solid links denote the stance leg, the dashed links denote the swing leg. This figure is reproduced from [Yeatman et al., 2019].

2.2 Methods

This section presents the theoretical framework for potential energy shaping with GRF-based tapering, the design of the exoskeleton and GRF force sensor, and the methods for the multi-task human subject experiment.

2.2.1 Potential Energy Shaping For Knee-Ankle Exoskeleton

2.2.1.1 Model

The biped model in Fig. 2.1 is restricted to the sagittal plane due to the planar actuation scheme of the exoskeleton. The masses of the human limb and the exoskeleton are combined together in the model. For control purposes, the dynamics of the stance and swing legs are modeled separately with coupled interaction forces. The generalized coordinates of the stance leg are given by $q_{st} = (p_x, p_y, \phi, \theta_a, \theta_k)^T \in \mathbb{R}^{5\times 1}$, where (p_x, p_y) represents the Cartesian coordinates of the heel with respect to the inertial reference frame (IRF). The heel angle ϕ is defined with respect to the vertical axis, and θ_a and θ_k are the stance ankle and knee angles, respectively.

We use the Euler-Lagrange method to derive the dynamics of the stance leg, where the corresponding Lagrangian $L(q_{st}, \dot{q}_{st}) = K(q_{st}, \dot{q}_{st}) - V(q_{st})$ is the difference between the kinetic energy and potential energy [Murray et al., 1994]. The kinetic energy $K(q_{st}, \dot{q}_{st}) = \frac{1}{2}\dot{q}_{st}^T M(q_{st})\dot{q}_{st}$ is based on the generalized mass/inertia matrix $M(q_{st}) \in \mathbb{R}^{5\times 5}$, and $V(q_{st}) \in \mathbb{R}$ is the gravitational poten-

tial energy. $V(q_{st}) = \sum_{i=1}^{n} m_i g h_i(q_{st})$ In the following equations, we omit the arguments q_{st} and $\dot{q}_{st}$ of the dynamic terms to abbreviate notation. Based on the Euler-Lagrange equation, the human-exoskeleton stance leg dynamics are given as

$$\frac{\mathrm{d}}{\mathrm{dt}}\partial_{\dot{q}_{st}} L - \partial_{q_{st}} L + A^T \lambda = M\ddot{q}_{st} + C\dot{q}_{st} + N + A^T \lambda = \tau, \tag{2.1}$$

where $C \in \mathbb{R}^{5\times5}$ is the Coriolis matrix, $N = \nabla_{q_{st}} V \in \mathbb{R}^5$ is the gravitational forces vector, and matrix $A \in \mathbb{R}^{3\times5}$ maps the ground reaction forces $\lambda \in \mathbb{R}^3$ into the dynamics. We denote the torque inputs as $\tau = \tau_{exo} + \tau_{hum} = Bu + Bv + J^T F$, where $B = [0_{2\times3}, I_{2\times2}]^T \in \mathbb{R}^{5\times2}$ maps the exoskeleton actuator torques $u \in \mathbb{R}^{2\times1}$ and human muscle torques $v \in \mathbb{R}^{2\times1}$ at the knee and ankle into the leg dynamics. The interaction forces $F \in \mathbb{R}^3$ between the hip and the swing leg are mapped to the system by the body Jacobian matrix J [Lv and Gregg, 2018].

For the swing leg model, the generalized coordinates are given as $q_{sw} = (h_x, h_y, \theta_{th}, \theta_{sk}, \theta_{sa})^T \in \mathbb{R}^{5\times1}$, where (h_x, h_y) are the positions of the hip with respect to the IRF, θ_{th} is the angle between the vertical axis and the swing thigh, and θ_{sk} and θ_{sa} are the swing knee and ankle angles, respectively. The swing leg dynamics have the same form as (2.1) except there is no ground contact, i.e., $\lambda = 0$.

2.2.1.2 Control

Our controller for the exoskeleton is based on the controlled Lagrangian method [Blankenstein et al., 2002], which maps the original open-loop system to a desired closed-loop system (i.e., feedback system). We wish to achieve a closed-loop system with a modified potential energy $\tilde{V}$ as

$$M\ddot{q}_{st} + C\dot{q}_{st} + \tilde{N} + A_l^T \lambda = Bv + J^T F, \tag{2.2}$$

where $\tilde{N} = \nabla_{q_{st}} \tilde{V} \in \mathbb{R}^{5\times1}$ represents the modified potential forces vector. Based on [Blankenstein et al., 2002], systems (2.1) and (2.2) match if and only if there exists a full rank left annihilator of B in the orthogonal projection form, i.e., $B^{\perp}B = 0$, such that

$$0 = B^{\perp}(N - \tilde{N}), \tag{2.3}$$

holds true along all trajectories $(q_{st}, \dot{q}_{st})$. Equation (2.3) is called the *matching condition* for potential energy [Lv and Gregg, 2018]. The corresponding feedback control law is explicitly given by

$$u = (B^T B)^{-1} B^T (N - \tilde{N}), \tag{2.4}$$

which only depends on the configuration vector q_{st} [Lv et al., 2018].

Given the left annihilator matrix

$$B^{\perp} = \begin{bmatrix} I_{3\times 3} & 0_{3\times 2} \\ 0_{2\times 3} & 0_{2\times 2} \end{bmatrix},$$

the matching condition (2.3) suggest the first three rows of the modified $\tilde{N}$ must be equal to those of N [Lv and Gregg, 2018]. To provide gravity compensation, we define the closed-loop potential force vector as $\tilde{N} = [N_{1:3}^T, \mu \cdot N_{4:5}^T]^T$, where $N_{i:j}$ contains the ith to jth elements of the vector N, and μ is a constant scaling coefficient. The resulting control law only depends on the foot orientation, ankle angle, and knee angle. The coefficient μ is selected to be less than one so that the exoskeleton compensates for a fraction of the gravitational torques at the ankle and knee joints, providing virtual body-weight support (BWS). The controller for swing period is derived in a similar manner using the swing leg coordinates [Lv and Gregg, 2018].

Note the model (2.1) does not know the state of the contralateral leg, and it is practically impossible to measure the interaction forces F between the hip and swing leg. Hence, the potential energy shaping controller compensates for a fraction of the full body weight during stance, even when part of the body weight is supported by the other leg or a chair. We attend to these issues by implementing a GRF-based torque tapering strategy, where a scaling factor ε multiplies the exoskeleton torque commands from (2.4) during the stance phase. The scaling factor ε is a function of the vertical ground reaction force measured by a custom force sensor in the Comex 1 foot plate, which is described next.

2.2.2 Mechanical Design of Exoskeleton and GRF Sensor

The partial-assist device (Comex 1) for which the controller is designed is shown in Fig. 2.2a. The device can produce 30 Nm continuous torque (60 Nm peak) at the knee and ankle using 200 W frameless BLDC motors (Emoteq) with a 24:1 transmission ratio. The transmission comprises a belt stage and a custom planetary gearbox inside the driven sprocket. The motors are driven with sinusoidal commutation by Elmo Gold Twitter drives (rated to 30 A). The control system includes the onboard sensors and computation needed to implement torque control laws, including Sunrise torque sensors for closed-loop torque control running at 800 Hz on a National Instruments myRIO microcontroller. High-resolution relative encoders measure joint angles/velocities, and a 6-axis Microstrain IMU measures orientation. The system is powered by an onboard Lithium-Ion battery pack. The unpowered backdrive torque is about 3 Nm, allowing the user to freely control their joint kinematics. The device weighs about 4.5 kg and includes safety features such as hard stops and current limiters at both joints.

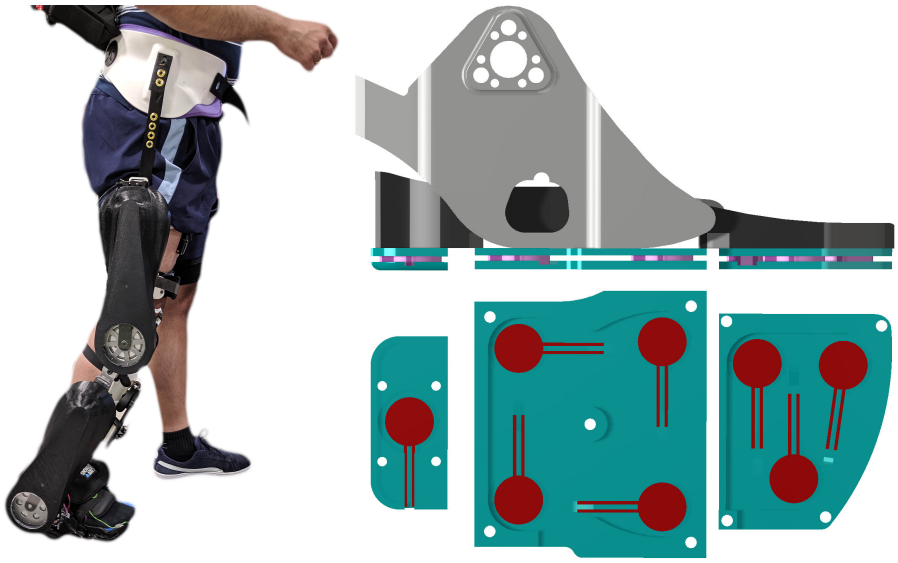

(a) (b)

Figure 2.2: (a) Comex 1 exoskeleton being worn by a healthy user. (b) Top: Sagittal view of Comex 1 foot plate, showing the rigid structure (gray), insole (black), force sensor plates (blue), and force-channeling pucks. Bottom: Top section view showing the layout of FSRs (red) within the force sensor plates (blue).

The foot sensor used in this work was designed to record the wearer's vertical ground reaction force with the accuracy of an instrumented force plate, while maintaining the profile and level of portability necessary to incorporate it into the underfoot region of Comex 1's footplate - see Fig. 2.2b. This was accomplished using a structure inspired by force plate construction, wherein each section includes two rigid plates, held apart by circular spacers that each sit atop a FlexiForce A401 (Tekscan, South Boston, MA) force sensitive resistor (FSR). Due to the gap between the rigid plates being held open by the spacers, all force applied to the plates' large surface areas travels through the spacers and, as a result, the FSRs. A thin layer of compressible foam is placed above and below the FSRs to ensure sufficient pressure distribution between the spacer and the lower plate. By funneling the force to the FSRs in this manner, we are able to avoid having large portions of the foot which do not transmit their force to a sensor due to their lack of surface area coverage. This is an issue that can also be addressed by using FSR-style sensors with large surface areas (e.g., Tekscan F-Scan), but high cost and limited durability keep this from being an ideal solution.

The FSRs from the heel and middle section of the sensor are connected to each other in parallel and form the total heel resistance. Similarly, the 3 FSRs from the toe section are connected in parallel, forming the total toe resistance. The change in resistance of the heel and toe (related to the force being applied at these locations) is sensed and amplified by an operational amplifier

circuit recommended in the Tekscan data sheet [Tekscan, 2020]. This circuit also has the additional function of linearizing the non-linear resistance-force relationship. Finally, MyRIO software is used to calibrate the sensors before each experiment to achieve a final readout normalized to body weight.

2.2.3 Human Subject Experiment Methodology

The human subject experiment was designed to demonstrate the potential benefit of the knee-ankle exoskeleton during multiple, common ADLs. These tasks were: sit to stand, stand to sit, treadmill walking, and stair climbing. The primary aim of the experiment was to show a reduction in effort of the muscles related to the joints assisted by Comex 1. We assessed activation levels of the following muscles: vastus medialis oblique (VMO), biceps femoris (BF), tibialis anterior (TA), and soleus (SOL), which function as a knee extensor, knee flexor, dorsi-flexor, and plantar-flexor respectively. A single, male human subject (mass: 80 kg, height: 1.78 m) was enrolled for the study, which was approved by the Institutional Review Board at the University of Texas at Dallas and the University of Michigan.

The sit to stand, and stand to sit tasks were completed as part of a repetitive sit-stand cycle which consisted of four phases: sitting, sit to stand, standing, and stand to sit. Each phase lasted 1.5 s (cued using a metronome set to 40 BPM). A total of nine repetitions were carried out for each of the three modes tested: bare (without exoskeleton), passive (exoskeleton un-powered), and active (exoskeleton assistance). The level of assistance was set to $\mu = 0.17$ and $\mu = 0.4$ for stance and swing respectively for the active mode. The subject was instructed to maintain the same sit-stand technique for all three modes to minimize any bias in the results. The next task performed was level walking on a treadmill. The walking speed and cadence were kept the same for all three modes, and were set to the subject's self selected levels (speed of 2 MPH and cadence of 75 steps/min). These were determined while the subject walked with Comex 1 on passive mode. Feedback of the selected cadence was provided using a metronome, and the subject was asked to comply with it to the best of his ability. A total of 30 gait cycles were collected for each of the three modes tested. While the subject was allowed to use the treadmill handle bars during practise, this was disallowed during the trials which were recorded. The last task tested was stair climbing. An internal staircase of the building housing the laboratory was used for this purpose. Data was collected in two sets for each mode, where each set consisted of climbing up the full staircase acquiring four gait cycles. Thus eight gait cycles were collected for each of the three modes. A metronome set at 40 BPM was provided to help the subject keep the cadence consistent. While this cadence is lower than the average for healthy subjects, this ensured longer muscle loading times to better distinguish the effect of Comex 1 assistance, and also is closer to the low cadence of stroke

patients who are the intended end users of the device.

We used a Delsys system to acquire electromyography (EMG) data from the four muscles VMO, BF, TA, and SOL of the right limb (the side with Comex 1). The skin was appropriately prepared to reduce skin-electrode impedance. An inter-electrode distance of 10 mm was used. All EMG data was sampled at 2000 Hz and smoothed with a low-pass, zero-lag, second-order Butterworth filter (6 Hz cutoff). All data was normalized with respect to the maximum value of the mean of the ensemble average of each task for each muscle [Yang and Winter, 1984], i.e., as a percentage of the maximum voluntary contraction level (%MVC). EMG data corresponding to each sit to stand, and stand to sit repetition was cropped based on the deflection and return to steady state of the sagittal femur angle (measured using an accelerometer built into the EMG sensor). The walking and stairs trials were cropped using spikes in the accelerometer data corresponding to heel strike. The cropped trials were then integrated with respect to time to represent muscular effort as %MVC.s.

2.3 Results

2.3.1 Tapering Simulation Using Normative Kinematic Data

In this simulation, we examine the exoskeleton torques provided by inputting normative human kinematic data during level-ground walking [Embry et al., 2018] into the controller (2.4). We set the scaling factor $\varepsilon = \sin(\frac{f}{f_{bw}} \cdot \frac{\pi}{2})$, which multiplies the exoskeleton torques during the stance phase, where f represents the vertical ground reaction force measured by the force plate, and f_{bw} represents the weight of the human subject. Once f reaches f_{bw}, the scaling factor becomes one, and the whole body weight acts on the contact foot. The reason for setting $\varepsilon = \sin(\cdot)$ is to have a smooth transition when f is around f_{bw}.

Fig. 2.3 compares the simulated exoskeleton joint torques with normative joint torques for level-ground walking [Embry et al., 2018]. Results show that potential energy shaping with tapering better matches the human torque profiles than without tapering, suggesting the tapering strategy will deliver more appropriate assistance in the subsequent experiments with ADLs.

2.3.2 Foot Sensor Validation

The foot sensor design was validated by wearing Comex 1 during overground walking, in which the wearer stepped on a portable force plate (Kistler). The foot sensor (via myRIO) and force plate recordings were started and stopped at the same time, and sampled at the same rate. The data in Fig. 2.4 were trimmed to contain just the stance phase of the step on the force plate, and normalized

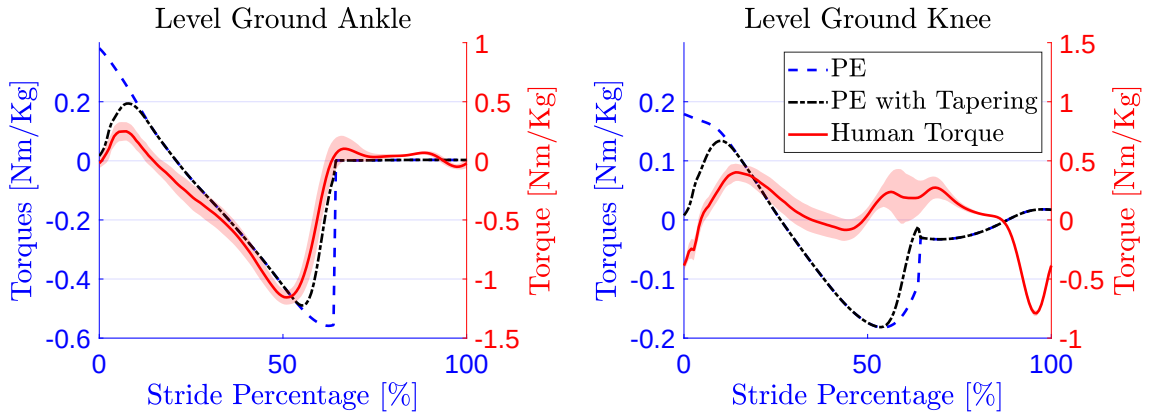

Figure 2.3: The torques acting on ankles and knees based on level ground walking on a treadmill with walking speed 1.0 m/s. The red solid lines represent the averaged human torques (10 subjects) with variance. PE represents the potential energy shaping method. Positive values represent ankle dorsiflexion torques and knee extension torques.

using the subject's body weight. This trial resulted in a correlation coefficient of 0.99 between the foot sensor and force plate data (taken as gold standard), with a mean square error (MSE) of 0.03 between the two signals. Further analysis of the graph shows that the difference between the peaks in both signals is negligible, showing the linear behavior of the force sensor.

2.3.3 Experiments with Activities of Daily Living

The primary objective of the human subject experiment was to determine the effect of Comex 1 assistance torques on the muscles related to the knee and ankle joint movements during the four tested tasks. Fig. 2.5 shows the ensemble average (across repetitions) of time-normalized EMG for all muscles (VMO, BF, TA, and SOL), tasks (sit to stand, stand to sit, level walking, and stair climbing), and exoskeleton modes (bare, passive, and active). Also shown are the simultaneously recorded exoskeleton assistance torques pertaining to the muscles (knee torques are overlayed for VMO and BF, whereas ankle torques are overlayed for TA and SOL). Generally during active mode, a reduction in agonist EMG (agonist muscular activation) was observed during periods of higher torque assistance levels of the related joint compared to bare and passive modes. A detailed analysis of Fig. 2.5 is given in Section 2.4 where we dissect the EMG patterns found for the various phases of the tasks and their potential bearing on stroke rehabilitation. We show quantitative comparisons of mean muscular effort for the various tasks and muscles in Tables 2.1-2.4.

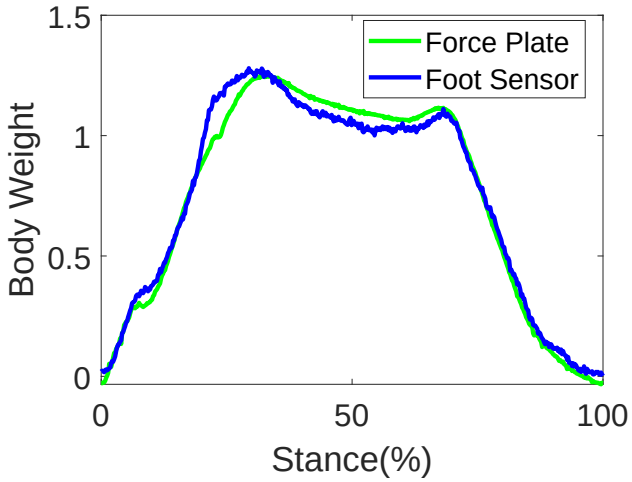

Figure 2.4: Comparison of the simultaneously recorded foot sensor and force plate readings for one stance cycle during level overground walking. Both readings are normalized to body weight, and temporally normalized to a percentage of the stance phase. A correlation coefficient of 0.99, and a mean square error of 0.03 was found between the two signals.

Table 2.1: Effort comparisons for Sit to Stand: showing mean ($\pm$ SD) for muscles (columns) and modes (rows).

Effort [%MVC.s]	VMO	BF	TA	SOL
Bare	78.8 (6.2)	86.0 (8.8)	63.2 (15.2)	33.6 (8.2)
Passive	67.6 (7.9)	96.9 (15.3)	54.7 (7.9)	46.4 (10.9)
Active	34.1 (3.9)	61.6 (8.6)	30.0 (4.3)	49.7 (9.7)

Table 2.2: Effort comparisons for Stand to Sit: showing mean ($\pm$ SD) for muscles (columns) and modes (rows).

Effort [%MVC.s]	VMO	BF	TA	SOL
Bare	98.8 (13.6)	93.8 (11.6)	85.2 (13.8)	59.2 (14.1)
Passive	87.4 (7.2)	72.1 (7.4)	85.9 (9.4)	68.4 (16.8)
Active	51.1 (5.2)	47.1 (7.0)	50.0 (10.8)	48.5 (7.5)

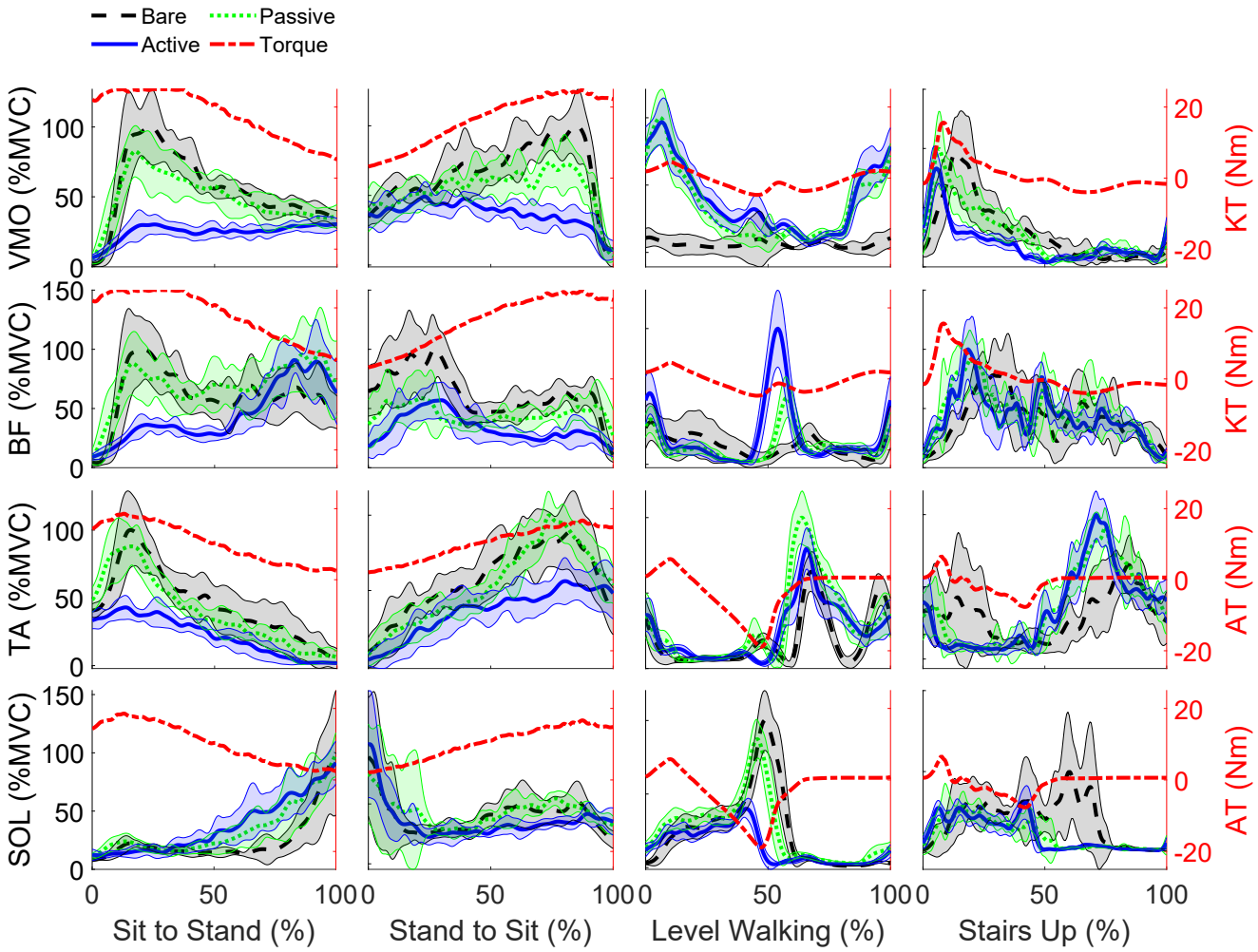

Figure 2.5: Comparisons of ensemble averaged EMG between the three exoskeleton modes tested (bare, passive, and active), along with the assistance torque for the corresponding joint. The four activities tested (sit to stand, stand to sit, level walking, and stairs up) are shown column wise, whereas the four muscles tested (VMO, BF, TA, and SOL) are shown row wise. Rows one and two represent the muscles primarily responsible for controlling the knee joint and torque provided by Comex 1 at the knee (KT). Rows three and four represent the muscles primarily responsible for controlling the ankle joint and the torque provided by Comex 1 at the ankle (AT). Shaded regions represent the SDs about the mean EMG profiles. A positive KT represents a knee extension torque, whereas a positive AT represents a dorsi-flexion torque.

Table 2.3: Effort comparisons for Walking: showing mean (± SD) for muscles (columns) and modes (rows).

Effort [%MVC.s]	VMO	BF	TA	SOL
Bare	10.4 (9.3)	23.8 (11.1)	32.3 (3.6)	42.9 (5.4)
Passive	62.7 (6.1)	25.0 (3.0)	54.4 (4.7)	46.4 (2.8)
Active	71.9 (7.2)	38.8 (6.9)	44.6 (4.7)	26.3 (2.2)

Table 2.4: Effort comparisons for Stairs: showing mean (± SD) for muscles (columns) and modes (rows).

Effort [%MVC.s]	VMO	BF	TA	SOL
Bare	73.0 (9.9)	102.3 (15.6)	73.3 (15.9)	96.5 (12.8)
Passive	82.6 (12.8)	137.7 (11.2)	104.9 (10.7)	64.7 (11.9)
Active	50.9 (4.1)	111.4 (10.8)	87.3 (10.6)	56.6 (5.6)

2.4 Discussion

The main objective of this study was to demonstrate the efficacy of a task-invariant controller for a backdrivable knee-ankle exoskeleton in providing partial assistance to a healthy human subject during multiple ADLs. Our previous work had established the theoretical basis for using an energy shaping controller in an exoskeleton [Lv et al., 2018]. In Section 2.2.1 we re-analyzed the potential energy shaping controller and highlighted a solution for multi-support phases of ADLs. In Section 2.3.1, we showed via simulation that scaling (or tapering) its output with the body weight normalized vertical ground reaction force better matches it with normative joint moments for level walking. A similar case can be made for the other ADLs, i.e., sit to stand, stand to sit, and stair climbing. In Sections 2.2.2 and 2.3.2 we showed the implementation of a FSR-based foot force sensor for tapering, and demonstrated that its performance closely matches that of a commercial force plate (correlation coefficient 0.99, and mean square error 0.03).

Using Comex 1 with the improved control scheme and custom force sensor, we presented the effects of partial-assistance on muscular activation (EMG) across multiple ADLs. While EMG plots of all muscles tested have been shown for all tasks performed, we discuss the more biomechanically meaningful results below. Potential energy shaping (which is a position based control strategy) is highly suited for assisting in tasks with slower dynamics, such as sit to stand and stand to sit. These two tasks primarily require knee extension, hip extension, and dorsi-flexion torques

[Millington et al., 1992]. During sit to stand these occur in the form of concentric contractions, and during stand to sit, as eccentric contractions. Accordingly, we found large reductions in VMO (knee extensor), BF (hip extensor), and TA (dorsi-flexor) activations for active mode in both these tasks when compared to bare and passive modes (see Tables 2.1 and 2.2 for mean effort values). Accordingly, the reductions in activations were aligned with the period of higher exoskeleton assistance torques as can be seen in Fig. 2.5. The reduction in BF activation is interesting, as no direct hip assistance torque was provided. However, we attribute this to an indirect effect on hip moment, possibly due to a change of strategy to a more knee dominant one. Another role of BF is in creating a knee flexion moment, and its co-contraction along with VMO acts to stabilize the knee joint. Therefore, another explanation could be the reduced need to stabilize the knee joint with exoskeleton assistance. Generally, agonist-antagonist co-contraction is higher for a more difficult task [Pfusterschmied et al., 2013], which was likely reduced due to the decreased difficulty in active mode.

Stair climbing during stance can be considered to have similar biomechanics to sit to stand, whereby knee extension, hip extension, and dorsi-flexion torques are required during early to mid stance to elevate the body's center of mass (COM) [Nadeau et al., 2003]. Additionally, a plantar-flexion torque during late stance is used to push off, similar to level walking [Nadeau et al., 2003]. Accordingly, we found reductions in VMO, and TA activations during early to mid stance, and also SOL activation during late stance (see Table 2.4 for mean effort values for the full stair cycle). Additionally, Comex 1 provided knee flexion torques during swing to help raise the shank, and is the likely cause of the reduction seen in BF EMG for active mode during early to mid swing (see Fig. 2.5). Overall, reductions in muscle activations aligned with the respective assistance torques, showing the contribution of Comex 1 towards the net joint torques.

Level walking has the fastest dynamics out of the four tasks tested, and a potential energy shaping control scheme that is based purely on joint angular positions (and not on velocity) would have reduced benefits compared to the slower tasks e.g., sit to stand. For example, the knee joint kinematics in early stance change rapidly in response to the impact of heel strike, but the magnitude of change of the knee angle is relatively small [Mentiplay et al., 2018]. In this case, the quadriceps primarily work to counteract momentum, rather than the effect of gravity (which a potential energy shaping controller is designed to counteract). Nevertheless from Fig. 2.5, it can be seen that Comex 1 did provide a mild supportive knee extension torque during early stance. This however did not translate to a reduction in VMO activation with the particular subject. A possible explanation for this is that the subject changed his gait to walk with a locked knee during bare mode, leading to minimal VMO activation. During passive, and active modes, his VMO activation was much higher than bare. This is likely due to the added weight of Comex 1 significantly increasing the momentum of the swing leg before heel strike, which needed to be countered by the VMO.

The assistance torque at the ankle is of a significantly larger magnitude compared to the knee during walking (Fig. 2.5), and therefore we expected to find beneficial effects for this joint. Indeed a large reduction in SOL activation was found during pushoff for active mode, which aligns well with the delivery of the plantar-flexion assistance torque. Interestingly, the assistance dorsi-flexion torque provided during early stance did not result in a significant reduction in TA activation in this phase. However, the dorsi-flexion torques provided during swing (to assist with foot clearance), did translate to a reduction in TA activation for active mode compared to passive mode, but not compared to bare mode. The likely reason for this is that dorsi-flexion assistance torques during swing are less than 1 Nm in amplitude, which is less than the backdrive torque of 3 Nm; therefore the difference in activation is likely only found with respect to passive mode. Table 2.3 provides mean effort values for the walking task, where we see only SOL had an overall mean effort reduction, when we consider the full gait cycle.

2.5 Conclusion and Future Work

In conclusion, this study demonstrated benefits of a potential energy shaping controller with GRF feedback when implemented in a backdrivable knee-ankle exoskeleton for assisting multiple ADLs. The controller provided reductions in muscular activation for tasks with slower dynamics and larger changes in joint angles, e.g., sit to stand, and significant benefit was apparent in certain phases of walking tasks, e.g., during push-off. Further testing needs to be done on a larger cohort of subjects to verify the behavior of the controller on a broader range of gait patterns. Additionally, work needs to be done to improve the benefit provided in the swing phase during level walking, e.g., by taking into consideration backdrive torque when prescribing the torque output. Lastly, we will validate the total energy shaping controller that accounts for joint velocities [Lin et al., 2019], so that tasks with faster dynamics can be better supported.

CHAPTER 3

Efficacy Testing Advanced Energy Shaping Controllers on Healthy Individuals

This chapter presents work from two studies. Study 1 was published in 2022 in the *IEEE Open Journal of Control Systems* [Lin et al., 2022]; authors: Jianping Lin, Nikhil V Divekar, Gray C Thomas, Robert D Gregg. Study 2 is under review for publication; authors: Jianping Lin, Gray C Thomas, Nikhil V Divekar, Vamsi Peddinti, Robert D Gregg.

3.1 Introduction

Throughout the course of my dissertation I collaborated on several research studies in the Locolab, by leading the in-vivo efficacy testing of several assistive devices which include (but are not limited to) the efficacy testing of task-invariant exoskeletons on healthy human subjects. In this chapter, after providing a brief synopsis, I present the human subject methods and results from *two* such collaborative studies. These studies contributed to the rationale for the novel controller framework and experimental designs I developed in subsequent chapters. Accordingly, at the end of the chapter I provide a combined discussion of the methods and results of the two collaborative studies in context of this dissertation.

Specifically, study 1 performed preliminary validation (n=3) of two advanced, data-driven energy shaping approaches under the collective MTOES framework: 1) with phi (PHI) which incorporates the global thigh angle, and 2) without-phi (WOP) which excludes it from the shaping framework. For human subject experiments, the controllers were implemented on the Comex 1 knee-ankle exoskeleton equipped with the vGRF sensor I developed in chapter 2, which significantly improved the MTOES optimization results. Study 2 generalized the MTOES framework to various modular configurations (ankle/knee/hip, unilateral/bilateral) and performed pre-clinical validation (n=8) using the MBLUE hardware on the knee and hip unilateral and bilateral modules. The primary hypothesis of both experiments was a holistic reduction in muscular effort (EMG) with exoskeleton assistance across multiple tasks.

3.2 Synopsis: Study 1

Study 1 utilized our prior IDA-PBC method [Lin et al., 2021] to include unactuated coordinates such as leg orientation in a passivity-based, energy-shaping controller for optimal assistance of all primary activities of daily life. In addition to global orientation, we included the vertical GRF in the basis functions (that map joint kinematics to joint moments) to address prior problems with excessive torque as weight transfers from the assisted leg to the (unmodeled) contralateral leg during double support [Divekar et al., 2020]. Incorporating these additional variables increased the number of candidate basis functions allowed by the IDA-PBC framework. This thereby improved the flexibility of the optimization process to fit the outputs of a single control law to normative human joint torques across all primary activities of daily life: level-ground walking, walking at variable inclines/declines, stair ascent/descent with variable step heights, and sit-to-stand. We formulated and solved this optimization problem using convex programming tools. No prior controller had demonstrated biomimetic assistance for such a wide variety of tasks without switching or adaptation between tasks. We assessed the muscular effort of multiple able-bodied human subjects with an experimental implementation of this task-invariant control method on a knee-ankle exoskeleton (Comex 1) to assist the primary activities of daily life (detailed below).

3.3 Human Subject Methods: Study 1

The following study was approved by the Institutional Review Board at the University of Michigan (HUM00164931). We enrolled five able-bodied human subjects (s1, male, mass: 78 kg, height: 1.78 m; s2, male, mass: 75 kg, height: 1.75 m; s3, female, mass: 50 kg, height: 1.62 m; s4, male, mass: 83 kg, height: 1.79 m; s5, female, mass: 60 kg, height: 1.75 m) to demonstrate the controller's ability to assist multiple tasks. Two subjects (s4, s5) were excluded due to failure of a foot FSR causing unusual control torques, which was noticed after the experiment. The remaining subjects had substantial (s1), moderate (s2), or minimal (s3) experience with Comex 1. We assessed muscle activation via EMG (Delsys Inc.) of vastus medialis oblique (VMO), rectus femoris (RF), biceps femoris (BF), tibialis anterior (TA), gastrocnemius (GM), and soleus (SOL), which function as a knee extensor, knee extensor/hip flexor, knee flexor, dorsiflexor, plantarflexor/knee flexor, and plantarflexor respectively.

The experiment comprised level treadmill walking at self-selected speed (1 m/s for s1-2, 0.8 m/s for s3), incline/decline treadmill walking on a $\pm 5.2^{\circ}$ slope at 0.6 m/s and a $\pm 12.4^{\circ}$ slope at 0.6 m/s, repetitive sit-stand cycles with a metronome set to 45 beats-per-minute (BPM), and stairs ascent/descent over 7 inch steps with a 60 BPM metronome. The tasks were repeated for three exoskeleton modes: bare (no exoskeleton), active exoskeleton with ϕ (PHI), and active exoskeleton

without ϕ (WOP). The level of assistance (LOA)% for the active modes was set to 60% for s1 and 50% for other subjects, based on their comfort level during practice trials. We collected at least 30 gait cycles for each treadmill task, 18 gait cycles for each stair task, and 18 sit-stand cycles. Subjects were instructed not to use the treadmill handrails except to prevent a fall (which never occurred).

The walking trials were cropped into gait cycles by detecting heelstrike with a heel-mounted accelerometer. Sit-stand-sit trials were cropped into individual repetitions using a thigh-mounted accelerometer built into the EMG sensor. Each muscle's EMG was demeaned, bandpass filtered (20 - 200 Hz), smoothed with a moving 100 ms window RMS, and then normalized with respect to the maximum peak of the ensemble averages (across repetitions) of the three exoskeleton modes [Yang and Winter, 1984]. This was done for each task and muscle separately, resulting in the signals being converted to a percentage of the maximum voluntary contraction level (%MVC) for a consistent and fair comparison across subjects. After normalizing the EMG to % MVC, the integral with respect to time was calculated to represent muscular effort as % MVC.s, similar to [Divekar et al., 2020] presented in chapter 2.

We performed intra-subject statistics on the EMG effort data. Since these data were not normally distributed according to the Shapiro Wilk test for normality, we applied non-parametric tests for checking the statistical significance of the effect of controller mode on EMG effort for each subject, similar to [Kumar et al., 2020]. We first used the Friedman's test to check the null hypothesis that muscle effort data corresponding to the three modes came from the same population. When the null hypothesis was rejected ($\alpha = 0.05$), we performed post-hoc pairwise comparisons between modes using the Wilcoxon signed-rank test with the null hypothesis that no median difference existed between EMG effort from different modes.

For comparing controller torques during the experimental trials to torques from the normative datasets [Camargo et al., 2021; Laschowski et al., 2021], we used two metrics. The first metric used was a Cosine Similarity (SIM), which is a judgment of orientation that measures the pattern of the normalized able-bodied torques. The second metric used was the Variance Accounted For (VAF) which measures the variability of the data that can be explained by a fitted regression model. The definitions are

$$\begin{aligned}
\mathrm{SIM}(A,B) &= \frac{100 \cdot A \cdot B}{\|A\|_2 \|B\|_2}, \\
\mathrm{VAF}(A,B) &= 100\left(1 - \frac{\mathrm{variance}(A-B)}{\mathrm{variance}(A)}\right).
\end{aligned}$$

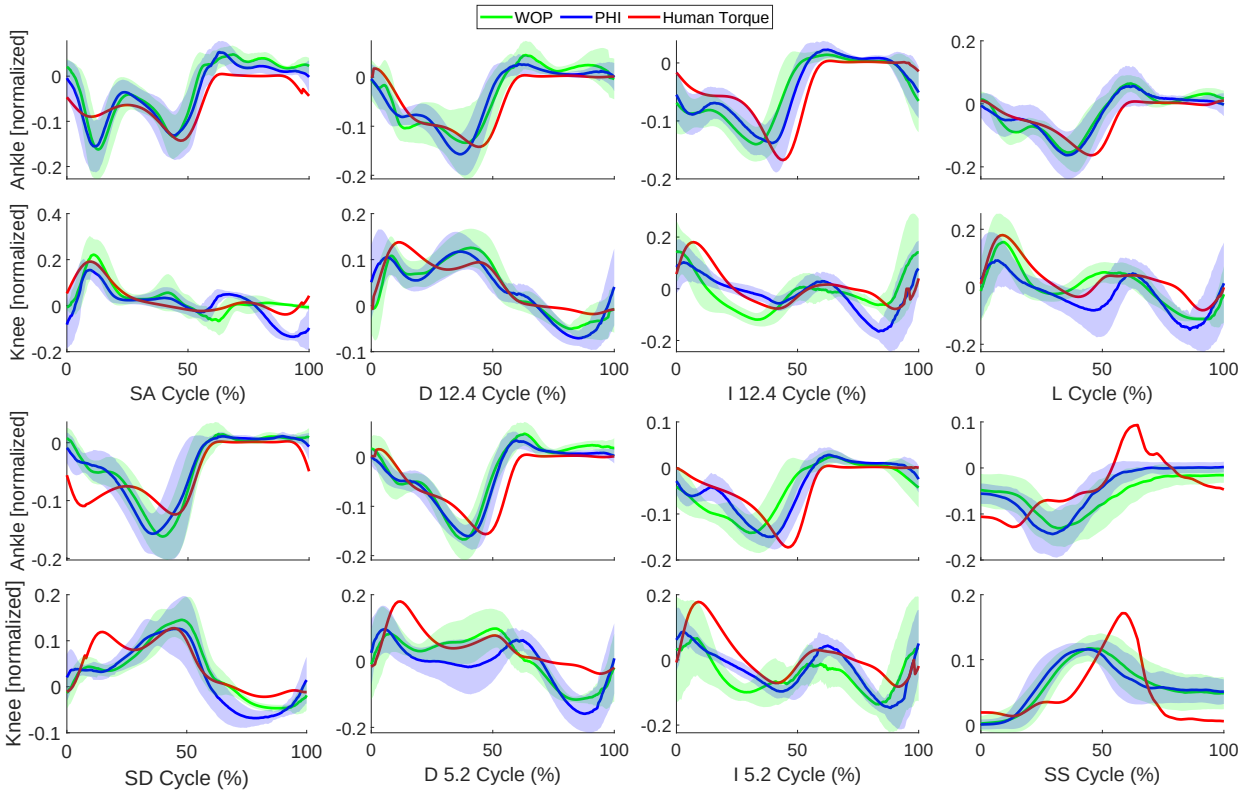

Figure 3.1: Comparisons of across-subject averaged normalized command torques (PHI and WOP methods) and normalized able-bodied human torques for experiment tasks {stair ascent/descent (7inch), decline $(-5.2^\circ, -12.4^\circ)$ and incline $(5.2^\circ, 12.4^\circ)$, level ground (1 m/s), stand-to-sit}. The blue solid (PHI method) and green solid (WOP method) lines represent the mean commanded exoskeleton torque (normalized by L2 norm) across all repetitions for the active modes. The red solid line represents the normative human joint torques (normalized by L2 norm) in [Camargo et al., 2021; Laschowski et al., 2021]. Positive torques represent ankle dorsiflexion and knee extension.

3.4 Human Subject Results: Study 1

Fig. 3.1 shows that, even in the experiment with subject kinematics being influenced by the exoskeleton's mass and joint torque, the averaged command torques (PHI and WOP methods) match with the normalized able-bodied human torques from [Camargo et al., 2021; Laschowski et al., 2021] in most tasks with SIM $= 81.6 \pm 6.5\%$, VAF $= 60.4 \pm 16.3\%$ for PHI; and SIM $= 80.1 \pm 9.0\%$, VAF $= 50.8 \pm 19.2\%$ for WOP, where torque trajectories are normalized to the L2 norm and standard deviations are given over tasks.

The ensemble-averaged VMO, RF, BF, TA, GM, and SOL EMGs for bare and active modes are shown in Fig. 3.2 for s1, who was the best responding subject to exoskeleton assistance. In general the task-specific dominant muscles (for the stance phase) had reduced effort and peak EMG for

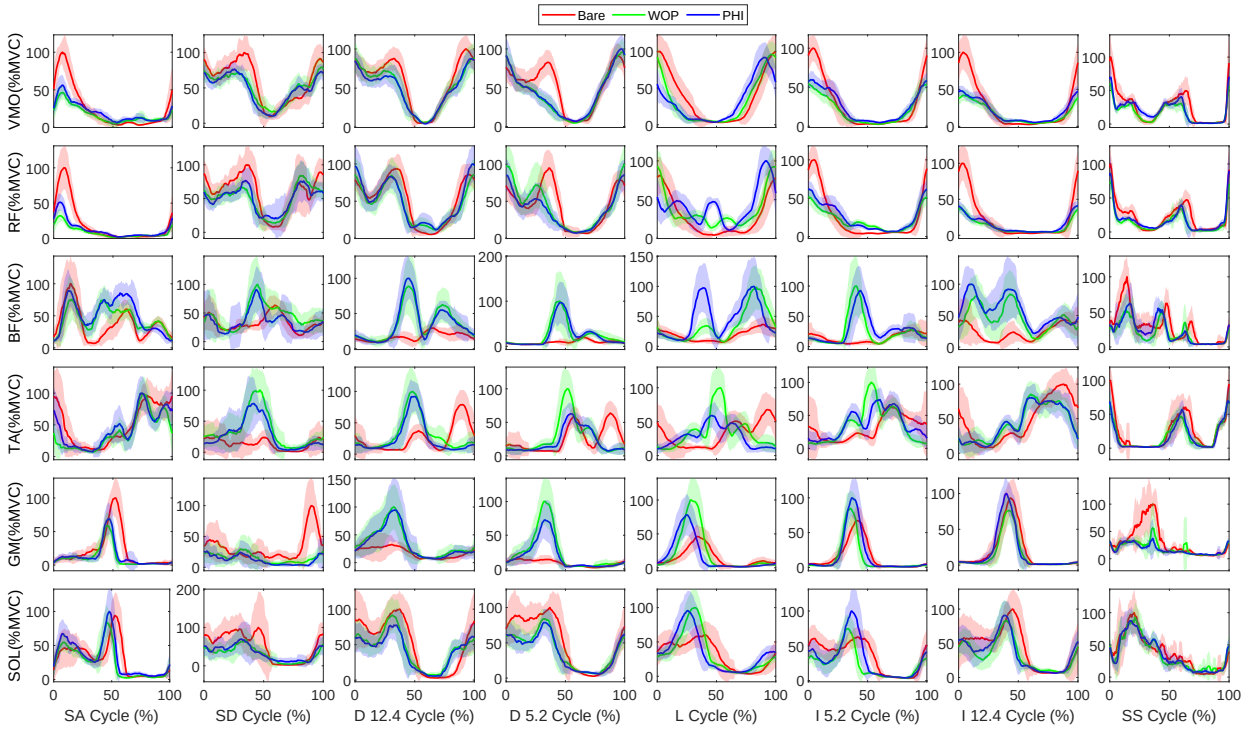

Figure 3.2: Subject 1 EMG comparisons between bare and active modes (PHI and WOP methods) for each muscle (VMO, RF, BF, TA, GM and SOL) and task {Stairs Ascent/Descent (7in step height), Decline $(-5.2°, -12.4°)$ at 0.6 m/s, level ground (1 m/s), Incline $(5.2°, 12.4°)$ at 0.6 m/s, and Sit-Stand cycle (45 BPM)}. The red solid (bare), blue solid (PHI method), and green solid (WOP method) lines represent the time-normalized ensemble averages across all repetitions.

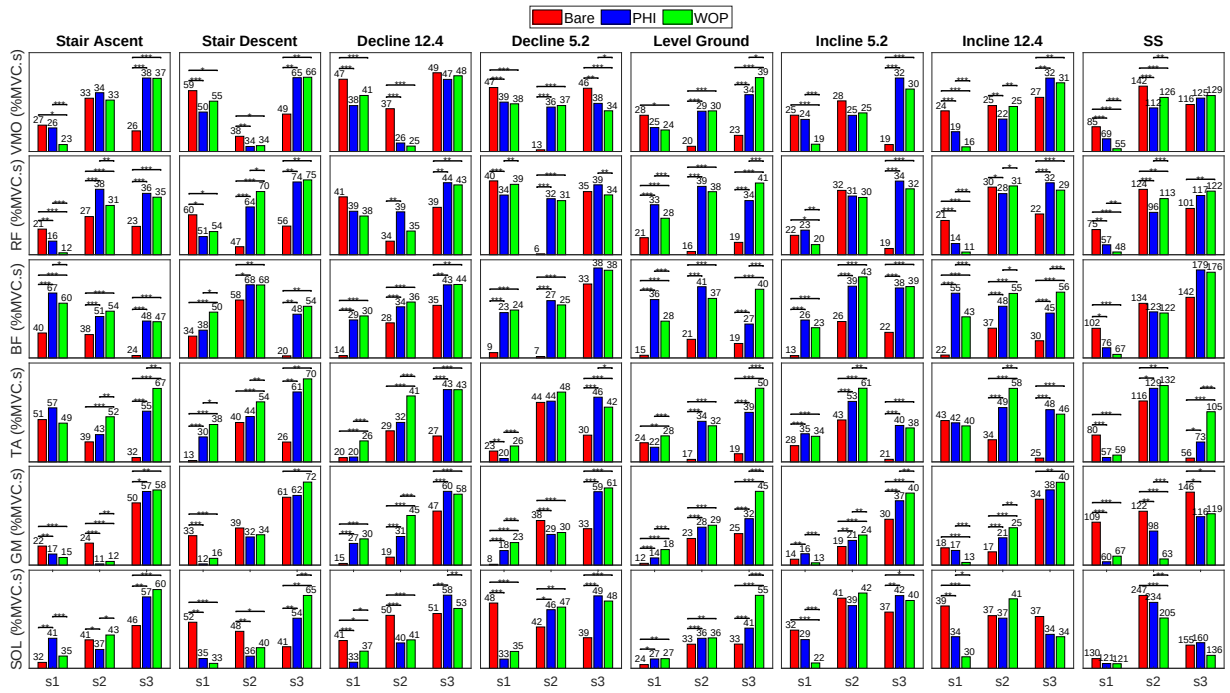

Figure 3.3: Individual subject comparisons of mean effort across repetitions. Effort is compared between bare, active with PHI method, and active with WOP method for each muscle pair (VMO, RF, BF, TA, GM and SOL) and task {Stairs Ascent/Descent (7in step height), Decline ($-5.2°, -12.4°$) at 0.6 m/s, level ground (1 m/s for s1 and s2, 0.8 m/s for s3), Incline ($5.2°, 12.4°$) at 0.6 m/s, and Sit-Stand cycle (45 BPM)}. * represents statistical difference ($p < 0.05$). ** represents $p <= 0.01$. *** represents $p <= 0.001$.

the active modes in most tasks—VMO, GM, and SOL for treadmill and stairs tasks, and VMO for sit-stand. Fig. 3.3 quantifies this trend for EMG effort and provides intra-subject statistics for the various muscles and tasks.

3.5 Synopsis: Study 2

This study introduced and validated an improved, modular version of the optimized energy-shaping controller framework developed in study 1 above to cater to the different configurations of *M-BLUE* and other exoskeleton designs. First, we introduced a general-purpose, modular, convex-optimization-based framework for multi-task optimized energy shaping (*M-TOES*). This framework extended our previous optimization framework (in study 1) by adding certain key features of modular energy bases, convex penalties on incorrect torque sign, and unification of stance and swing controllers by use of the vertical GRF. Second, we rigorously analyzed the behavior of the target energy resulting from these controllers, including all possible power leaks due to practical relaxations of the matching conditions (criteria that determine the allowable kinematic inputs to the basis functions) and passivity. Third, we empirically validated the stability, modularity, and task-invariance of the resulting controllers with $N = 8$ able-bodied participants performing the primary activities of daily life with four different configurations of the *M-BLUE* system: unilateral hip, bilateral hip, unilateral knee, and bilateral knee. For each modular configuration of the device, the *M-TOES* controller is optimized across multiple tasks (including multi-speed walking, ramps, stairs, start-stop, and sit-to-stand tasks) from able-bodied datasets [Camargo et al., 2021; Laschowski et al., 2021]. The human subject experiments are detailed below.

3.6 Human Subject Methods: Study 2

In study 2, the *M-TOES* controller was generalized for different joint modules, and implemented on the *M-BLUE* exoskeleton system. The experimental methods for validating different configurations with healthy human subjects performing multiple ADLs are presented next.

3.6.1 Hardware Implementation: Study 2

The controller was implemented on *M-BLUE* shown in Fig. 3.4 (see [Nesler et al., 2022] for details). The unilateral knee and hip modules weigh 2.36 kg and 2.15 kg, respectively, including the battery. *M-BLUE* combines commercial off-the-shelf orthoses with a quasi-direct drive actuator—the T-motor AK80-9 which comprises a high-torque electric motor with an internal 9:1 planetary gearbox. This actuator is highly backdrivable with less than 0.5 Nm static backdrive torque. It can

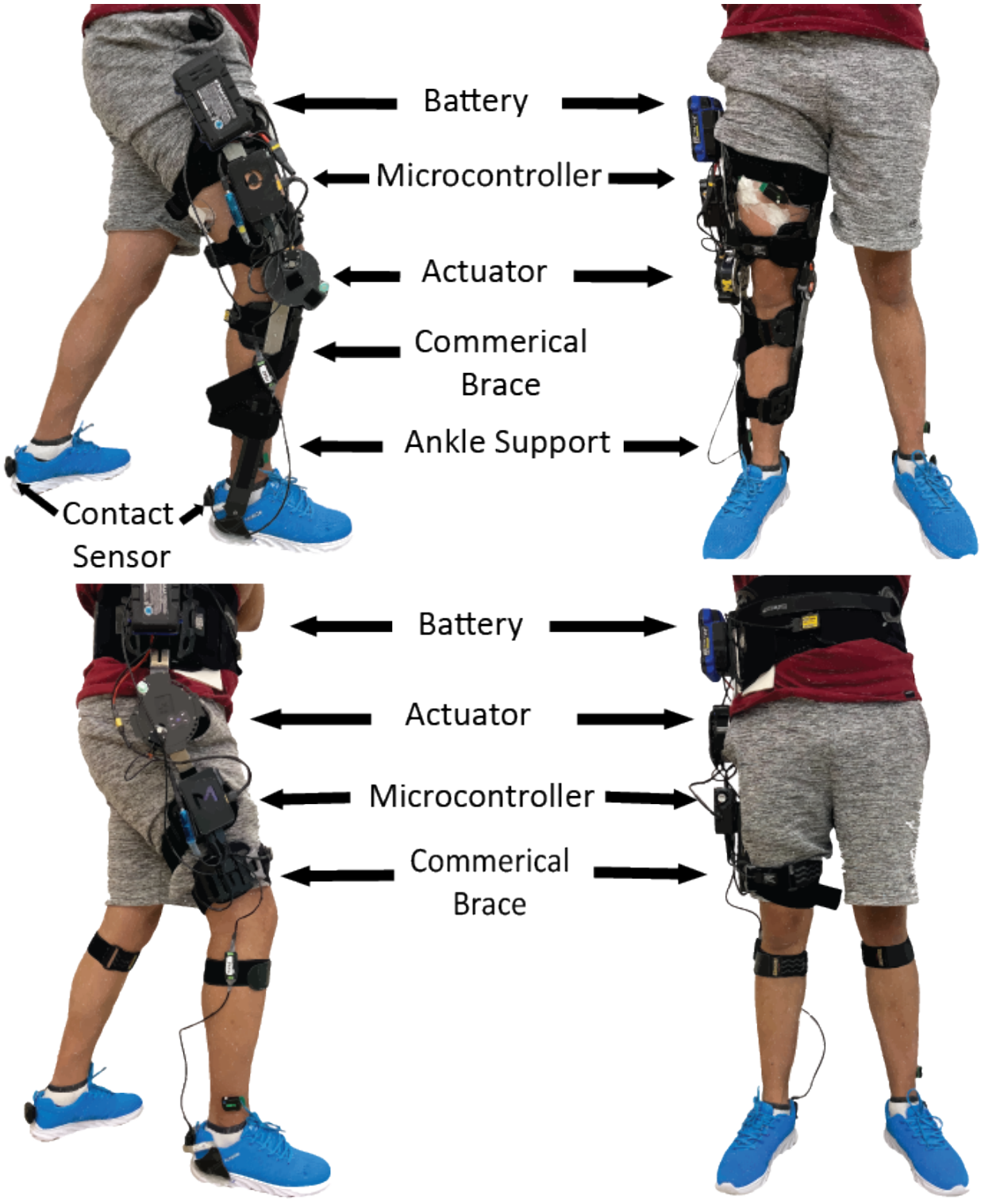

Figure 3.4: *M-BLUE* hip-only and knee-only exoskeleton configurations worn by a healthy user (with an unpowered ankle brace in the knee-only configuration to support the mass of the knee actuator).

provide 9 Nm continuous torque and 18 Nm peak torque according to the manufacturer, though we verified up to 30 Nm peak torque using the Dephy FASTER ActPack driver in our own bench-top calibration [Nesler et al., 2022]. This modular exoskeleton facilitates bilateral/unilateral knee and/or hip configurations to match different use cases.

The high-level control loop ran at $\sim$ 200 Hz on an 8 GB RAM Raspberry Pi 4B for each leg, where bilateral configurations communicated with each other through ZeroMQ, a TCP based package. Sagittal-plane joint angles and global segment angles were measured by two 6-axis Microstrain IMUs attached to the brace straps around each limb segment. The joint angles were obtained by taking the difference between the global angles of adjacent segments, which mostly bypassed the compliance between the actuator and limb segment to give more accurate joint measurements than the actuator encoders. In fact, soft-tissue and strap compliance caused vibrations when using the joint encoders, which was avoided by using the IMU-based joint measurements. *M-BLUE* was powered by a 24 V, 2 Amp-hour Kobalt powertool battery ($\sim$ 470 g) attached to a 3D printed adapter mounted on the side of each orthosis.

The vGRF was measured by a commercial footwear sensor (IEE Smart Footwear) placed underneath the shoe insole. Similar to zero-order hold, a parallel thread was created to read vGRF continuously at $\sim$ 55 Hz, which gave the latest vGRF every 0.02 s and avoided slowing down the main control loop at 200 Hz. The sensor was calibrated using a predefined calibration procedure before each use to achieve a final readout normalized to body weight in the same manner as the vGRFs from the normative dataset used for the controller simulation. An infinite impulse response (IIR) second-order low-pass filter (50 Hz cutoff frequency) was applied to the vGRF for noise reduction purposes.

Safety features such as mechanical hard stops, thermal protectors, software program interventions, and current limiters were present at all joints. We also implemented a motor current limiting policy to prevent overheating the motor windings.

3.6.2 Experimental Protocol: Study 2

The study was approved by the Institutional Review Board at the University of Michigan (HUM00164931). We enrolled eight able-bodied (AB) human subjects (see Table 3.1) to demonstrate the ability of *M-BLUE* with *M-TOES* to assist multiple tasks. We assessed muscle activation via wireless EMG (Delsys Inc.) of vastus medialis oblique (VMO), rectus femoris (RF), biceps femoris (BF), and gluteus maximus (GLUT), which function as a knee extensor, knee extensor/hip flexor, knee flexor, hip extensor, respectively. We used low-profile neonatal sensors for VMO, RF, and BF.

Participants performed the same activities of daily life (ADLs) with five exoskeleton conditions: bare (no exoskeleton), active bilateral hip exoskeleton (HipB), active unilateral hip ex-

Table 3.1: Subject Demographics

Subject	AB01	AB02	AB03	AB04	AB05	AB06	AB07	AB08
Sex	M	M	F	M	F	M	F	F
Mass (kg)	80	80	60	88	63	70	55	58

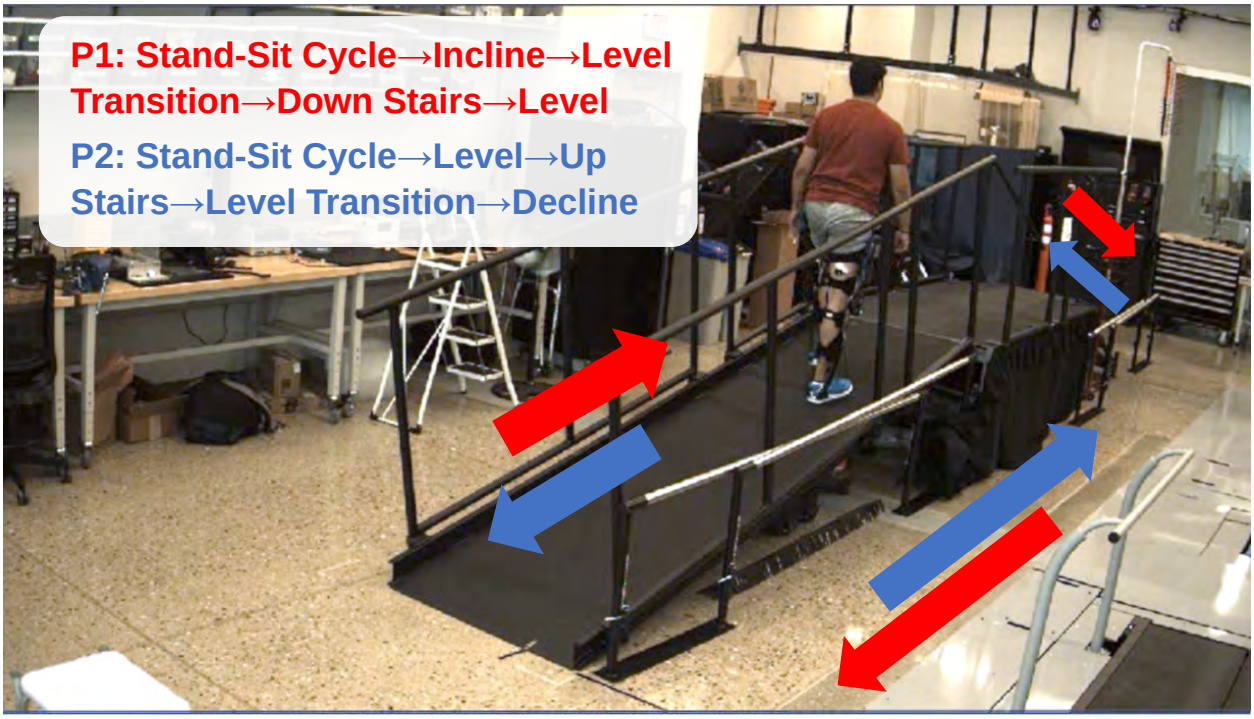

Figure 3.5: AB01 with bilateral knee *M-BLUE* walked on a circuit. One trial consists of Part 1 (P1) and Part 2 (P2).

oskeleton (HipU), active bilateral knee exoskeleton (KneeB), and active unilateral knee exoskeleton (KneeU). The LOA% for the active modes was set based on the subjects' comfort level during practice trials and fixed for the entire experiment. Each trial comprised two parts of an ADL circuit at a self-selected speed, as shown in Fig. 3.5. Part 1 (P1) includes five sections: stand-sit cycle (SS), followed by incline walking (II, 12°), level walking on the platform, stair descent (SD, 6 inch), and level walking (LL) over ground. Part 2 (P2) reverses the direction and also includes five sections: stand-sit cycle, followed by level walking over ground, stair ascent (SA, 6 inch), level walking on the platform, and decline walking (DD, 12°). All incline/decline and upstairs/downstairs sections started with the right foot contacting the ramp/stairs first to get the maximum number of strides for the right leg (not required for level walking). We collected 5 trial repetitions for each exoskeleton condition, providing a minimum of 20 gait cycles of level walking, 10 gait cycles per stairs task, 10 gait cycles per ramp task, and 10 stand-sit cycles. At least five minutes of acclimation time was provided for each exoskeleton condition, and a five minute break was provided between conditions. Subjects were instructed not to use the handrails except to prevent a fall.

The walking trials were separated into different tasks using a stopwatch and VICON video, and cropped into gait cycles by detecting heelstrike with a heel-mounted accelerometer. Stand-sit cycles were cropped into individual repetitions using a thigh-mounted accelerometer built into the EMG sensor. Each muscle's EMG was demeaned, bandpass filtered (20 - 200 Hz), smoothed with a moving 100 ms window RMS, and then normalized with respect to the maximum peak of the ensemble averages (across repetitions) of all the active modes [Yang and Winter, 1984]. This was done for each task and muscle separately, resulting in the signals being converted to a percentage of the maximum voluntary contraction level (%MVC) for consistent comparison across subjects.

3.6.3 Statistical Analysis: Study 2

The subject-wise muscular efforts analysis involved a linear mixed model (LMM) in MATLAB with restricted maximum likelihood estimation of parameters. Data from eight subjects were tabulated with information consisting of muscle effort change, exoskeleton condition (Bare, HipB, HipU, KneeB, KneeU), weight, LOA, and gender. We quantified muscular effort (%MVC.s) by integrating normalized EMG over time from the beginning to the end of five repeat trials for each exoskeleton condition [Divekar et al., 2020]. We subtracted the %MVC.s of active conditions by the %MVC.s of the bare condition to determine the effort change. We defined exoskeleton conditions as categorical variables and fit a LMM, where the condition, weight, LOA, and gender are

fixed effects:

$$\begin{aligned}\text{Effort Change} \sim \text{Controller} + \text{Weight} + \text{Gender} \\ + (1|\text{Muscle}) + (1|\text{Task}) + (1|\text{Subject}),\end{aligned}$$

where $(1|\cdot)$ represents random effects. Statistical significance of each fixed effect parameter was determined by a two-tailed t-test. As a secondary analysis, a LMM without the random effects of task and muscle,

$$\begin{aligned}\text{Effort Change} \sim \text{Controller} + \text{Weight} + \text{Gender} \\ + (1|\text{Subject}),\end{aligned}$$

was applied to each muscle and task separately.

3.7 Experimental Results: Study 2

This section presents the experimental outcomes of our study on the eight able-bodied participants. The bilateral knee condition of participants AB02 and AB03 were excluded due to a failure in the synchronization between the left and right Raspberry Pi units. Moreover, the BF muscle's EMG data for participant AB04 were excluded because of a sensor failure, which was detected after the completion of the experiment.

Both of the unilateral configurations (KneeU and HipU) significantly reduced the muscular effort required to complete the ADL circuit, with statistically significant fixed effects in our primary LMM ($p < 0.001$, Fig. 3.6). The HipU configuration reduced effort by an average of 2.71 %MVC.s, 95% CI [1.16, 4.27], and the KneeU configuration by 3.40 %MVC.s, 95% CI [1.85, 4.95]. There was also a significant gender effect, a penalty of 3.00 %MVC.s, 95% CI $[0.46, 5.55]$ for women in all exoskeleton–bare comparisons ($p = 0.021$). This penalty is comparable in magnitude to the benefits from the unilateral controllers. Thus, there was only a net benefit for male subjects. A correlation was observed between weight and muscular effort, leading to an average reduction of $0.02 \cdot \text{mass}$ %MVC.s, 95% CI $[-0.02, 0.06]$. However, this correlation was not statistically significant, indicating that gender and weight were distinct effects.

The two bilateral configurations (KneeB and HipB) had a statistically null effect on muscular effort ($p > 0.05$). Considering the gender effect, this amounts to a net penalty for women. No significant effect was found for subject mass ($p > 0.05$).

The across-subject muscle activation results for each task, configuration, and muscle offer a very detailed analysis of the controller's effect (Table 3.2). Muscle effort comparisons were made

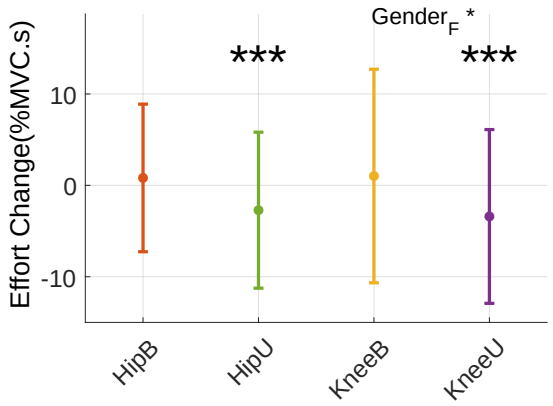

Figure 3.6: Across-subject comparisons of total muscle effort during five repetitions. Muscle effort is compared between the bare mode and different exoskeleton configurations for combined muscles. A positive value represents the total muscle effort increment with respect to the bare mode. * represents statistical difference ($p < 0.05$), ** represents $p <= 0.01$, *** represents $p <= 0.001$.

between the bare mode and various exoskeleton configurations, where a positive value represents each muscle pair's effort increment (%MVC) with respect to the bare mode. These results can be interpreted through the measured control torques and ensemble-averaged VMO, RF, BF, and GLUT EMGs for subject AB01 in Fig. 3.7 and Fig. 3.8.

3.8 Discussion

The results of study 1 are promising but are subject and task specific. Subject 1 exhibited more holistic muscular benefits in most tasks, with minimal muscle-task combinations in which the exoskeleton proved to be a hindrance. Comparatively, subject 2 and subject 3 exhibit no pattern in benefits or hindrances across muscles or tasks. Study 2 is larger (n=8) and allows the assessment of results via more powerful group statistics, rather than having to perform individual assessments like in study 1. Furthermore, the MBLUE exoskeleton used in study 2 is much lighter (by a factor of 2) and seven times more backdrivable (24:1 gear ratio of Comex 1, vs. 9:1 gear ratio of MBLUE) than the Comex 1 exoskeleton used in study 1. However, study 2's results similarly show a lack of consistency in muscular effort reductions across muscles, tasks, and modular configurations. While the unilateral modules achieved significant reductions in muscular effort in males, the bilateral modules demonstrated a non-significant *increase*. I discuss some possible reasons behind the inconsistent results below.

Being data-driven, the M-TOES controllers tested in these studies produce stable torques, well matched to normative joint moments when normative kinematics are provided in feedback. How-

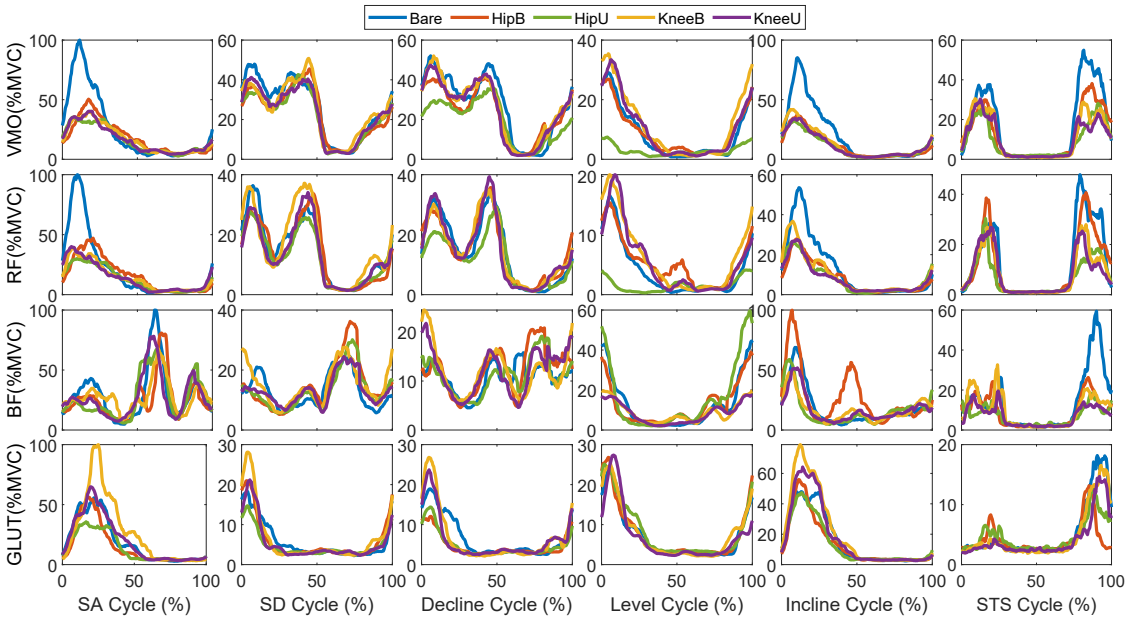

Figure 3.7: Subject 1 EMG comparisons between bare and different exoskeleton configurations for each muscle (VMO, RF, BF, and GLUT) and task {stair ascent/descent (6inch), decline/incline (12°), level ground, and sit-stand cycle}. Results are time-normalized ensemble averages across all repetitions.

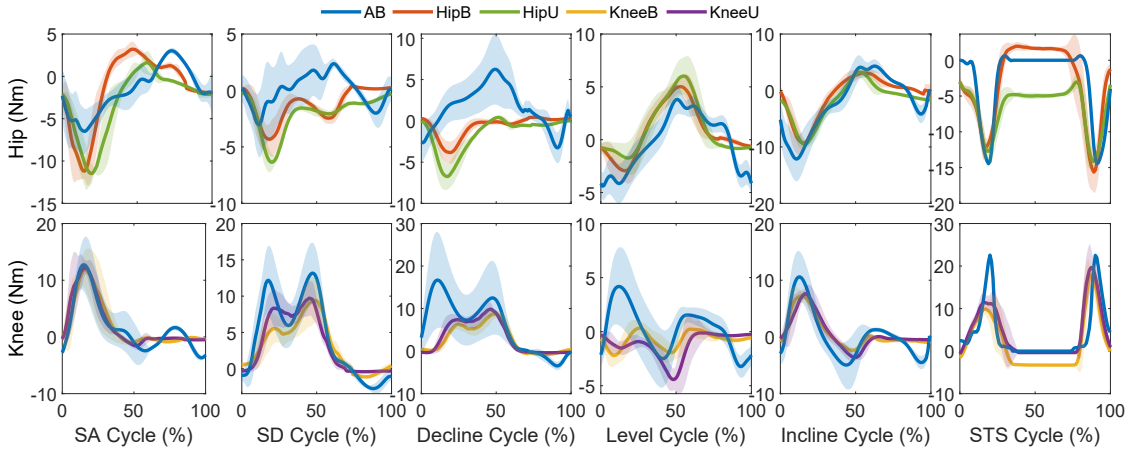

Figure 3.8: Subject 1 averaged normalized command torques for experiment tasks {stair ascent/descent (6inch), decline/incline (12°), level ground, stand-sit cycle}. The red (HipB), green (HipU), yellow (KneeB), and purple (KneeU) lines represent the mean commanded exoskeleton torque across all repetitions for the active modes. Normative AB human joint torques (blue lines) have been scaled by LOA% for better comparison. Positive torques represent hip flexion and knee extension.

Table 3.2: Across-subject comparisons of muscle effort change (mean ± standard deviation in %MVC.s) over different tasks, configurations, and muscles.

		SA	SD	DD	LL	II	SS
VMO	KneeB	-3.3(15.0)	0.2(10.8)	-2.0(8.9)	4.6(2.8) ***	-3.0(9.7)	-16.9(26.7)
	KneeU	-6.4(10.9)	-4.3(6.2)	-3.9(7)	2.1(2.3) *	-4.6(6.1)	-20.7(18.7) **
	HipB	1(6.1)	1.5(6.2)	2.4(4.8)	2.2(2.3) *	-0.1(7.0)	6.2(18)
	HipU	-3.4(6.5)	-3.58(3.4)	-1.1(4.7)	0.2(2.5)	-3.47(6.6)	-7.2(17.4)
RF	KneeB	-1.3(7.7)	2.8(6.4)	-1.8(4.1)	4.0(3.2) **	-1.6(5.9)	-16.6(10.2)
	KneeU	-6.4(6.0) *	-6.6(4.6) **	-5.3(3.7) ***	1.1(1.1)	-5.0(5.1) *	-18.9(9.9) **
	HipB	-2.0(5.4)	-2.5(4.9)	0.1(4.0)	1.5(2.5)	-1.4(4.4)	1.1(18.1)
	HipU	-4.7(9.1)	-5.4(3.7) *	-2.6(3.2)	0.2(2.4)	-2.4(4.35)	-1.5(25.5)
BF	KneeB	4.2(10.4)	6.7(5.5) **	0.2(4.7)	2.2(9.4)	1.1(12.0)	-5.8(10.8)
	KneeU	-0.5(9.4)	-0.2(5.1)	-1.1(3.6)	-1.9(4.8)	-6.0(8.1) *	-10.7(12.0) *
	HipB	1.5(7.1)	4.1(4.1) *	1.5(3.4)	1.4(2.4)	-1.4(10.6)	1.4(16.6)
	HipU	-1.5(8.4)	0.7(3.6)	-0.5(3.1)	1.0(1.5)	-7.6(7.0) *	-7.5(18.4)
GLUT	KneeB	17.7(7.5) ***	9.1(7.9) ***	3.8(3.5) **	5.4(3.7) **	10.2(5.5) ***	1.2(12.7)
	KneeU	3.2(6.5)	2.5(3.6)	1.4(2.3)	4.8(7.1) **	3.1(5.0)	-0.4(10.3)
	HipB	1.3(7.1)	0.5(3.7)	-0.8(2.6)	0.6(2.8)	0.4(7.3)	-2.1(13.7)
	HipU	-3.2(5.1)	-0.5(2.4)	-1.3(2.5)	-0.8(1.5)	-3.5(4.1)	-5.7(10.8)

A positive value represents the total muscle effort increment with respect to the bare mode. * represents statistical difference ($p < 0.05$), ** represents $p <= 0.01$, *** represents $p <= 0.001$.

ever, on conduction of initial pilot testing, we realized they are capable of producing unhelpful torques for edge case kinematics (i.e., kinematics that fall outside of the training dataset), likely due to over-fitting and use of hundreds of sinusoidal torque basis functions in the optimization (much like a Fourier series expansion). As an example: if a participant squatted lower than the deepest squat in the dataset, a torque sign flip occurred at the normative kinematic boundary. Thus, while the elaborate mathematical modeling and derivations guarantee stability (bounded torques), and passivity for continuous dynamics (bounded net energy injection by the exoskeleton provided no impact dynamics present), they cannot guarantee "assistance" especially for kinematics that fall outside the multi-dimensional volume of the training dataset (as in the case for the impaired populations). Nevertheless, these issues can be worked-around using saturation limits on the feedback kinematics to contain them within normative ranges—this was eventually implemented in the studies. However, this assistance scheme is also susceptible to slight offsets (errors) in the dataset.

Moreover, rather than differences in absolute amplitudes, humans seem highly sensitive to the % difference in exoskeleton torques vs. their own joint moments, particularly if the % difference is negative, i.e., the biological and exoskeleton torques are of opposite signs. This issue became apparent when our pilot subjects complained of hindrance in their late stance—where the subjects preferred a mild knee flexion torque, and the controller (as per the dataset) was providing a mild extension torque, inhibiting the free transition to early swing. The effect of this can be observed in the high BF activations with exoskeleton assistance in Fig. 3.2. In general, the process of fixing such small localized errors in torque magnitude (customization) is very cumbersome in the M-

TOES framework and sometimes ends up in a compromise in peak torque for the sake of subject comfort (Fig. 3.8).

Overall, while study 2 showed the potential benefits of the modular, and highly-backdrivable MBLUE exoskeleton by assisting in unilateral configurations, the M-TOES framework was not suitable for the application to LLC and impaired populations. LLC requires a bilateral knee configuration, for which the M-TOES could not assist in, and the unique requirements of impaired populations require a clinically intuitive controller that is easily customizable and robust to pathological kinematics that fall grossly outside the training dataset. These limitations paved the way for the novel controller I develop in the next chapter.

CHAPTER 4

Development of a Versatile, Clinically Intuitive and Easily Customizable Bilateral Knee Controller

The work in this chapter is under review for publication; authors: Nikhil Divekar, Gray Thomas, Avani Yerva, Hannah Frame, Robert Gregg.

4.1 Introduction

The behavior of a majority of controllers targeting "task-invariance" (including those developed in our prior work) is limited by and restricted to a normative dataset that informs their crucial data-driven optimization processes [Lin et al., 2022; Molinaro et al., 2022; Medrano et al., 2023]. In summary, the optimization aims to find optimal coefficients for a large set of torque basis functions (parameterized by normative kinematics and GRF) to achieve the corresponding normative torques (joint moments) in the dataset. This approach has a few drawbacks that may hinder the translation of excellent in-silico results to meaningful in-vivo benefits. The first is the problem of "over-fitting". When in-vivo kinematics fall outside of the training dataset, the resultant torque can deviate significantly from biomimetic behavior. Further, errors/offsets in the training dataset can manifest into unhelpful torques during in-vivo use. Moreover, correcting such localized undesirable behaviors may require setting manual "kinematic thresholds" on feedback signals and/or manually adjusting the dataset and re-optimizing across all tasks before re-validating the behavior in-vivo—overall a cumbersome cyclical process which may culminate in compromised assistance torque magnitudes at the critical phases of tasks.

The proceeding sections develop an intuitive physically inspired controller that is aimed to tackle these limitations. While I show the results of a data-driven optimization as a proof of concept of the multi-task torque tracking ability of the carefully chosen and curated torque basis functions, the controller is not by any means bound by these results. In fact, the optimization results only provide an initial starting point for the important basis function coefficients, enabling a second in-vivo optimization process that "fine-tunes" the controller as per the desired application. Therefore,

while the controller developed here was for multi-terrain lifting-lowering-carrying (LLC) tasks, it can be generalized to all common activities of daily living (ADLs) by making appropriate adjustments to the lifting-lowering spring to suit the sit-stand-sit task in the ADLs. Accordingly, this readily customizable controller was used for assisting LLC in chapter 5 and for assisting impaired individuals in chapter 6.

4.2 Controller design

The objective of our control law is to approximate the biological knee moment (torque) across common LLC tasks using kinematic and GRF feedback (Fig. 4.1). To make the controller stable and predictable, we take inspiration from the energy-shaping framework that our group previously used to design energetically passive controllers within the stance or swing phase [Lv et al., 2018]. This style of controller alters the dynamics of the user's legs in an assistive manner without time-based trajectories or explicit classification of locomotion type. A theoretical guarantee of passivity provides certainty that the total energy of the human user's leg remains under human control. However, such strict energetic passivity only allows energy injection when switching between stance and swing controllers, which precludes continuous energy injection throughout the stride. We therefore relax the passivity requirement in our controller design to permit both small continuous injections and large event-based injections of energy as in [Lin et al., 2022]. As an example of the former, we use a gravity compensation term at the knee that depends on the global angle of the shank during phases of underactuation [Lin et al., 2022]. As an example of the latter, a pre-loaded *ascent spring* activates when the foot touches down in order to propel the user up stairs or ramps, where the amount of energy injection is a predictable function of the initial knee flexion angle.

Unfortunately, the approach in [Lin et al., 2022] relies on data-driven optimization to choose dozens of unintuitive controller parameters, which are difficult to adjust for different use cases like LLC. To build an intuitive and customizable controller (depicted in Fig. 4.2), we begin with a short list of basic physical components that obey the assumptions of [Lin et al., 2022]. These components include springs, dampers, inertia compensation, and gravity compensation, and since each one maps from measurable quantities to torque, they can serve as basis functions to parameterize the control law. We then deviate from the energy shaping framework [Lin et al., 2022] by heuristically modulating these core torque bases into specialized task- and phase-specific behaviors. We obtain task-specific stance torque bases (e.g., ascent spring) that are suitable for specific task categories (e.g., incline walking), and general swing torque bases (e.g., modified gravity compensation) that are universally helpful in swing. A part of this specialization involves "phase sensitization"

by using a robust phase variable (the leg angle)—this, for example, suppresses the ascent spring in late stance where it would hinder the transition to swing.

Next, the process of "task sensitization" modulates the specialized stance torque basis functions to accommodate differences between activities and variations within activities. For example, the aforementioned ascent spring injects net positive energy only for incline or upstairs tasks (with higher energy injected for steeper inclines), and a non-ascent spring-damper absorbs energy only for decline, downstairs, and level walking tasks. Essentially, task sensitization involves scaling the specialized basis functions by smooth functions of task-sensitive signals (e.g., by the height differential between the two ankle joint centers at heel-strike is sensitive to terrain incline). Summing the task-sensitized stance basis functions gives the task-invariant stance torque function which is parameterized fully by kinematic and GRF feedback (similarly for the task-invariant swing torque function, Fig. 4.2). Finally, the convex combination of the task-invariant stance and swing torque functions (weighted based on GRF feedback) provides the final task-invariant knee torque. The next sections provide a detailed description of the controller and its data-driven and in-vivo optimizations.

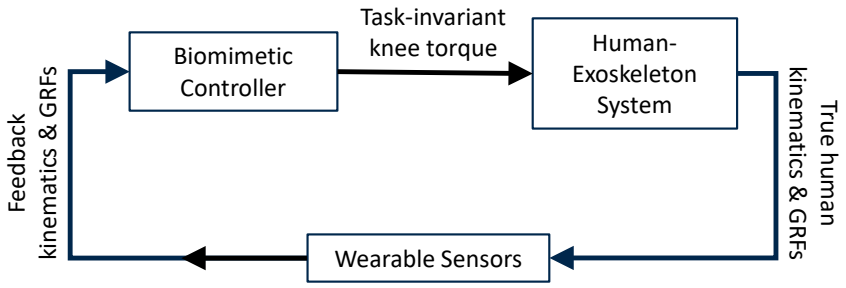

Figure 4.1: System diagram. Diagram shows biomimetic controller, human exo system and sensor feedback.

4.2.0.1 Biomimetic stance basis functions

For ramp/stairs ascent tasks, the knee primarily produces net positive work and is actively involved in driving the body through the gait in stance phase. The ascent spring was designed as a virtual unidirectional torsion spring located at the knee joint. This spring has a fixed neutral point at 0 degrees knee flexion, and is unlatched for hyperextension angles. This spring is virtually pre-loaded "free of cost" in the swing phase, and then injects energy at heelstrike depending on the amount of knee flexion at heelstrike. The ascent spring torque has the form

$$\tau_{\mathrm{a}} = k_{\mathrm{a}} \cdot \theta_{\mathrm{k}} \cdot \sigma(\theta_{\mathrm{la}}, m_{\theta_{\mathrm{la}}}, d_{\theta_{\mathrm{la}}}) \tag{4.1}$$

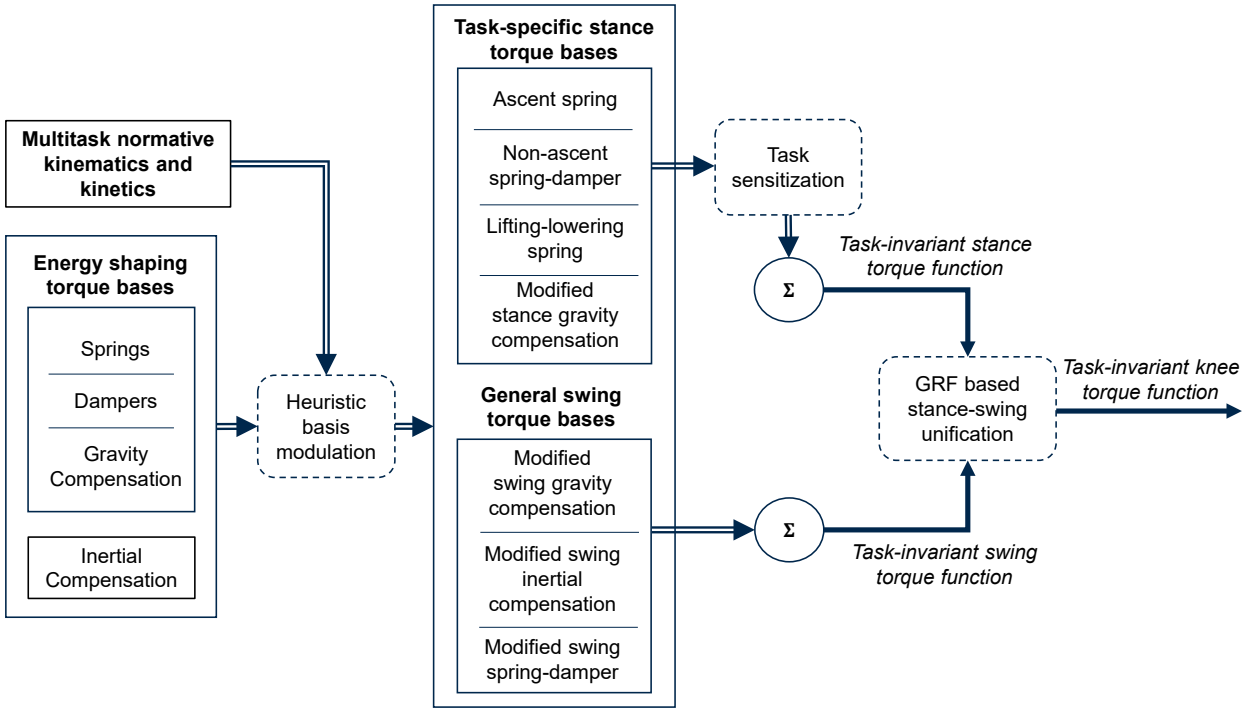

Figure 4.2: Control diagram. Diagram shows process of creating biomimetic functions using core energy shaping functions and modifying them heuristically. Solid arrows represent scalar functions, whereas double arrows represent sets of scalar functions.

where k_a is the ascent spring constant and θ_k is the knee angle. The sigmoid function σ is generally defined as

$$\sigma(\theta, m, d) = \frac{1}{1 + e^{-m \cdot (\theta + d)}}, \tag{4.2}$$

mapping θ from $(-\inf, \inf) \mapsto (0,1)$ given sigmoid slope m and offset d. In this case, θ_{la} is the so called "leg angle" [Villarreal and Gregg, 2014], i.e., the angle of the line between the hip joint center and the ankle joint center with respect to vertical. The sigmoid slope $m_{\theta_{\text{la}}}$ and offset $d_{\theta_{\text{la}}}$ were chosen such that the sigmoid function of the "leg angle" acts to inhibit the effect of the ascent spring in late stance.

For non-ascent tasks—level-walking, stairs descent, and ramp descent—the knee primarily produces net negative work and is involved in absorbing impact at heelstrike and subsequently lowering the body smoothly. The non-ascent spring is a virtual unidirectional torsion spring at the knee with a variable neutral point, which is set as the angle of the knee at heelstrike. The spring absorbs energy by loading itself along with the knee flexion after heelstrike. Since the spring is unidirectional, it does not apply any torque for knee flexion angles less than the angle at heelstrike. A special energy absorption limiting feature was added based on subject feedback, which acts

as a taper in torque for large knee flexion angles beyond the angle at heelstrike and allows for a smoother transition to mid-stance. This was implemented by allowing the virtual spring to undergo "plastic deformation", i.e., a decrease in stiffness for strains beyond the elastic limit. To provide damping for impact absorption, a unidirectional virtual damper was added parallel to the spring—the damper provides no resistance for knee extension velocities. The spring damper has the form

$$\tau_{\text{na}} = [K_{\text{na}}(\theta_{\text{k}_\text{d}}^{\max}) \cdot \theta_{\text{k}_\text{d}} + c_{\text{na}} \cdot \dot{\theta}_{\text{k}} \cdot \text{step}(\dot{\theta}_{\text{k}})] \cdot \text{step}(\theta_{\text{k}_\text{d}}) \cdot \sigma(\theta_{\text{la}}, m_{\theta_{\text{la}}}, d_{\theta_{\text{la}}}), \tag{4.3}$$

where $K_{\text{na}}(\theta_{\text{k}_\text{d}}^{\max})$ is the non-ascent spring stiffness function based on $\theta_{\text{k}_\text{d}}^{\max}$, the maximum knee flexion (spring deflection) angle achieved for the current gait cycle, where $\theta_{\text{k}_\text{d}} = \theta_{\text{k}} - \theta_{\text{k}_{\text{hs}}}$ for knee angle θ_{k} and its value at heel strike $\theta_{\text{k}_{\text{hs}}}$. In particular, $K_{\text{na}}(\theta_{\text{k}_\text{d}}^{\max}) = k_{\text{na}} \cdot \sigma(\theta_{\text{k}_\text{d}}^{\max}, m_{\text{na}}, d_{\text{na}})$ where k_{na} is the stiffness of the non-deformed non-ascent spring; the sigmoid function tapers this spring stiffness to emulate the plastic deformation process beyond the elastic region. Additionally, c_{na} is the damping coefficient for knee velocity $\dot{\theta}_{\text{k}}$. Unit step functions $\text{step}(\cdot)$ are used to make the spring and damper unidirectional so they only apply knee extension torques and only for knee flexion angles more than the spring neutral point ($\theta_{\text{k}_{\text{hs}}}$). Similarly to the ascent spring, the "leg angle" inhibits the activation of the non-ascent spring in late stance via the last sigmoid function.

At the core, the LL spring is a standard virtual torsion spring at the knee with a fixed neutral point of 0 degrees knee flexion. The spring stiffness is however tapered in a nonlinear fashion dependent on knee angular velocity and knee angle itself. At a high level, the spring was designed to become more compliant with higher magnitudes of knee flexion angular velocity, such that it minimally impedes the intentional lowering (knee flexion) portion of LL but also provides a strong boost for the intentional lifting (knee extension) portion. Further, we modified the angular velocity dependence by the depth of the squat, i.e., the amount of knee flexion angle. For deeper squats the spring stiffness is less sensitive to knee flexion angular velocity. This feature helped to provide a bracing effect at the bottom of the squat (a biomechanically compromised position) as the knee flexion velocity decreased. The LL spring has the form

$$\tau_{\text{LL}} = k_{\text{LL}} \cdot \theta_{\text{k}} \cdot \sigma(\dot{\theta}_{\text{k}}, m_{\text{LL}_1}, x_1 \cdot \sigma(\theta_{\text{k}}, m_{\text{LL}_2}, d_{\text{LL}}) + x_2) \cdot F_{\text{GRF}}^{\text{ipsi}} \tag{4.4}$$

where k_{LL} is the spring constant of the LL spring, x_1, $x_2 \in \mathbb{R}$ scale and shift the knee angle-modulating sigmoid respectively, and $F_{\text{GRF}}^{\text{ipsi}}$ is the GRF normal to the ipsilateral foot normalized by body weight.

The basis function for partial gravity compensation during stance has the form

$$\tau_{\text{grav}_{\text{st}}} = g_{\text{st}} \cdot \sin(\theta_{\text{th}}) \cdot F_{\text{GRF}}^{\text{ipsi}} \cdot \text{step}(\theta_{\text{th}}) \tag{4.5}$$

where g_{st} scales the magnitude of gravity compensation for stance, and θ_{th} is the global thigh segment angle. The unit step function restricts the torque to only flexion torques which were found to be helpful in propelling the body forward in late stance and allow a smooth transition to the flexion torque required for foot clearance in early swing.

4.2.0.2 Task sensitization

We scaled the task-specific stance torque bases by task functions, i.e., sigmoid functions parameterized by important "task variables" to make their amplitudes sensitive to the current task. To modulate the torque basis functions based on terrain incline (and implicitly distinguish between ascent and non-ascent tasks), we made use of the height (y-coordinate) of the ankle joint center (AJC) of the leading leg relative to the trailing leg's AJC at the latest heel-strike. We denote this task variable here as $\delta_{\text{AJC}_{\text{y}}}$. We assumed a subject height of 1.8 m with thigh and shank lengths of 0.468 m and 0.446 m, respectively. To modulate the gait vs. non-gait (LL) basis functions, we made use of four task variables: the distance between the AJCs of the two legs, i.e., $\delta_{\text{AJC}_{\text{dist}}}$, the GRF at the ipsilateral and contralateral heels normalized by body weight ($F_{\text{heel}}^{\text{ipsi}}$ and $F_{\text{heel}}^{\text{contra}}$), and the GRF at the contralateral foot denoted $F_{\text{GRF}}^{\text{contra}}$. Prior to operating on the torque basis functions, all task variables are transformed to a number in the range $[0, 1]$ by intuitively constructed sigmoid functions, such that they only work to scale down the torque of the torque basis functions they act on, and thereby preserve boundedness of torque. The modulated (task sensitive) stance basis functions are presented next.

The modulated LL torque basis is

$$\tau_{\text{LL}}^{\text{mod}} = \tau_{\text{LL}} \cdot \sigma(F_{\text{heel}}^{\text{ipsi}}, -m_{\text{F}}, d_{\text{F}}) \cdot \sigma(F_{\text{heel}}^{\text{contra}}, -m_{\text{F}}, d_{\text{F}}) \cdot \sigma(\delta_{\text{AJC}_{\text{dist}}}, m_{\text{AJC}_{\text{dist}}}, d_{\text{AJC}_{\text{dist}}}).$$

Note that our bipedal model is co-planar with a common hip joint center (HJC), such that zero distance between the two AJCs represents perfect symmetry of the bilateral joint configuration (assuming either knee cannot be hyper-extended). We assumed this case implies a squatting posture. We also assumed both heels will be in contact with the ground when squatting assistance is required as per the recommendation of "driving though the heels," although this assumption can be relaxed (via the modulating sigmoid) for users not able to keep their heels on the ground during squatting.

The modulated ascent spring torque basis is

$$\tau_{\mathrm{a}}^{\mathrm{mod}} = \tau_{\mathrm{a}} \cdot \sigma(\delta_{\mathrm{AJC_y}}, m_{\mathrm{AJC_y}}^{\mathrm{a}}, d_{\mathrm{AJC_y}}^{\mathrm{a}}) \cdot \sigma(\delta_{\mathrm{AJC_{dist}}}, -m_{\mathrm{AJC_{dist}}}, d_{\mathrm{AJC_{dist}}}).$$

The first sigmoid modulates the torque based on height of the leading leg's AJC relative to the trailing leg's AJC, both measured at the latest heelstrike to obtain a constant value throughout the gait cycle. This mimics a higher support torque and corresponding higher energy injection for climbing steeper inclines (stairs or ramps). The last sigmoid prevents activation of the ascent spring for symmetric (squatting) postures.

The modulated non-ascent spring torque basis is

$$\begin{aligned}\tau_{\mathrm{na}}^{\mathrm{mod}} = \; & \tau_{\mathrm{na}} \cdot \sigma(\delta_{\mathrm{AJC_y}}, m_{\mathrm{AJC_y}}^{\mathrm{na}}, d_{\mathrm{AJC_y}}^{\mathrm{na}}) \cdot \sigma(F_{\mathrm{heel}}^{\mathrm{contra}}, m_{\mathrm{F}}, d_{\mathrm{F}}) \cdot \\ & \sigma([\sigma(\delta_{\mathrm{AJC_{dist}}}, -m_{\mathrm{AJC_{dist}}}, d_{\mathrm{AJC_{dist}}}) + \sigma(F_{\mathrm{GRF}}^{\mathrm{contra}}, m_{\mathrm{F}}, d_{\mathrm{F}})], m_{\mathrm{sat_1}}, d_{\mathrm{sat_1}}).\end{aligned}$$

The first sigmoid serves a similar purpose as it does for the ascent spring with the difference being that energy is absorbed rather than injected in the first half of the stance cycle. The second sigmoid down-modulates the spring torque when significant weight transfer to the leading leg is unlikely, i.e., when the trailing heel is on the ground (contralateral heel GRF is high). The third sigmoid ensures the non-ascent spring remains inactive during LL (low AJC distance at latest heelstrike), but transitions to an active state as the contralateral foot is lifted off (low contralateral GRF)—this enables LL to carrying transitions.

The modulated stance gravity compensation torque basis is

$$\tau_{\mathrm{grav_{st}}}^{\mathrm{mod}} = \tau_{\mathrm{grav_{st}}} \cdot \sigma(\delta_{\mathrm{AJC_{dist}}}, -m_{\mathrm{AJC_{dist}}}, d_{\mathrm{AJC_{dist}}}) \cdot \sigma(F_{\mathrm{heel}}^{\mathrm{contra}}, m_{\mathrm{F}}, d_{\mathrm{F}}).$$

Both sigmoids ensure the gravity compensation sigmoid is not active during non-gait tasks (LL).

Finally the stance torque is simply the sum of the modulated basis functions, i.e.,

$$\tau_{\mathrm{st}} = \tau_{\mathrm{LL}}^{\mathrm{mod}} + \tau_{\mathrm{a}}^{\mathrm{mod}} + \tau_{\mathrm{na}}^{\mathrm{mod}} + \tau_{\mathrm{grav_{st}}}^{\mathrm{mod}}. \tag{4.6}$$

4.2.0.3 Swing basis functions

For the swing phase of the gait cycle, we provide angular velocity-modulated gravity compensation, inertial compensation, and a unidirectional virtual spring/damper for all tasks. The purpose

of the gravity compensation is to provide assistance to lift the shank in early swing for leg clearance. To prevent the gravity compensation from hindering the free pendular downswing in mid-swing, it is modulated by angular velocity. The angular velocity-modulated gravity compensation basis function has the form

$$\tau_{\text{grav}_{\text{sw}}} = g_{\text{sw}} \cdot \sin(\theta_{\text{sh}}) \cdot \sigma(\dot{\theta}_{\text{k}}, m_{\text{grav}_{\text{sw}}}, d_{\text{grav}_{\text{sw}}}), \tag{4.7}$$

where g_{sw} scales the magnitude of gravity compensation for swing, and θ_{sh} is the global shank angle.

The purpose of inertial compensation is to provide additional assistance to accelerate the shank forward in mid-swing. The inertial compensation basis function has the form

$$\tau_{\text{inertial}_{\text{sw}}} = a_{\text{sw}} \cdot [1 - e^{-x_3 \cdot \ddot{\theta}_{\text{k}}}] \cdot \text{step}(-\theta_{\text{sh}}) \cdot \text{step}(-\ddot{\theta}_{\text{k}}), \tag{4.8}$$

where a_{sw} is the maximum inertial compensation torque, x_3 modifies the sensitivity of the torque to knee angular acceleration $\ddot{\theta}_{\text{k}}$, and the step functions ensure the inertial compensation torque is zero for angular acceleration in flexion and for shank orientation anterior to vertical.

The virtual spring/damper prevents knee hyperextension and provides bracing at small knee flexion angles in late swing to mimic the flexion torque pulse seen in normative gait. The spring/damper has the form

$$\tau_{\text{sd}_{\text{sw}}} = [k_{\text{sw}} \cdot e^{\theta_{\text{k}} - \theta_{\text{k}}^{\text{eq}}} + c_{\text{sw}} \cdot \dot{\theta}_{\text{k}} \cdot \text{step} \cdot (\dot{\theta}_k)] \cdot \text{step}(\theta_{\text{k}} - \theta_{\text{k}}^{\text{eq}}), \tag{4.9}$$

where k_{sw} is the spring constant, $\theta_{\text{k}}^{\text{eq}}$ is the constant spring neutral angle, and c_{sw} is the damping coefficient. The step functions make the spring and damper unidirectional, such that they only apply knee flexion torques and only for knee flexion angles less than the spring neutral point.

The swing torque is simply the sum of the swing basis functions:

$$\tau_{\text{sw}} = \tau_{\text{grav}_{\text{sw}}} + \tau_{\text{inertial}_{\text{sw}}} + \tau_{\text{sd}_{\text{sw}}}. \tag{4.10}$$

4.2.0.4 Task-invariant knee torque function

The final control torque is a convex combination of the stance and swing torques parameterized by the ipsilateral GRF as follows:

$$u_{\text{controller}} = \alpha \cdot \tau_{\text{st}} + [1 - \alpha] \cdot \tau_{\text{sw}} \tag{4.11}$$

where $\alpha = \sigma(F_{\text{GRF}}^{\text{ipsi}}, m_{\text{GRF}_u}, d_{\text{GRF}_u})$. For comfort purposes, especially at heel-strike during ascent tasks, the rate of torque increase in the extension direction (slew rate) was limited to 200 $Nm \cdot s^{-1}$.

4.3 In-silico optimization results

The coefficients for the springs and dampers, gravity compensation gains, and slopes and offsets of important sigmoids were optimized within physically sensible bounds, using FMINCON in MATLAB to minimize the L2 norm of error between the corresponding control torques and normative human torques (scaled to provide 25% assistance for a 80 kg male subject of 1.8 m height) for multiple tasks: level walking at 0.5 $m \cdot s^{-1}$ and 1.5 $m \cdot s^{-1}$ (LW 0.5 and LW 1.5); incline (I 5.2, I 11) and decline (D 5.2, D 11) walking with two slopes 5.2° and 11°; stairs ascent (SA 4, SA 7) and descent (SD 4, SD 7) with two step heights 4 in and 7 in; and Lifting-lowering (LL) for a fast speed. Fig. 4.3 shows the fitting results, and Table 4.1 shows the variation accounted for percentage (VAF%) metric for assessing the fitting goodness for each task.

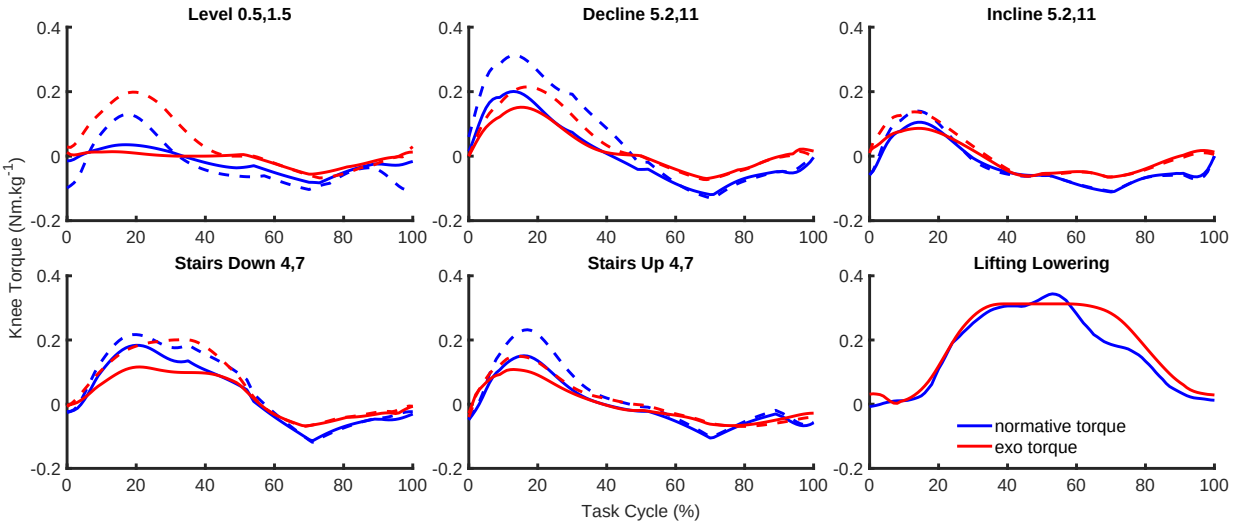

Figure 4.3: In-silico controller validation: normative vs optimized controller torques for multiple tasks. For each task, the red lines represent simulated controller torques given normative kinematic and GRF inputs, whereas the blue lines represent normative human torques from an able-bodied dataset [Camargo et al., 2021]. The dotted lines represent the faster or steeper tasks. The level walking task is optimized with two speeds (0.5 $m \cdot s^{-1}$ and 1.5 $m \cdot s^{-1}$). The incline and decline walking tasks are optimized with two slopes 5.2° and 11°. The stairs ascent and descent tasks are optimized at two step heights 4 in and 7 in. Lifting-lowering is optimized for a fast speed.

Table 4.1: VAF% between optimized control torques and normative torques for multiple tasks.

Task	**LW 0.5**	**LW 1.5**	**D 5.2**	**D 11**	**I 5.2**	**I 11**	**SD 4**	**SD 7**	**SA 4**	**SA 7**	**LL**
VAF (%)	67	77	86	83	84	91	88	95	89	87	94

4.4 Discussion

In this chapter we took a more fundamental controller development approach to overcome the limitations of prior task-invariant controllers. Mainly, the limitations were a lack of intuitive customization capability and although stable, no predictability on the helpfulness of torques for kinematics that fall grossly outside the normative dataset as for impaired individuals. We firstly studied the clinical gait analysis literature to gain both a qualitative and causal understanding of the high torque exhibiting regions of the knee joint torque profiles in the different categories of tasks encountered in LLC., e.g., ascent vs descent tasks, or gait vs non-gait tasks. This allowed us to carefully select a minimal set of physically inspired (inherently passive and predictable) torque basis functions (springs, dampers, gravity compensation, inertial compensation) and biomimetically modify them to produce the general torque profiles for each task category. By then scaling them with task and phase sensitive signals, such as the leg angle (a robust pseudo-phase variable), and the height differential between the leading vs. trailing ankle joint centers at heelstrike (sensitive to terrain incline), we ensured the torques are smoothly down-modulated in the low or negative torque phases of the respective task, and the entirety of other tasks. This process produced an intuitive and readily customizable "task-invariant" basis function set that was not strictly dependent on the outcome of a data-driven optimization process. Although we indeed performed a data-driven optimization (see Fig. 4.3) and achieved a good match with the normative torques (Table 4.1), the torque basis coefficients were not bound to its results allowing a second phase of in-vivo subjective feedback based manual optimization for LLC (in chapter 5) and impaired individuals (in chapter 6) to produce the most helpful and biomimetic torques in all tasks.

CHAPTER 5

A Backdrivable Knee Exoskeleton Mitigates Fatigue During Lifting, Lowering, and Carrying Over Terrains

The work in this chapter is under review for publication; authors: Nikhil Divekar, Gray Thomas, Avani Yerva, Hannah Frame, Robert Gregg.

5.1 Introduction

Fatigue is inevitable and detrimental in physically demanding jobs. According to the National Safety Council (USA), 69% of workers across the construction, manufacturing, transportation, and utility industries get fatigued, increasing the risk of injuries and incidents on the job [National Safety Council, 2018]. Fatigue causes a decrease in workers' cognitive and physical function (performance) in their assigned tasks [Zhang et al., 2015; Enoka and Duchateau, 2016]. This fatigue-induced performance decline becomes crucially deleterious (injurious) when there is a minimum performance level constraint imposed by factors outside the workers' control, e.g., rate of lifting and placing determined by the speed of a conveyor belt [CCOHS, 2019]. More than a million people in the USA suffered a non-fatal work-related musculoskeletal disorder in 2022 [BLS, 2022], most commonly low back pain (LBP) [Wami et al., 2019], costing employers millions of dollars every year in worker compensation [Bone and joint initiative USA, 2018]. Repeated lifting-lowering (LL) activities are highly associated with overexertion and LBP incidence [Wang et al., 2015], and significant research effort has been put into investigating the effect of LL techniques on LBP.

There are two common lifting techniques: stooping—lifting with the back and a flexed lumbar spine—and squatting—lifting with the legs while maintaining a neutral lumbar spine [Straker, 2003]. Compared to squat, the stoop technique consumes less energy [Welbergen et al., 1991] and is associated with less perceived lower-limb exertion and fatigue [Hagen and Harms-Ringdahl,

1994; Hagen et al., 1993]. On the other hand, the squat is associated with less lumbar shear forces and reduced lumbar passive tissue stress compared to stoop [Bazrgari et al., 2007; Potvin et al., 1991]. Further, the squat technique is favored over stooping by people who have previously incurred low back injuries [Damkot et al., 1984; Straker and Duncan, 2000]. This could be an instinctual self-protective choice that prioritizes the safety of the ligaments and discs of the lumbar spine, which are stressed during stooping, over the muscles of the lower limbs, which are stressed during squatting [Potvin et al., 1991; van der Have et al., 2019]. Moreover, the national workplace labor guidelines [NIOSH, 2007], military manual lifting guidelines [Marilyn Sharp et al., 2006; US ARMY, 2000], and physical therapists [Nolan et al., 2018] recommend the squat lifting technique to prevent LBP, especially for lifting weights that can be placed between the feet. Overall, squatting is often considered safer but is more energetically demanding and fatiguing on the lower limbs, especially the quadriceps.

Indeed a significant correlation exists between quadriceps muscle activation and the metabolic cost of squatting [Jeong et al., 2023]. Quadriceps fatigue has been shown to influence lifting technique, causing a transition from squatting to stooping as quadriceps fatigue progresses [Trafimow et al., 1993]. Consequently, high quadriceps fatigue is associated with higher effort of the lower back extensor muscles during repeated LL [Sasaki et al., 2008], which could increase the chance of overuse injuries. Quadriceps fatigue can also lead to a diminished capacity to handle perturbations while squatting [Ballantyne and Shields, 2010], and a loss of balance during lifting can result in unnatural, risky loads on the lower back. In addition to LL, quadriceps are critically involved in carrying tasks over stairs and ramps, which are demanding activities that further contribute to quadriceps fatigue and consequent balance loss [Givoni et al., 2007]. Fatigue could potentially be mitigated through the use of orthotic devices (i.e., exoskeletons) that assist the wearer during lifting-lowering-carrying (LLC) activities over multiple terrains, which has recently motivated a field of research and development [Ali et al., 2021].

The majority of orthoses developed for the purpose of mitigating LBP directly support the lumbar spine rather than the quadriceps [Theurel and Desbrosses, 2019; Kermavnar et al., 2021]. A low back belt or back support are basic examples of this intervention approach, but the National Institute for Occupational Safety and Health does not recommend back belts due to the lack of supportive evidence for their effectiveness [NIOSH, 2020; Azadinia et al., 2017]. More sophisticated passive hip-back orthoses [Bosch et al., 2016] reduce lumbar moments during forward bending tasks but hinder active hip flexion or lumbar flexion in walking [Baltrusch et al., 2019]. Newer commercial devices like HeroWear circumvent this issue with a clutch that allows manually disengaging the device when unrestricted lumbar flexion and/or hip flexion is desired [Goršič et al., 2021]. Powered (active) hip-back orthoses can modulate their assistance with software (i.e., the control strategy) rather than a mechanical clutch as the task changes [Koopman et al., 2019; Heo

et al., 2020]. However, designing a versatile control strategy is challenging: while LL was facilitated, walking was hindered by the active hip-back exoskeleton in [Poliero et al., 2020]. A subsequent study [Poliero et al., 2021] overcame this limitation but relied on explicit task classification and electromyography sensing which is cumbersome to setup and calibrate. Moreover, the lumbar (back only) and hip-back devices (passive and powered alike) do not directly support the quadriceps muscles that are critically involved in both squatting and load carrying. On the other hand, a powered ankle exoskeleton induced indirect reductions in quadriceps activation during squatting in [Kantharaju et al., 2022; Jeong et al., 2023]. These surprising findings were attributed to the closed-chain dynamics of squatting, where assistive torques at the ankle induced helpful reaction torques at the knee [Kim and Yoo, 2017]. However, this dynamics phenomenon cannot be leveraged for open-chain tasks like carrying. To most effectively assist the quadriceps in multi-terrain LLC, assistance torque needs to be *directly* applied to the knee via a *knee* orthosis/exoskeleton.

Knee orthoses must be highly versatile to handle the multi-terrain LLC that is performed in many work environments [NIOSH, 2007; Orr et al., 2021; Chung et al., 2005; Work Fit, 2023; HC Chung and MJJ Wang, 2001]. The knee joint kinetics and kinematics vastly vary between the various activities that fall under general LLC such as squatting, level walking, and stairs and ramp ascent and descent [Chan et al., 2022; Camargo et al., 2021]. Numerous knee orthoses, both passive and active, have been developed for various applications [Zhang et al., 2020]. State-of-the-art passive knee orthoses naturally fall short of the versatility required for the LLC application, as a fixed spring (even with an elaborate mechanical clutch) simply cannot recreate biomimetic assistance over a variety of tasks. Such devices have therefore been limited to supporting only squatting at best [Ranaweera et al., 2018; Hidayah et al., 2021]. Active knee orthoses on the other hand have the potential to provide versatile assistance for multi-terrain LLC. Traditionally, the development of active orthoses has favored rigid (highly geared) actuators that track predefined kinematics to assist severely impaired individuals [Zeilig et al., 2012; Harib et al., 2018]. However these orthoses are not suitable for the LLC application as the combination of rigid actuators and kinematic control hinders the voluntary motion of healthy individuals. The commercial pneumatic knee exoskeleton ROAM Forge, for example, needs to be manually turned off for dynamic gait (non-squatting) tasks since it impedes knee flexion during the swing phase [WIRED, 2021]. Only recently has there been a paradigm shift towards lightweight orthoses fitted with low-impedance (highly-backdrivable) actuators [Laschowski and McPhee, 2023], however their control strategies still lack the versatility to seamlessly support all tasks involved in multi-terrain LLC.

The overall goal of a partial assistance controller for an application like LLC is to use readily measurable signals (lower-limb segment and joint angles/velocities, foot pressure, etc.) to command a biomimetic assistance torque over a wide range of tasks. A direct approach is to use inverse dynamics to estimate joint torque from measured ground reaction forces (GRFs), but this has only

been successfully applied to the ankle [Gasparri et al., 2019]—the first major joint in the kinematic chain from the ground up. Dynamic modeling errors, sensor noise, and missing GRF components present significant issues for more proximal joints, which can instead be controlled via explicit representations of gait phase and task that parameterize a biomimetic torque model. Machine learning methods are commonly used to classify between distinct activity modes (e.g., for a hip exoskeleton in [Kang et al., 2022]), but this discretization of activities does not allow seamless adaptation to continuous variations in the environment or user behavior. A Kalman filter-based approach enabled biomimetic ankle torque adaptation based on continuous estimates of gait phase, ground incline, and walking speed [Medrano et al., 2023], but this approach did not consider stair or LL tasks. Using a combination of activity classification and user torque estimation via a dual Kalman filter, a hip-knee-ankle exoskeleton reduced quadriceps and plantar-flexor muscle activation during LL and walking [Sado et al., 2019]. However, this approach similarly lacked key activities like stairs and ramps and further did not test the efficacy of the exoskeleton in fatigued conditions. Recently, an implicit task representation was proposed to directly predict human hip torques using deep learning with a multi-activity able-bodied dataset [Molinaro et al., 2022]. Although promising results were achieved offline without the need for explicit task recognition, this black-box method does not provide formal safety guarantees, lacks a biomechanically intuitive means of customization for LLC tasks, and has not been generalized to more complicated joint kinetics like that of the knee.

Our group has investigated another implicit task representation based on the nonlinear control method of *energy shaping*, which alters the dynamics (potential forces, Coriolis forces, etc.) of the human-exoskeleton system in closed loop by applying joint torques as functions of the system states (joint and segment angles/velocities) [Lin et al., 2019, 2022]. The solutions to partial differential equations called the "matching conditions" determine the realizable alterations to the dynamics of an underactuated system, which can be used to define a set of admissible torque basis functions that parameterize the controller. Based on the spring-loaded inverted pendulum (SLIP) walking model, our early work [Lin et al., 2019] utilized a minimal basis set (including gravity compensation and virtual springs and dampers at the actuated joints) to provide assistive knee and ankle torques for incline, decline, and level walking. Though intuitive, this controller could only handle limited walking tasks, and the controller torque was not biomimetic especially in late stance. Our latest work [Lin et al., 2022] used a data-driven approach to find the optimal coefficients for a large set of torque bases to closely predict normative human torques [Camargo et al., 2021] given normative kinematic inputs over the primary activities of daily life. The drawbacks of this approach were: 1) a non-intuitive combination of hundreds of torque basis functions making manual controller customization for LLC very difficult, 2) susceptibility to "overfitting" resulting in unhelpful torques for input kinematics that grossly deviated from the training dataset, and 3) experimental results demonstrating inconsistent reductions in muscle effort across tasks.

In summary, a crucial gap exists in state-of-the-art exoskeletons for LLC, which involves repetitive, high-stress, and fatiguing tasks. Although effective assistance has been demonstrated for specific use cases such as *stooping*, no exoskeleton has thus far demonstrated versatile and effective assistance during multi-terrain LLC, including (but not limited to) the clinically recommended *squat* technique. These activities critically involve the quadriceps muscles, but assisting the knee joint over a wide range of activities presents significant challenges in actuation and control. This chapter addresses these challenges by implementing the novel energy-based control strategy developed in chapter 4 on a highly-backdrivable, bilateral knee exoskeleton (*M-BLUE*) to provide assistance and mitigate fatigue during multi-terrain LLC. Briefly, the implemented control strategy draws inspiration from 1) our prior work based on the SLIP model [Lin et al., 2019] and 2) fundamental concepts of clinical gait analysis to develop a biomechanically intuitive and minimal set of torque basis functions that holistically assist multi-terrain LLC. The quasi-direct drive actuators of the *M-BLUE* knee exoskeleton [Nesler et al., 2022] enables the controller to augment voluntary motion with meaningful torque assistance yet minimal backdrive torques. Experiments with eight healthy participants tested our hypothesis that aiding the quadriceps with this versatile knee exoskeleton would induce 1) performance benefits during repetitive LL when squatting posture is enforced in a highly-fatigued state, and 2) muscular benefits during multi-terrain LLC in a non-fatigued state. The results suggest this exoskeleton can be applied to mitigate quadriceps fatigue in real-world workplace conditions in which low back injuries tend to occur.

5.2 Materials and methods

5.2.1 Experimental Protocol

The controller was implemented on an improved, bilateral version of our M-BLUE knee exoskeleton module [Nesler et al., 2022] as shown in Fig. 5.1. Each module has a highly-backdrivable commercial actuator (T-Motor AK80-9), comprising a high-torque motor and an internal 9:1 planetary gearset. The motor is driven by the FASTER motor controller by Dephy, Inc with custom firmware to bypass the default thermal limits. We implemented a thermal model-based torque limiter that smoothly tapers the actuator torque based on estimated coil temperature, allowing short (1-2 s) bursts of much higher peak torques (limited to 25 Nm) than the default setting. We also implemented a ground reaction force sensor (IEE Sense) based on a matrix of force sensitive resistors (FSRs). Finally, we improved comfort and practicality by attaching the Raspberry Pi computation unit on-board, implemented waist-mounted "plug-and-play" power tool batteries for better familiarity with construction workers, and included a waist suspension strap to prevent exoskeleton slipping/sliding.

We sought to study the effects of the novel controller/exoskeleton on performance, posture, muscle activity, and user perception during assisted multi-terrain LLC in fatigued and non-fatigued conditions. The study was approved by the Institutional Review Board at the University of Michigan (HUM00164931). Eight (n=8) able-bodied healthy participants (4 males, 4 females, age 25 $\pm$ 1 years) who had prior knowledge and experience of the squat lifting technique completed this study. The experiment was divided into two sessions: 1) fatiguing session and 2) non-fatiguing session, which were completed on two separate days at least 1 week apart to provide adequate recovery time.

Before starting session 1 participants underwent exoskeleton acclimation for approximately 15 minutes in which they traversed the multi-terrain circuit until they felt comfortably attuned to the behavior of the exoskeleton. For the ascent tasks, the experimenter explained the intuitive concept of utilizing a pre-loaded spring (likened to a spring loaded toy car). For descent and level walking tasks, we explained the concept of a bracing knee spring that prevents knee buckling. Finally for the LL task, the concept of a velocity dependent torsion spring was explained by likening it to intent detection. For the lowering (negative work) portion, we explained that the knee spring will resist their downward motion less if it detects a stronger intention to lower (faster knee bending). For the lifting portion, since the direction of velocity and spring torque is the same, we explained the controller would feel similar to a conventional torsion spring.

After the acclimation with the exoskeleton, we acquired important gait parameters of each participant in the *bare* condition for each portion of the circuit except level walking. For ascent tasks (ramp and stairs) we acquired their maximum knee extension velocity in stance, and similarly for descent tasks we acquired their maximum knee flexion velocity in stance. For LL we acquired the maximum knee extension velocity of the lifting portion. These parameters later served as experimental controls in session 2.

5.2.1.1 Session 1 (fatiguing) protocol

The purpose of session 1 was to assess the effect of the exoskeleton on *post-fatigue* LL performance when enforcing the squat form, and to acquire a subjective assessment of its effectiveness on *post-fatigue* multi-terrain LLC. Accordingly, participants performed continuous squat LL repetitions with a 9 kg kettlebell until "failure" with no pausing allowed between repetitions. Participants were instructed to verbally declare failure when they felt they could no longer complete the next repetition with proper squat form without needing a pause. Declaring fatigue initiated a time trial of 10 fatigued LL repetitions in which participants were permitted to pause long enough after repetitions to complete the next repetition with perceived good squat form. The participants

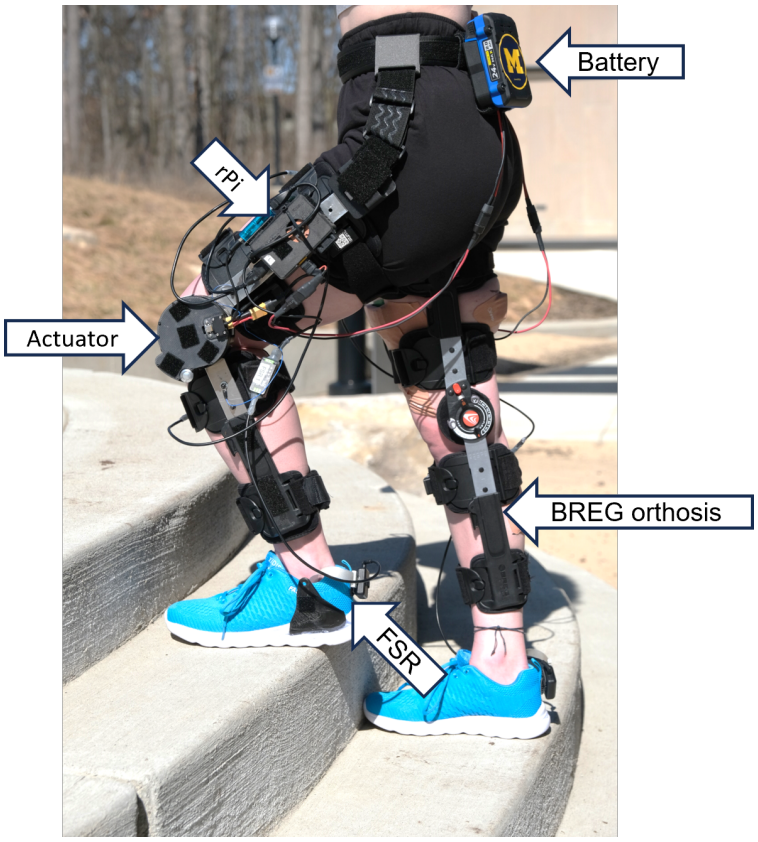

Figure 5.1: M-BLUE bilateral knee exoskeleton. Diagram shows the highly-backdrivable actuator (T-Motor AK80-9 with Dephy motor driver), Raspberry Pi for computation, 24V power tool battery, force sensitive resistor (FSR) system, retrofitted onto a commercial BREG knee brace.

were oblivious to the timed nature of the trial and were instructed to focus their attention on their posture. This process was repeated without the exoskeleton (bare) and with the exoskeleton. The order of conditions was alternated between participants, and a minimum break of 15 minutes (or longer if the participant desired) was enforced between conditions. For the exoskeleton condition, the fatiguing repetitions were performed with the exoskeleton in passive mode, for which the exoskeleton has an imperceptible $\sim$ 1 Nm backdrive torque for the joint accelerations encountered during LL [Nesler et al., 2022]. With the use of a wireless push button, the researcher changed the exoskeleton to active mode immediately after "fatigued" was declared by the participants, providing them with assistance during the post-fatigue repetitions.

Immediately after completing the 10 post-fatigue LL repetitions, the participants walked over a multi-terrain circuit while carrying the 9 kg mass. The circuit comprised a 3.7 m ramp inclined at 15°, a short level platform of 2 m, and a 5 step staircase with 18 cm step height. The circuit was traversed in a continuous, "freestyle" fashion in both directions and included a squat LL repetition on both ends of the circuit to emulate a workplace multi-terrain LLC scenario. Two roundtrip laps

of the circuit were completed for each condition. After completing the circuit with the second condition, participants rated the effectiveness of the exoskeleton assistance over the multi-terrain circuit by filling out a modified QUEST questionnaire (see Tab. 5.1 for the list of questions). The questionnaire gathered discretized ratings of 1-5 (not satisfied at all, not very satisfied, somewhat satisfied, quite satisfied, and very satisfied, respectively) for all steady-state portions of the circuit (ramp and stairs ascent/descent, level walking, LL). The participants only considered the effectiveness of the exoskeleton during the *post-fatigue* circuit traversal.

Table 5.1: Modified QUEST list of questions for participants

How satisfied were you with the device assistance during:
• Lifting and Lowering
• Ramp Ascent
• Stairs Ascent
• Ramp Descent
• Stairs Descent
• Level Walking

The table lists the questions asked in the modifed QUEST questionnaire. The assessment was to be given on a discretized scale of 1-5 (not satisfied at all, not very satisfied, somewhat satisfied, quite satisfied, and very satisfied respectively).

5.2.1.2 Session 2 (non-fatiguing) protocol

The purpose of this session was to assess the effect of the exoskeleton on quadriceps effort in six tasks (ramp ascent/descent, stairs ascent/descent, level walking, and squat LL) in a non-fatigued state. Accordingly, participants traversed each portion of the circuit (stairs ascent/descent, ramp ascent/descent, LL) and a 10 m level walkway multiple times until we collected at least 10 gait/task cycles for each task in which the corresponding maximum velocities in stance were within $\pm 10\%$ of their baseline values collected during acclimation. Since level walking is relatively more common and natural than the other tasks, we did not enforce a velocity constraint and instead asked participants to walk at their natural "self-selected" speed. The tasks were repeated with both bare and exo conditions, with the order of the conditions alternated between subsequent participants. For the stairs and ramp descent tasks, participants were reminded to carefully walk and lower themselves down, and *not* skip or hop down in order to emulate safe carrying etiquette. Since a variety of stair ascent styles exist: knee dominant (most common), hip dominant, ankle dominant, etc., it was plausible for newly acclimated participants to change their climbing style in response to the assistive knee torques, potentially confounding the EMG comparisons between conditions. We thus encouraged the participants to use the most common knee dominant style for both conditions

(during both acclimation and data collection trials), which turned out to be the natural style for all participants.

5.2.2 Data Collection

5.2.2.1 Post-fatigue LL performance

Post-fatigue LL performance was evaluated by the time to complete 10 LL repetitions after the participant exclaimed "fatigued." A LL repetition started with the participant standing in the upright posture without the weight, followed by lifting the weight from the ground attaining the upright standing posture, and lastly lowering the weight back to the ground, and standing upright once again without the weight. It was common for the participants to declare fatigue mid-way during a repetition, and therefore the time measurement was started from the instance the last fatiguing repetition was fully completed. Since pausing between repetitions was allowed in the 10 post-fatigued repetitions, most participants took a 2 -3 s pause right after declaring fatigue—this time was included in the time to complete metric. The time to complete analysis was performed offline using the sagittal plane 2D video recordings of the LL task.

5.2.2.2 Post-fatigue LL posture

Although squatting posture was an experimental control in session 1, we performed an exploratory analysis of lifting posture (peak thorax lean) to see if the exo helped participants maintain a better squat form. A Vicon motion capture system (Oxford Metrics, Oxford, UK) was used to collect three-dimensional marker trajectories for session 1's LL trials. Retro-reflective markers on the torso were placed at C7, T10, CLAV, and STRN to define the thorax segment [Vicon Motion Systems, 2023]. Three additional "backup" markers were placed on the shoulders and lower back to aid in post-process "gap filling". After appropriate data cleanup, gap filling, and filtering, we calculated the sagittal plane global thorax angle with respect to upright standing (zero degrees) [Vicon Motion Systems, 1997]. The peak global thorax angle was found for each post-fatigue lifting and lowering squat (20 post-fatigue squats total), and averaged across repetitions to get the thorax lean (stooping) angle for each subject and condition.

5.2.2.3 Multi-terrain Quadriceps Effort

In session 2, after appropriate skin preparation, we secured five electromyography (EMG) electrodes (Trigno Avanti and Snap, Delsys, Massachusetts, USA) onto the subject's right vastus medialis oblique (VM), vastus lateralis (VL), rectus femoris (RF), biceps femoris (BF), and

semitendinosus (ST) to assess muscle activation. Participants performed a maximum voluntary contraction (MVC) procedure comprising explosive jump squats (eliciting maximal dynamic contraction) and maximal isometric contraction against manual resistance, which enabled EMG data to be normalized to %MVC.

To assess muscular effort we calculated the mean of the MVC-normalized RMS signal for each gait/task cycle. The RMS signal provided by the Delsys EMG acquisition software was used for this purpose (RMS window length: 125 ms, 122 ms overlap). The muscle recruitment pattern of the individual quadriceps muscles varies both intra- and inter-participant, but the force exerted by these muscles is similar for the same level of neural activation (due to similar cross-sectional areas). Since we were interested in gross quadriceps effort, and to reduce the number of degrees of freedom in our statistical analysis, we averaged the muscle efforts of the 3 quadriceps muscles that we recorded to get a gross quadriceps effort metric.

5.2.3 Statistical Analysis

We first confirmed normality of our data using QQ-plots. Muscular effort was analyzed using a linear mixed model (LMM) in MATLAB with restricted maximum likelihood estimation of parameters. Data from our eight subjects were tabulated with information consisting of quadriceps muscle effort, condition (bare, exoskeleton), and gender (male, female). We defined exoskeleton conditions and gender as categorical variables and fit a separate LMM for each task, where the condition and gender are fixed effects and subject is a random effect:

$$\text{Effort} \sim \text{Condition} + \text{Gender} + (1|\text{Subject}).$$

The LMM provided the effect sizes and uncorrected p-values for the fixed factors. We corrected the p-values for multiple comparisons (six tasks) using the Holm Bonferroni correction. For the post-fatigue performance and posture metrics, a similar LMM included additional fixed effects of order (bare vs. exo condition) and pre-fatigue workload (number of LL repetitions required to fatigue), without having to correct for multiple comparisons. Quadriceps effort and post-fatigue performance were log-transformed prior to analysis. Although our power analysis resulted in a participant sample size of 10, we decided to stop our study early because of a strong trend seen in our primary metrics of performance and effort reduction, and considering the risk to participants of this high-fatigue protocol. The criteria for early stoppage demands a further correction to the p-value as per the Pocock boundary, which we applied to all our metrics.

5.3 Results

In chapter 4 we designed a multi-terrain LLC controller based on heuristic modification and modulation of several torque basis functions that modify the closed-loop human-exoskeleton dynamics according to the method of energy shaping. Briefly, the coefficients of the basis functions were first chosen using data-driven optimization to match controller torques (given normative kinematic/GRF inputs) to normative human torques over multiple tasks as done in [Lin et al., 2022]. Fig. 4.3 shows the simulation results based on an optimization pipeline in Matlab using *fmincon*. The controller and human torques match well overall, demonstrating that the controller can provide assistive torques to the critical phases of stance and swing across the various tasks (without explicit task classification). The optimized controller was then implemented on an improved, bilateral version of our highly-backdrivable M-BLUE knee exoskeleton (9:1 gear ratio, 25 Nm peak output torque, $<$2 Nm peak backdrive torque) shown in Fig. 5.1 and detailed in the Methods. This provided a starting point for a manual coefficient tuning process based on subjective feedback in pilot testing. After a satisfactory controller was obtained, the same set of coefficients were used for all participants (n=8) in this study.

The study comprised two sessions: fatiguing and non-fatiguing. Fatigue is inevitable and causes deleterious symptoms of reduced performance and increased risk of injury [National Safety Council, 2018; Zhang et al., 2015; CCOHS, 2019]. Accordingly, performance on a time trial is one of the classical measures of fatigue [Enoka and Duchateau, 2016]. Session 1 tested the hypothesis that the exoskeleton improves *fatigued* LL performance (time trial of 10 fatigued LL reps) compared to no exoskeleton (bare), when squatting posture is enforced. Participants performed repeated squat LL until fatigue-induced failure (without power in the exoskeleton condition), immediately followed by 10 timed squat LL cycles (with power in the exoskeleton condition). Participants were instructed to take the minimum required pause between repetitions in order to complete the next repetition with good squat posture, emulating a typical time trial while ensuring safe posture. Although squatting posture was an experimental control, we performed an exploratory analysis of peak thorax lean to see if the exoskeleton helped participants maintain a better squat form. Session 1 also gathered qualitative subjective feedback of exoskeleton effectiveness in post-fatigue multi-terrain LLC. At least one week later, session 2 tested the hypothesis that the exoskeleton reduces quadriceps effort during multi-terrain LLC in a non-fatigued state. A recent study similarly investigated *back* exoskeleton-induced improvements in worker performance with time trials of various activities [Luger et al., 2023], along with assessing muscular, postural, and perceptual benefits.

For all metrics, we used linear mixed models (LMMs) with condition (bare, exo) and gender (male, female) being fixed effects and participant being treated as a random effect. For post-fatigue performance and posture metrics, we included additional effects of order (for the bare vs. exo condition) and pre-fatigue workload (number of pre-fatigue LL repetitions required to reach fatigue). Although our power analysis originally called for ten participants, we concluded our study early after completing eight participants due to 1) the unavoidable risk and discomfort of the fatiguing protocol, and 2) the strong trends observed in our primary metric. The p-values of all metrics tested were therefore corrected as per the early stoppage criteria (Pocock boundary) by scaling by a factor of 1.7. We also corrected for multiple testing (six tasks) for the quadriceps effort metric using the Holm Bonferroni method. Gender, order, and workload were found to be non-significant factors in all statistical tests reported below.

5.3.1 Performance and postural benefits in post-fatigue lifting-lowering

The results confirmed our hypothesis that the knee exoskeleton improves post-fatigue LL completion time. Compared to bare, the bilateral knee exoskeleton induced a significant ($p<0.001$) 33% reduction, 95% CI [21%, 43%], in the time to complete 10 LL repetitions post-fatigue, corresponding to raw un-adjusted averages of 50 seconds (bare) and 35 seconds (exo). Fig. 5.2 shows the completion time distributions, and Fig. 5.3 shows the ensemble averaged durations for 10 LL repetitions before and after fatigue was declared. We also found that the pre-fatigue workload (number of pre-fatigue LL repetitions performed in exo condition as a percentage of bare condition) was uncorrelated ($r = -0.11$) with the post-fatigue completion time (exo condition as a percentage of bare condition, Fig. 5.4). Hence, although the exo condition required fewer repetitions to reach fatigue than bare, this did not bias the post-fatigue results.

Compared to bare, the bilateral knee exoskeleton also induced a non-significant 3° reduction, 95% CI [$-2°$,8°], in peak thorax lean during post-fatigue LL, corresponding to raw un-adjusted averages of 54° (bare) and 49° (exo). See Fig. 5.5 for the peak thorax lean distributions, and Fig. 5.6 for the ensemble averaged deviations in peak thorax lean from the minimum peak thorax lean for each participant. Fig. 5.8 shows individual data points for the post-fatigue LL completion time and thorax lean metrics, and Fig. 5.7 shows the ensemble averaged thorax lean (sagittal thorax angle) profiles.

The average subject feedback rating for effectiveness of exoskeleton assistance in traversing the various tasks in post-fatigue LLC was 4.5 out of 5 on the modified QUEST questionnaire. The individual task averages were 4.8 for LL, 4.8 for stairs ascent (SA), 4.8 for stairs descent (SD), 4.3

for ramp ascent (RA), 4.4 for ramp descent (RD), and 3.8 for level walking (LW). See Fig. 5.9 for the distribution of ratings for the tasks.

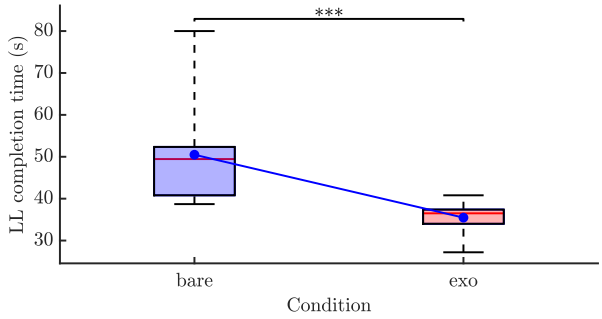

Figure 5.2: Completion times for post-fatigue LL . The box plots show the distributions of the time taken to complete 10 repetitions of LL post-fatigue, for bare and exo conditions. The blue line connects the mean values for each condition. * represents statistical difference ($p < 0.05$), ** represents $p <= 0.01$, *** represents $p <= 0.001$.

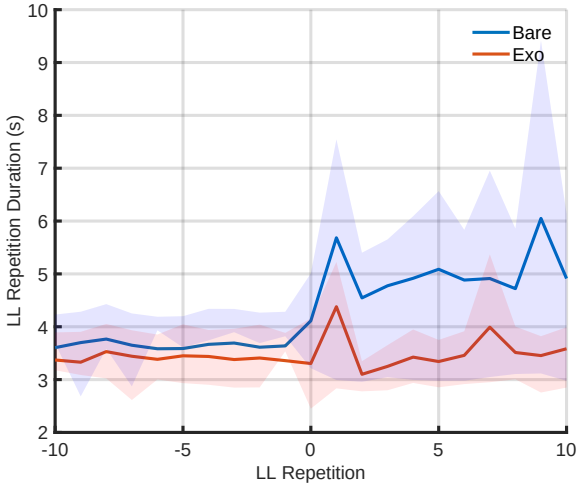

Figure 5.3: Repetition durations for Pre- and post-fatigue LL. The ensemble averaged plots depict the pre- and post-fatigue LL repetition durations for bare and exo conditions. Repetition 0 is defined as the point when fatigue was announced, beyond which exoskeleton assistance was activated for the exo mode.

5.3.2 Muscular effort in non-fatigued lifting-lowering-carrying

We estimated quadriceps effort during six different LLC tasks for bare and exoskeleton-assisted conditions in a non-fatigued state. Muscle effort was calculated as the mean RMS EMG over the gait/task cycle. Quadriceps effort was estimated by taking the mean of the efforts of the vastus

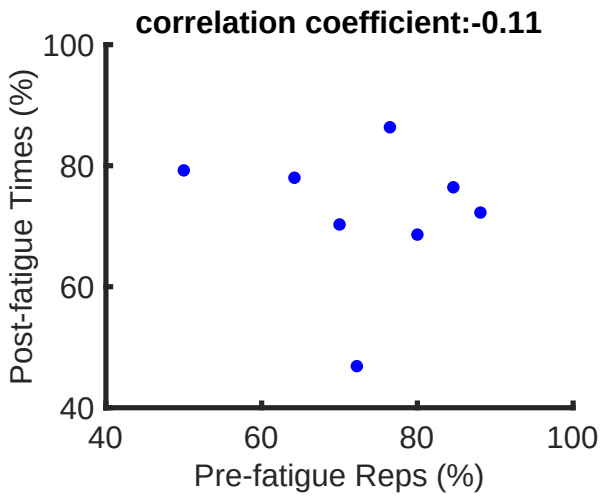

Figure 5.4: Pre-fatigue workload change vs. post-fatigue performance change in LL . The figure shows the correlation between the number of LL repetitions performed in pre-fatigue exo condition as a percentage of bare condition, vs. post-fatigue 10 repetition completion time for the exo condition as a percentage of the bare condition.

medialis oblique (VMO), vastus lateralis (VL), and rectus femoris (RF). The results confirmed our hypothesis that the knee exoskeleton reduces quadriceps effort during non-fatigued, multi-terrain LLC, with the caveat of LW having a non-significant reduction. Compared to bare, the exoskeleton significantly reduced mean quadriceps effort by 28% [21,34]% for LL ($p<0.001$), 16% [10,21]% for RA ($p<0.01$), 27% [16,36]% for SA ($p<0.01$), 13% [5,20]% for RD ($p<0.05$), 13% [6,20]% for SD ($p<0.05$), and 5% [-14,20]% for LW (n.s.). Fig. 5.10 shows the distributions of quadriceps effort for the conditions and tasks tested.

A good qualitative match can be observed between the ensemble-averaged quadriceps EMG profiles and the exoskeleton torque profiles in Fig. 5.11, demonstrating appropriate timing and magnitude of the assistance torque. Because our prior work found that a different exoskeleton/controller caused high hamstrings activation in late stance [Divekar et al., 2020; Lin et al., 2022], we also examine hamstrings EMG profiles in Fig. 5.12 by taking the mean of the biceps femoris (BF) and semitendinosus (ST) recordings. It can be qualitatively seen that the current exoskeleton/controller do not cause any noticeable increase in hamstrings activation compared to bare.

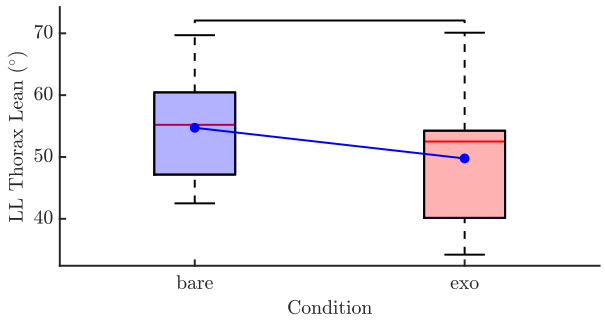

Figure 5.5: Peak thorax lean for post-fatigue LL. The box plots show the distributions of the peak thorax lean associated with post-fatigue LL, for bare and exo conditions. The blue line connects the mean values of each condition.* represents statistical difference ($p < 0.05$), ** represents $p <= 0.01$, *** represents $p <= 0.001$.

5.4 Discussion

State-of-the-art exoskeletons fall short on providing versatile assistance to the critically-involved quadriceps during multi-terrain LLC, which comprise varied tasks including high-torque closed-chain squat lifting as well as open-chain gait tasks such as level walking, ramps, and stairs. In particular, prior LLC studies have not demonstrated holistic (multi-terrain) and multifaceted (performance, muscular, perceptual, and postural) exoskeleton benefits, especially in high-fatigue physical states which are correlated with LBP incidence. This chapter addresses these gaps with the following major contributions. We implemented the novel versatile energy-based control strategy developed in chapter 4 on a highly-backdrivable, bilateral knee exoskeleton to provide assistance and mitigate fatigue during multi-terrain LLC. The resulting control torques are well matched to biological torques in-silico (Fig. 4.3) and to quadriceps activations in-vivo (Fig. 5.11) for all tasks in multi-terrain LLC. The other major contribution is the *first* experimental demonstration of a versatile knee exoskeleton that provides 1) significant performance benefits to squat LL in a highly-fatigued condition (Fig. 5.2), and 2) holistic muscle effort reductions (Fig. 5.10) during multi-terrain LLC in non-fatigued conditions. These results suggest the presented exoskeleton can be applied to mitigate fatigue in real-world workplace conditions in which low back injuries tend to occur.

5.4.1 Biomimetic quadriceps assistance improves performance and posture in post-fatigue LL

Fatigue is inevitable in physically demanding jobs and is a causal factor for work-related musculoskeletal disorders [National Safety Council, 2018]. Our results primarily demonstrate that the

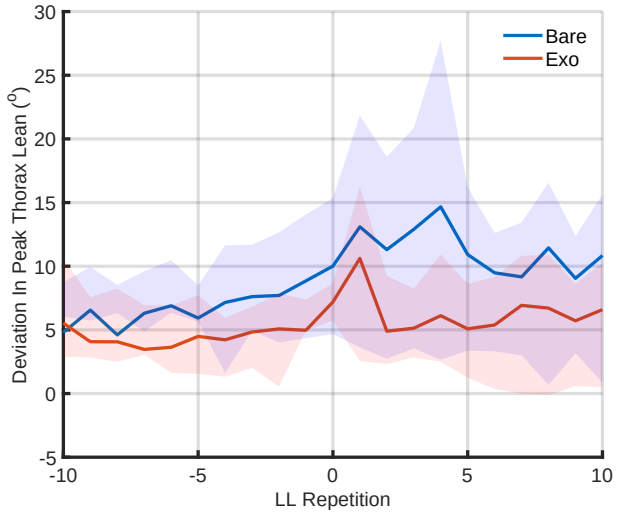

Figure 5.6: Peak thorax lean deviations for pre- and post-fatigue LL. The ensemble averaged plots depict the deviations in peak thorax lean for bare and exo conditions. The deviations are calculated from the minimum peak thorax lean observed for each participant in the exo and bare conditions combined. Repetition 0 is defined as the point when fatigue was announced, beyond which exoskeleton assistance was activated for the exo mode.

exoskeleton can mitigate the deleterious effects of fatigue on LL performance [Zhang et al., 2015], which also has implications on injury risk. Specifically, when minimum performance requirements are not able to be met by workers due to fatigue, they may adopt a compromised posture (stoop) resulting in injury [CCOHS, 2019]. Therefore, by improving performance in a fatigued state, the exoskeleton not only improves worker productivity, but also potentially mitigates the associated risk of injury.

Neuromuscular fatigue can be quantified by the decrease in the muscle's peak force production ability (or peak torque/moment of the corresponding joint). The peak knee torque for a fast squat is about 1.4 Nm $\cdot$ kg^{-1} [Chan et al., 2022], or about 100 Nm for an average person. During the fast LL squats performed in our study, the peak knee torque is required at the bottom of the squat to redirect the body's downward momentum upwards. The bottom of the squat is also where we observed the peak in post-fatigue thorax lean (Fig. 5.7), a likely consequence of participants trying to reduce the moment arm on the knee (and stress on the fatigued quadriceps) in this biomechanically compromised position. The peak of 25 Nm in our exoskeleton assistance torque (about 25% of the normative squat torque) was indeed well aligned with this high-torque squat phase, resulting in good alignment with the quadriceps EMG peaks in the non-fatiguing LL task (Fig. 5.11). Accordingly we found a 28% reduction in mean quadriceps effort and a 33% decrease in peak activation for non-fatigued LL with exoskeleton assistance. To compare, a 60% reduction

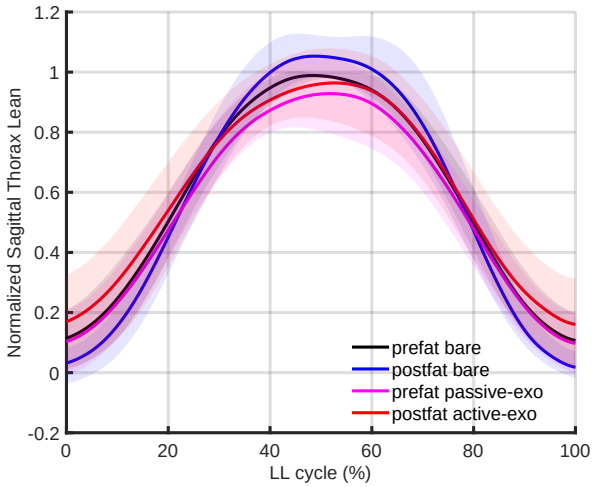

Figure 5.7: Pre- and post-fatigue thorax lean profiles for LL in bare vs. exo conditions. The figure shows the across subject ensemble averaged thorax lean (sagittal thorax angle) profiles normalized to the peak value in the pre-fatigue bare condition. The prefat (pre-fatigue) plots consider the 10 LL repetitions before fatigue was declared, and similarly the postfat (post-fatigue) plots consider the 10 LL repetitions after fatigue declaration. The lifting and lowering repetitions are combined and time normalized from 0 to 100% of the squat cycle. The shaded regions show the SD about the mean.

in quadriceps activation was found with just 16 Nm peak assistance torque in a recent squat-only exoskeleton study [Arefeen and Xiang, 2023]. However, the posture of the subjects in [Arefeen and Xiang, 2023] was highly bent-over during the squat lifts, suggesting a much lower net knee extension torque was required for their task (for which 16 Nm is a higher percentage).

A *fatiguing* squat study reported a 25% decline in maximal quadriceps force after fatiguing exercises [Longpré et al., 2015], but we did not measure maximal quadriceps forces pre- and post-fatigue in our study. If we make relatively broad assumptions of a linear relationship between EMG and force [Staudenmann et al., 2010], and consider fast LL as a maximal activity for the quadriceps, the 33% savings in peak quadriceps force afforded by the exoskeleton was likely sufficient to fully overcome the supposed 25% deficit in force from the induced fatigue. This could explain how the exoskeleton assistance enabled the subjects to significantly reduce their time to complete 10 LL repetitions post-fatigue by 33% and with better posture (3 degrees decrease in global thorax angle), see Fig. 5.5. In fact, the exoskeleton assistance practically maintained the pre-fatigue LL duration levels in post-fatigue (Fig. 5.3), suggesting a full replenishment of the post-fatigue quadriceps force deficit. On the other hand, the LL durations in the bare condition increased with post-fatigue repetitions, indicating an increasing trend in fatigue. The mean LL repetition durations prior to declaring fatigue have quite similar magnitudes for both conditions, suggesting the

similarity in bare and *passive*-exo conditions. After participants declared fatigue, both conditions had a peak LL duration at the 1^{st} repetition because they were allowed to pause just enough to recover and continue. The exo condition likely had a smaller pause because participants had more confidence continuing after fatigue when assistance was expected. The post-fatigue LL feedback rating is also the highest amongst the tasks—almost a perfect 4.8/5—supporting the effectiveness of the exoskeleton assistance at a perceptual level.

The exoskeleton's replenishment of the diminished quadriceps force in post-fatigue LL explains the observed reduction (although statistically non-significant) in peak thorax lean for the exo condition compared to bare. Fig. 5.6 depicts ensemble averaged deviations in peak thorax lean from the minimum thorax lean observed for each participant in both conditions before and after fatigue. Both conditions have similar magnitudes before declaring fatigue (repetition 0), indicating the bare and *passive*-exo conditions had a similar influence on peak thorax lean as expected. Similar to the trend in LL repetition durations, the deviation in peak thorax lean is noticeably higher for the bare condition after fatigue. Without exoskeleton assistance, the participants likely offloaded their highly-fatigued quadriceps by leaning more forward and thus reducing the moment arm on their knees. This was likely a subconscious behavior because participants were reminded to maintain proper squat posture at all times and take a longer pause if they perceived a compromised posture. This observation agrees with a classic study showing quadriceps fatigue leads to a compensatory change in posture (more stooping) [Trafimow et al., 1993]. Importantly, our study is the first to show a trend towards the reversal of this compensatory change with exoskeleton assistance. This intervention addresses the root cause of postural changes (fatigued quadriceps) rather than simply alerting the user by means of a vibrator as in [Picchiotti et al., 2019].

5.4.2 Biomimetic knee assistance reduces quadriceps effort in multi-terrain carrying

We also found a holistic decrease in quadriceps effort for all carrying tasks in the non-fatigued session (Fig. 5.11 and Fig. 5.10). To the authors' knowledge, this is the first knee exoskeleton study to demonstrate consistent reductions in quadriceps muscle effort (without negatively affecting the antagonistic hamstrings) in all the common gait tasks (level walking, stairs and ramp ascent/descent). One of the main factors in these consistent findings could be our mixed in-silico and in-vivo approach to the controller development, whereas prior "task-invariant" controllers (including our prior work) were limited by and restricted to a normative dataset that informed their data-driven optimization/learning processes [Lin et al., 2022; Medrano et al., 2023; Molinaro et al., 2022]. We firstly studied the clinical gait analysis literature to gain both a qualitative and causal

understanding of the high torque exhibiting regions of the knee joint torque profiles in the different categories of tasks encountered in LLC, e.g., ascent vs. descent tasks, or gait vs. non-gait tasks. This allowed us to carefully select a minimal set of physically inspired (inherently passive and predictable) torque basis functions (springs, dampers, gravity compensation, inertial compensation) and biomimetically modify them to produce the general torque profiles for each task category. By then scaling them with task- and phase-sensitive signals, we ensured the torques are smoothly down-modulated in the low or negative torque phases of the respective task, and the entirety of other tasks. This process produced an intuitive "task-invariant" set of basis functions that could be readily customized after an initial data-driven optimization process (see Fig. 4.3). In-vivo manual customization based on subjective feedback was crucial to producing the most helpful and biomimetic torques in all tasks. This final controller was identical between the participants enrolled in this study, i.e., no user-specific tuning was needed.

The peaks in assistive torques are well aligned with the peaks in quadriceps activations across tasks in Fig. 5.11, explaining the significant reductions in quadriceps effort in the exo condition. It should be noted that human muscles are much more efficient in performing negative work (as required in descent tasks) compared to positive (required in ascent tasks). It is therefore understandable that participants found the assistive torques the most helpful (according to subjective feedback) in the tasks requiring high positive work. Indeed, LL, stairs ascent, and ramp ascent (in order) had the highest reductions in quadriceps effort. The ramp and stairs descent muscle activation profiles exhibit a double peak: the first absorbs the initial impact of landing and the second smoothly lowers down the body. After initially optimizing the controller to match this double peak (Fig. 4.3), pilot tests revealed that assistive control torques in the second peak slightly hindered some subjects during the transition to late stance and swing. We therefore adjusted the leg angle-based sigmoid to down-modulate the non-ascent spring's torques earlier in phase, as can be seen in Fig. 5.11. Finally, level walking exhibited the lowest knee moments out of all tasks, and accordingly received the lowest assistance torque magnitude compared to other tasks. Although the assistive torque was well aligned to the quadriceps activation profile, this task got the lowest effectiveness rating in post-fatigue (3.8/5)—the most common feedback was that the exoskeleton did not help in level walking as much as the other tasks. In line with this finding, level walking was also the only task which had a non-significant reduction in quadriceps effort. We suspect that soft-tissue compliance precludes effective exoskeleton torque transfer during such a minimal and fast knee range of motion, and the knee simply does not need much assistance in level walking. Regardless, compared to our prior studies [Divekar et al., 2020; Lin et al., 2022], the presented controller/exoskeleton satisfactorily eliminated the problem of high peaks in hamstrings activation profiles in late stance in level walking (see Fig. 5.12). This is likely the result of 1) adding knee flexion torques via gravity compensation to aid the hamstrings in late stance, and 2) the use of a

significantly lighter exoskeleton.

5.4.3 Study limitations

The main limitation of this study was relying on participants' perception of their point of failure to control the level of fatigue between bare and exo conditions. Participants were reminded to declare fatigue in the second condition at the same level experienced in the first condition, where order was randomized. Fig. 5.3 shows the pre-fatigue repetition durations of both conditions were similar (bare having marginally higher durations). Since repetition duration is a classical indicator of fatigue [Enoka and Duchateau, 2016], we believe any discrepancy in fatigue level at time trial initiation (repetition 0 in Fig. 5.3) was negligible compared to the large difference in durations between conditions during the time trial (repetitions 1-10 in Fig. 5.3). While EMG could have potentially provided an estimate of neuromuscular fatigue, we chose not to encumber the subjects with EMG sensors to avoid discomfort and consequently affect the time trial. We were also wary of using EMG during the fatiguing trials because EMG RMS amplitudes during fatigue are unreliable and the ability to predict fatigue with the median frequency slope is highly subject-dependent [Lamers et al., 2020]. Nevertheless we expect the exoskeleton provided a similar reduction in quadriceps effort and peak activation during the fatiguing LL trial as it did in the non-fatiguing trials in session 2 when we did measure EMG.

Ideally, the condition leading up to fatigue would be the same (e.g., bare). However, substantial recovery from such acute exercise-induced fatigue happens in a matter of a few minutes [Larson and Potteiger, 1997], and therefore it was practically impossible to don the exoskeleton fast enough to capture the effect of fatigue. We therefore settled for the best compromise by having the participants perform the pre-fatigue LL repetitions in as close a condition to bare as feasible with the exoskeleton in passive mode. Fortunately, in this mode the exoskeleton applies a negligible backdrive torque (< 1 Nm [Nesler et al., 2022]) and weighs only 4.6 kg total across both legs. We took two steps to test the effect of this possible confound on the post-fatigue performance. First, we performed a correlation analysis between the % change in repetitions to reach fatigue and the % change in time to complete 10 LL repetitions post-fatigue (Fig. 5.4). We found no significant correlation between these two variables indicating that the effect of exoskeleton assistance on post-fatigue performance was not related to the potential difference in pre-fatigue workload (number of LL repetitions until failure). Second, we incorporated the effect of pre-fatigue workload in the LMM design and found it is non-significant in explaining the post-fatigue performance outcome.

Additionally, the two fatiguing conditions (bare and exo) were performed on the same day

(session 1), potentially causing greater fatigue for the second condition. This study design was intended to make it easier for participants to declare fatigue at a similar perceived point of failure. To minimize the possible confound, we gave participants ample time to rest between conditions and alternated the order of conditions between participants. Moreover, we incorporated the effect of order in the LMM and found it was non-significant in explaining the post-fatigue performance outcome. This protocol is similar to a recent study on the effect of exoskeleton assistance on LL endurance (lift-lower till failure), in which both bare (control) and exo conditions were tested on the same day with a short break between conditions [Rodzak et al., 2023].

Lastly, we did not directly test the exoskeleton's ability to delay LL fatigue, e.g., with an endurance test till failure. However, the significant reduction in quadriceps EMG during non-fatigued LL in session 2 suggests the exoskeleton could have this effect. Endurance testing with the exoskeleton is left to future work.

5.4.4 Future work

For loads/objects that cannot be placed between the feet, some amount of forward bending is inevitable which will create a non-negligible moment arm about the critical L5/S1 joint and increase the chance of injury. In the workplace, LLC loads come in a variety of shapes and sizes and hence it may become necessary to directly offload the lower back with a back or hip-back brace. The inherently modular nature of the knee exoskeleton presented in this study allows it to be readily interfaced with a hip-back exo to provide versatile assistance for LLC with the squatting technique shown in this chapter as well as stooping in future work. In fact we presented a modular knee-hip combination of our exoskeleton in prior work—albeit only performing a single LL task with a simple gravity shaping controller [Nesler et al., 2022]. In future work we hope to extend the control approach to the hip-back module and test the knee-hip-back configuration's efficacy in LLC with various types of loads.

Finally, the customizable "task-invariant" controller implemented in this chapter for LLC can easily be adapted for general purpose assistance for mobility impairments or augmenting healthy individuals by modifying the LL spring for sit-stand tasks (see chapter 6). The coefficients for the three types of springs and gravity compensation can be safely and independently tuned, enabling future customization to unique patient needs (see chapter 6). This control approach is also amenable to automation via human in the loop optimization that requires a small set of tunable parameters [Slade et al., 2022].

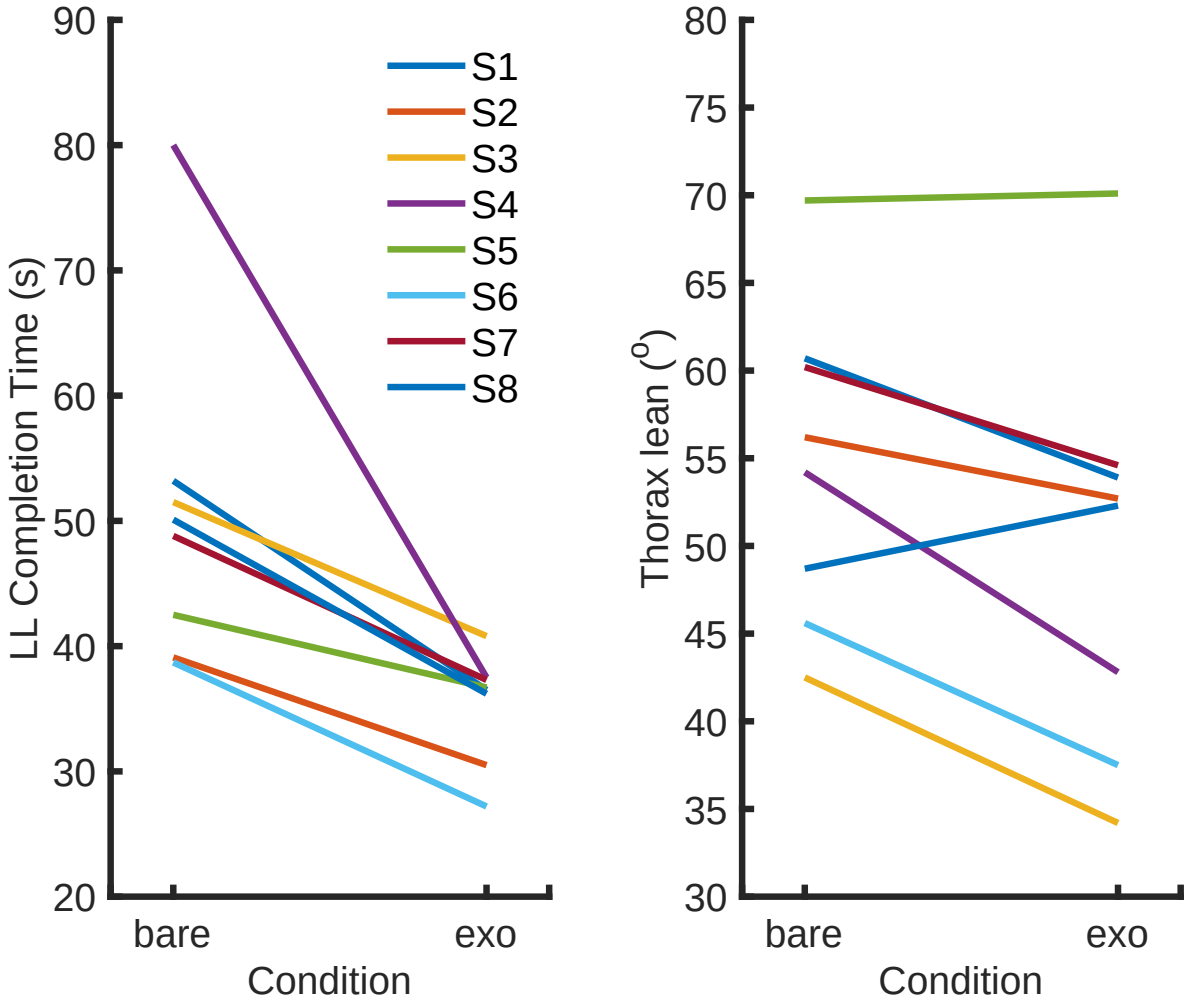

Figure 5.8: Individual post-fatigue completion times and thorax lean. The left figure shows the individual completion times averaged over the 10 post-fatigue LL repetitions. The right figure shows the individual peak thorax lean averaged over the 10 post-fatigue LL repetitions. Data points for all eight subjects (s1-s8) enrolled in this study are shown.

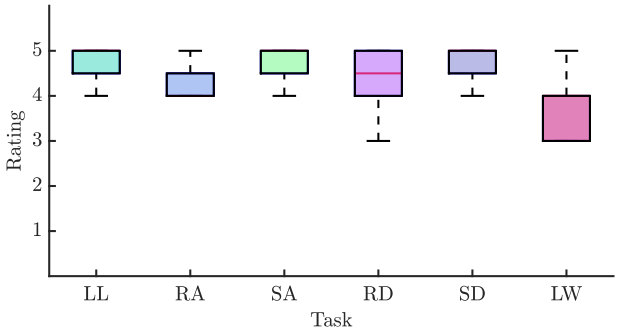

Figure 5.9: Modified Quest Summary. Box and whiskers plot showing the results of the modified QUEST for post-fatigue tasks of lifting-lowering (LL), ramp ascent (RA), stairs ascent (SA), ramp descent (RD), stairs descent (SD), and level walking (LW). Ratings are: 1 - not satisfied at all, 2 - not very satisfied, 3 - more or less satisfied, 4 - quite satisfied, and 5 - very satisfied.

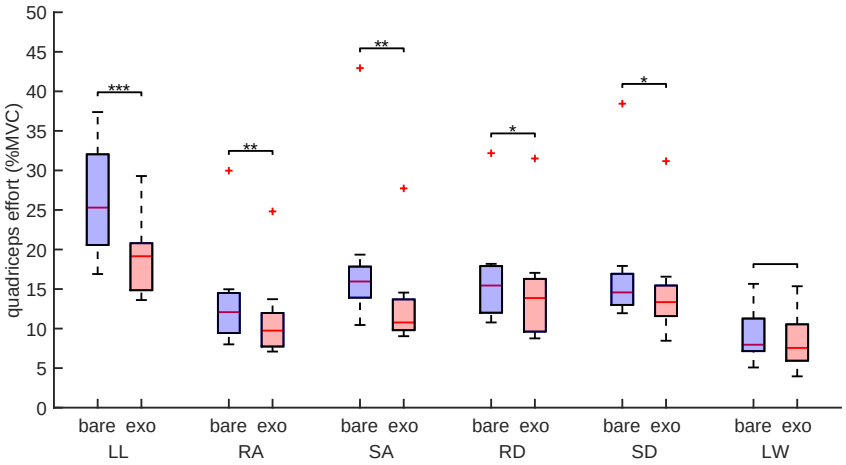

Figure 5.10: Quadriceps effort. The box plots show the distributions of the quadriceps effort, for bare and exo conditions and for all tasks (LL - lifting-lowering, RA - ramp ascent, SA - stairs ascent, RD - ramp descent, SD - stairs descent, LW - level walking). * represents statistical difference ($p < 0.05$), ** represents $p <= 0.01$, *** represents $p <= 0.001$.

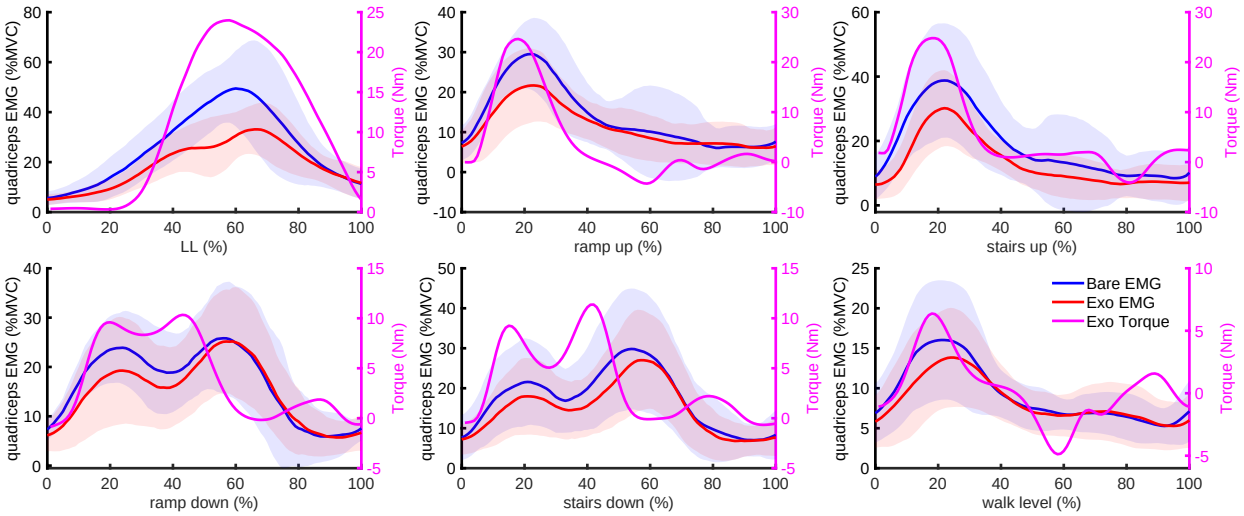

Figure 5.11: Quadriceps EMG and exoskeleton knee torque. The figure shows the ensemble-averaged quadriceps EMG profiles and the torque profiles of the exoskeleton for all tasks tested. Torques are positive in the extension direction.

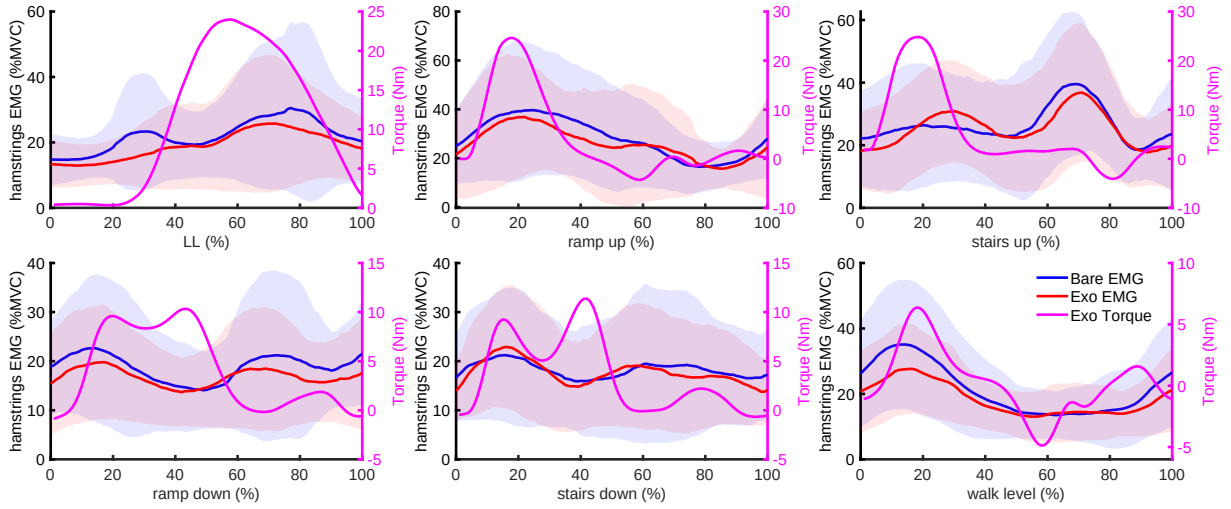

Figure 5.12: Hamstrings EMG and exoskeleton knee torque. The figure shows the ensemble averaged hamstrings EMG profiles and the torque profiles of the exoskeleton for all tasks tested. Torques are positive in the extension direction.

CHAPTER 6

Customizability and Preliminary Validation of a Versatile Bilateral Knee Exoskeleton for Assisting Impaired Individuals

6.1 Introduction

Individuals with impairments present a difficult challenge for task-invariant controllers. Specifically, controllers that are trained on normative datasets may prove overly generic to cater to the unique deficits present in impaired individuals. Moreover these controllers require a secondary optimization process (e.g., reinforcement learning, human in the loop optimization) which then tries to update the algorithm by incorporating the individual's personalized gait data. However this optimization process can take several hours of cyclical data collection and re-tuning, especially if the number of basis functions (control parameters) is large. While this may be doable for healthy individuals, it is highly burdensome and impractical for impaired individuals who usually have a small reserve of energy before fatiguing, e.g., individuals with multiple sclerosis (MS) and post-polio syndrome (PPS). Moreover, the clinician (physical therapist) is completely sidelined in this methodology, preventing them from contributing their expert knowledge. Patients may also prefer their therapist's involvement.

This chapter focuses on addressing these challenges with the novel bilateral knee controller developed in chapter 4, and the latest M-BLUE exoskeleton shown in chapter 5. First we go through the development of a clinician friendly android app (GUI) that facilitates wireless, live modification of the coefficients of the task sensitized torque bases and also displays live control torques from the exoskeleton for both legs. Next we present the individual case studies focusing on customizing the controller to suit each participant's highly unique gait deficits, and assessing the corresponding functional and biomechanical improvements with exoskeleton assistance.

We investigated two highly impaired cases of MS and PPS. The manual muscle test (MMT) and clinician assessment of the PPS patient revealed that he had a highly impaired (atrophied) right

leg from the hip down, and quadriceps weakness in his left side. Accordingly, discussion with the patient and on-site clinician highlighted the need to assist knee extension especially during sit-stand-sit and stairs ascent which the patient found the most challenging. Performance assessments during sit-stand and stair ascent were therefore our primary metrics. We hypothesized that after appropriate controller customization for the PPS patient, our novel bilateral exoskeleton would improve the results of the five times sit to stand (5xSTS) test, and time to ascend a 5-step staircase.

The MMT and clinician assessment of the MS patient revealed he had reduced knee flexion strength (greatly exacerbated by quadriceps spasticity) and severely hampered hip flexion capability. Functionally, his prominent deficit was leg clearance (worse on the left side) leading to compensatory circumduction. Accordingly, our primary metrics were sagittal knee and frontal shank kinematics. We hypothesized that after appropriate controller customization, exoskeleton assistance would increase the MS patient's peak knee flexion angle (assessing leg clearance), and reduce peak shank abduction angle (assessing circumduction).

For both patients, we performed a battery of assessments to explore the effects of exoskeleton assistance for a wide array of tasks (including exploratory assessments beyond the primary outcomes described above). We performed two common gait tests: the timed up and go (TUG) test and six meter walk test (6MWT). We also assessed the times to ascend and descend a staircase and ramp. Finally we acquired subjective feedback on exoskeleton effectiveness for the various tasks completed using a modified QUEST questionnaire.

6.2 Methodology

6.2.1 Clinician-friendly android app (GUI) interface development

I designed an android app, or graphical user interface (GUI) in Android Studio using the Java language. This work involved two main aspects: 1) designing the front panel (or what the user sees and how they interact), and the background interface which provides the functionality of the GUI. We wished the front panel to be user friendly to the clinician who will ideally leverage the intuitive customizability of the controller to provide the appropriate assistance levels for each category of task or task phase to the patient based on their unique deficits. Four customization options were provided: as can be seen in Fig. 6.2, i.e., the ability to modulate the assistance for - 1) aiding in upward propulsion in ascent tasks, aiding bracing (energy absorption) in descent tasks, 3) aiding the strength of upward propulsion for sit-stand (or more generally closed chain squatting) tasks, and 4) leg clearance in general swing. With intuitive graphics, the on-site clinician was easily able to control the behavior of the controller. The GUI also provides a secondary feedback panel which receives data from the bilateral exoskeleton modules and displays them as live bar graphs. In this

case we displayed live commanded torques (normalized to the saturation torque of 25 Nm). This feature allows the clinician to monitor the behavior of the controller and can determine if more assistance may be needed in certain difficult tasks or task phases. Buttons on the bottom right of the screen are provided to easily switch back and forth between the two front panels.

The background process development is quite an involved one, mainly consisting of using multi-threading to coherently and cohesively run the various networking, GUI, and live graphing processes. Upon startup, the network thread automatically initializes and tries to establish connections with the bilateral exoskeletons (equipped with Raspberry Pi's which perform their computing and networking). For this version of the app, the ip addresses and ports of the exoskeletons are hard-coded, as they are always the same being on an independent router. Similarly, the ip address and port of the android device is hard-coded on the exoskeletons' Raspberry Pis. Fig. 6.1 shows the full network setup implemented for our experiments. The android app is configured to continuously send the desired assistance levels to the exoskeletons, using the faster UDP protocol (vs. TCP which has packet receipt checks making it slower). Since we are not interested in a *particular* packet, but rather the speed of packets, UDP was the preferred choice over TCP. Pressing the "SEND" button on the GUI updates the assistance variables in memory with the levels seen on the GUI thus updating what gets sent. The "STOP" button acts as a soft toggle in case the clinician quickly wants to disable the assistance - this updates the assistance variables in memory to zero values. To resume assistance, "SEND" is pressed. The stop and resume feature proved very helpful during patient acclimation to the clinician and engineer alike especially to assess the effect of the exoskeleton by changing it to passive mode with "STOP". Moreover the GUI facilitated patient acclimation and controller customization by enabling a gradual increase in assistance of each of the four available categories to a level that was effective as well as comfortable for the patient.

6.2.2 Experimental protocol

The experiments with the impaired participants were approved by the IRB, and both (PPS and MS) participants provided their consent for the same. Both participants also met our inclusion criteria which required them to not have major balance issues (or any uncontrolled cardiovascular conditions), and be able to walk for 10 minutes with/without their assistance aid. The experimental protocol for both participants was spread out over 3 sessions completed on separate days. In session 1 we first completed the manual muscle test (MMT) and range of motion test (ROM). Next we collected their baseline gait metrics by performing the standard timed up and go (TUG), 6 meter walk test (6MWT), and 5 times sit-stand (5xSTS) tests. We additionally performed our own custom battery of tests which measured the participants' competency (time to complete) in ramp and stairs ascent/descent on the lab's multi-terrain circuit—see chapter 5 for specifics of the circuit.

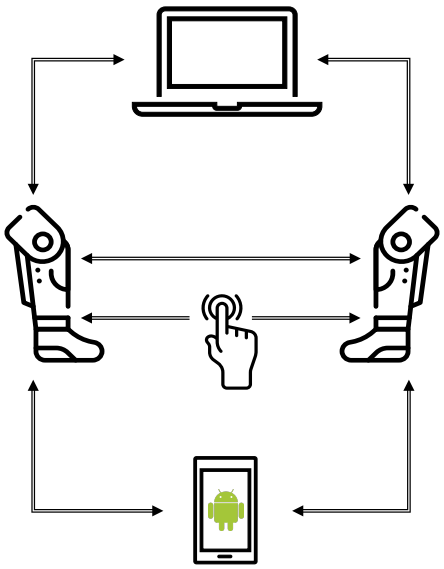

Figure 6.1: M-BLUE wireless networking setup. The figure shows the wireless communication between the different devices involved in the experimental setup. The two M-BLUE knee modules are configured in a paired TCP mode to establish an easy interface to exchange feedback sensor data which is critical in the bilateral controller framework. The experimental laptop communicates with each M-BLUE module, also via TCP. The push button is configured in broadcast UDP mode and is used to soft-toggle the exo power. The android GUI subscribes to and publishes to the two M-BLUE modules via UDP, and is used to update controller coefficients and display exoskeleton related information to the user (see Fig. 6.2).

If time permitted, session 1 ended with a short acclimation to the bilateral knee exoskeleton. In the case of the MS patient, this was initially limited to just observing one of the examiners using the exoskeleton on various parts of the circuit and listening to a concurrent verbal explanation of the assistance. Session 2 primarily consisted of acclimation with the exoskeleton. Firstly, with the help of our on-site clinician collaborator we carefully donned the bilateral knee exoskeleton on the participants. For the PPS participant this was a particularly unique challenge since he had a heavily atrophied right leg. Supplementary foam padding and careful strapping adjustments aided in this process. Next we used the android GUI to gradually introduce assistance torques to the participants as they traversed various parts of the circuit trying various tasks. This is also where I performed the custom modifications to the controller based on each subject's unique gait characteristics and deficits (detailed in the subject specific sections below). We concluded session 2 after the participants were able to successfully complete a few repetitions of all tasks in the experiment, i.e., level walking, STS, and ramp and stairs ascent/descent. The session 3 protocol was a repeat of session 1's with the exoskeleton. At the end of session 3 we collected subject feedback on the effectiveness of the exoskeleton according to our modified QUEST questionnaire

(see Table 6.1 for the list of questions). Each session lasted approximately 3 hours. During the baseline (bare) testing in session 1, we secured IMU sensors and foot pressure sensors on the participants in order to measure key gait signals. These same set of sensors were also present on the exoskeleton in the exo condition in session 3.

Table 6.1: Modified QUEST list of questions for impaired participants

How satisfied were you with the device assistance during:
• Sit-stand
• Ramp Ascent
• Stairs Ascent
• Ramp Descent
• Stairs Descent
• Level Walking

The table lists the questions asked in the modified QUEST questionnaire for impaired participants. The assessment was to be given on a discretized scale of 1-5 (not satisfied at all, not very satisfied, somewhat satisfied, quite satisfied, and very satisfied respectively).

6.3 Controller customization, results, and interpretation

6.3.1 Post-polio syndrome

Our PPS participant was male, aged 58 yrs, and weighed 73 kg. His manual muscle test (MMT) results and range of motion results are shown in Table 6.2 and Table 6.3 respectively. As can be seen from the MMT results, his right limb from the hip downward was heavily atrophied and practically had no power. Moreover, this leg is used as a "walking stick" to quote the participant. It could also be likened to a passive prosthesis.

We made a few adjustments to the controller to accommodate this asymmetry and still provide meaningful torques in a task invariant fashion—see Fig. 6.3 for the exoskeleton torque and knee angle profiles measured during the multi-terrain experiments. Firstly, the non-ascent spring damper dynamics can accommodate a wide range of leg masses, however the heavy atrophy on the right leg meant that the mass-spring-damper system became marginally unstable for any meaningful spring stiffness values. We therefore fully down-modulated this torque basis—since the current version of the GUI is setup to uniformly adjust the task- and/or phase-specific assistance levels of both legs, this change had to be hard-coded. Secondly, we had to modify the task-sensitization of the LL spring. The LL spring, which assists in symmetric closed-chain squatting or STS tasks, is scaled by the GRF of the ipsilateral leg to provide assistance proportional to the amount of loading on

Table 6.2: Manual muscle test (MMT) results for PPS participant

	Right	Left
DF	0/5	5/5
PF	1/5	5/5
KF	0/5	5/5
KE	0/5	3+/5
HF	0/5	4-/5

the respective leg and down-modulate when the participant is seated (see chapter 2 for a detailed explanation of vGRF tapering). This spring is also scaled by the ipsilateral and contralateral heel FSR signals to prevent it from activating when the user is not stably planted on the ground, i.e., both heels are required to at least impart 0.1 BWs of force on the ground for a meaningful activation level. With the heavy atrophy on the right leg, the participant was unable to apply any significant pressure to the ground to activate the LL spring, however, it was desirable to assist this leg. Since he retained good control of his better left leg, we scaled the LL spring of his highly atrophied leg by the GRF of the better contralateral leg. This was a welcome change as the participant was now able to control assistance to both legs using his better leg. This resulted in an impressive improvement in his 5xSTS test time which was the first of the two primary metrics (see Table 6.4). Accordingly, he rated the STS task highly (see Table 6.5).

The exoskeleton induced a marginal reduction in the time to complete stairs ascent (second primary metric), stairs descent, and ramp descent; while there was a marginal increase in the time to complete ramp ascent with the exoskeleton (see Table 6.4). Accordingly, the participant rated the stairs ascent task highly in Table 6.5 (same as STS) likely due to the assistance received to his weakened quadriceps in helping them perform positive work in these demanding tasks.

From Table 6.4 it can be seen that the participant was noticeably slower for the level walking tests (TUG and 6MWT) with the exoskeleton. This finding is in line with a recent study which tested a custom unilateral knee exoskeleton on three PPS participants and found drastically slower TUG and 10MWT times with the powered device compared to a simplistic passive brace [Yu et al., 2020]. The primary drivers in level walking are the hips and ankles, with the knee taking a minor passive role. The added mass/inertia of the exoskeleton were the likely reasons for our participant slowing down slightly in tasks which involved level walking.

6.3.2 Multiple sclerosis

Our MS participant was male, 60 yrs, and weighed 82 kg. The MMT (Table 6.6) and ROM (Table 6.7) tests and visual (functional) gait assessments conducted by the collaborating clinician revealed that the participant had a severe weakness of his left hip flexors. Furthermore, spasticity

Table 6.3: Range of motion (ROM) results for PPS participant

	Right	Left
DF	15°	5°
PF	40°	56°
KF	150°	125°
KE	5°	0°

Table 6.4: Gait test results for PPS participant

Test	Bare (s)	Exo (s)
5xSTS	18.9	11.8
TUG	13.0	15.2
6MWT	6.2	8.6
SA	8.3	8.1
SD	9.1	8.5
RA	8.2	8.4
RD	14.8	14.6

Table 6.5: Modified QUEST ratings for PPS participant

Task	Rating (out of 5)
STS	4
Level walking	2
Stairs ascent	4
Stairs descent	3
Ramp ascent	3
Ramp descent	2

in his quadriceps, combined with weak knee flexors, severely impaired his foot clearance. The participant compensated by circumducting his left leg. Moreover, his bare gait tests in Table 6.8 reveal the debilitating effect of his condition on his walking speed and also completion time of other gait tasks such as stairs and ramp climbing. Since he had intact quadriceps strength on both legs (Table 6.6), his sit-stand ability was unaffected as far as power was concerned, however balance was an issue (as with all tasks).

Like for the PPS patient, we performed controller customizations according to the MS patient's unique gait deficits to provide helpful torques in all tasks wherever possible with the bilateral knee exoskeleton (see Fig. 6.4). We first made a significant addition to the controller's swing basis set to provide meaningful knee flexion torque to address this participant's leg clearance issue. The original swing controller relies on gravity compensation to provide an anti-gravity swing torque, but the torque due to gravity on the knee is zero when the shank is vertical. Due to his severe impairment, the MS participant's left knee hardly exhibited 10° ROM during level walking (see Fig. 6.7), and therefore his shank did not appreciably rotate posterior to vertical. This resulted in an insignificant assistance torque from the gravity compensation basis function, so we implemented an additional specialized torque basis function to boost his leg clearance. To the final swing torque, we added

$$\tau_{\text{th}} = g_{\text{th}} \cdot \sin(\theta_{\text{th}} - \theta_{\text{th}}^{\text{offset}}) \cdot \text{step}(\theta_{\text{th}} - \theta_{\text{th}}^{\text{offset}}) \tag{6.1}$$

where g_{th} scales the magnitude of torque boost, θ_{th} and $\theta_{\text{th}}^{\text{offset}}$ are the global thigh angle (sagittal) and its offset respectively, and the step function ensures the basis function is off for anterior global thigh rotation angles higher than the offset value. See Fig. 6.5 for a simulation of control torques with and without the additional basis function for boosting leg clearance. This basis function was inspired by our group's complimentary work in the prosthetics field, where the global thigh angle plays an important role as a robust phase variable especially for walking tasks [Villarreal and Gregg, 2014]. Since the participant retained a reasonable amount of strength in his hip extensors, he could intuitively modulate the assistance from this new boost function by using the more intact proximal joint (hip) to control the highly impaired distal joint (knee). The global thigh angle offset was carefully chosen such that the participant would receive knee flexion assistance at a vertical global thigh angle, i.e., during mid-swing. The GUI, among other parameters, allows scaling the overall swing torque using the bottom-right icon and button set on the main panel (see Fig. 6.2). As a safety feature, coefficient updates by the GUI are limited to a reasonable amount. However, after initial acclimation trials, and consultation with the on-site clinician, we increased the hard-coded coefficient such that an average peak torque of 21 Nm was provided in swing for this participant. This magnitude of assistance in swing falls drastically outside any normative dataset, as it is more in line with the assistance fraction we provide in stance. However, this participant needed such high assistance torque during swing, and the high customizability of the controller made this change

possible. Fig. 6.6 shows controller simulations (including the swing boost basis function) with various swing assistance levels that can be set by the GUI—swing assistance level 4 was chosen for the MS participant.

The swing boost function induced marked improvements in the MS participant's primary metrics—substantial improvements in his leg clearance (tracked by the sagittal knee angle) and associated compensatory circumduction (tracked by the frontal global shank angle) as can be seen in Fig. 6.7 and Fig. 6.8 respectively. Receiving the greatly needed swing assistance was likely the reason he rated the exoskeleton assistance in level walking highly (see Table 6.9).

The second change we made was to remove the scaling of the STS (LL) torque relative to AJC_{dist}. Ideally, this ensures the activation of the STS torque only when the user attains a symmetrical starting posture. However during acclimation we realized the participant stands in a non-symmetrical posture. Since this was a precautionary task function, and given the very slow gait speed of the participant, its removal did not have any negative effect on the overall controller behavior outside of STS, and greatly improved the reliability of STS assistance. Similar to the PPS participant, we also removed the scaling with respect to the heel-FSR for his left (high impaired) leg for STS, allowing his better right leg's heel to control the behavior. These changes resulted in a marginal improvement in his 5xSTS speed shown in Table 6.8.

While we were able to drastically improve his leg clearance with the bilateral knee exoskeleton, the added mass and inertia of the exoskeleton proved to be burdensome on his already weakened hip flexors. For all gait tests (apart from 5xSTS) the participant slowed down in the exo condition compared to bare (see Table 6.8). This finding is in line with a large randomized clinical trial on the Keeogo (a commercial bilateral knee exoskeleton which claims to support multiple tasks) in which the exoskeleton significantly slowed down the MS participants in all gait performance tests., the TUG, 6 minute walk test, and timed stair test [McGibbon et al., 2018, 2023]. Interestingly, the Keeogo study carefully excluded participants who had trouble initiating walking movements with their hip flexors (i.e., an identical issue exhibited by our case study participant). We had no such exclusion criteria in our IRB approved protocol.

For level walking, the knee is primarily passive, while the ankle and mainly the hips are the primary drivers of the task. Since our knee module did not address his hip flexor weakness (and in fact added to the problem due to the added mass/inertia), the negative results of the 6MWT and TUG are expected. For stair and ramp climbing the same kinematic bottleneck of the weak hip flexors is present and hinders the initiation of the swing phase, especially for the ascent tasks. From the video analysis, it is quite obvious that the participant struggled to lift his leg to the level of the step in stair ascent, and the added mass of the exoskeleton makes this more difficult. While our exoskeleton did provide knee extension torque in stance to propel the body upwards and forwards on the stairs, our participant's quadriceps did not have deficit to begin with and therefore

Table 6.6: Manual muscle test (MMT) results for MS participant

	Right	Left
DF	4/5	3+/5
PF	4+/5	5/5
INV	1/5	2-/5
EV	1/5	2-/5
KF	3/5	4-/5
KE	5/5	5/5
HF	3-/5	2-/5
HE		

Table 6.7: Range of motion (ROM) results for MS participant

	Right	Left
DF	5°	-5°
PF	35°	40°
KF	135°	135°
KE	0°	0°
HF		
HE		

this assistance was likely unnecessary at the cost of further hindering his hip flexors. Accordingly, our MS participant slowed down less with the exo in the descent tasks (compared to ascent), since he could use gravity to aid his hip flexors to swing his leg through.

6.4 Discussion

In this chapter we successfully designed a clinician friendly android GUI that proved very helpful to our on-site clinician and also to the experimenters. We also successfully customized the bilateral

Table 6.8: Gait test results for MS participant

Test	Bare (s)	Exo (s)
5xSTS	20.3	18.4
TUG	27.5	46.8
6MWT	15.9	29.6
SA	19.7	26.2
SD	12.8	15.6
RA	17.4	27.2
RD	14.3	19.4

Table 6.9: Modified QUEST ratings for MS participant

Task	Rating (out of 5)
STS	3
Level walking	4
Stairs ascent	3
Stairs descent	4
Ramp ascent	3
Ramp descent	4

knee controller developed in chapter 4 to best assist each participant's unique deficits related to the knee joint. Fig. 6.3 and Fig. 6.4 show the exoskeleton torques and knee angles measured during the various tasks performed in our experiments for the PPS and MS participants respectively. From a biomechanics standpoint, the customized controller behavior was near ideal considering the particular deficits and compensatory gait adoptions of each participant. The participants predominantly adopted a "step-to" gait pattern due to one of their legs being substantially more impaired than the other. The PPS participant's right leg was heavily atrophied and impaired, and the MS participant's left leg was more severely affected. A common trend seen in Fig. 6.3 and Fig. 6.4 is the controller applying minimal torques to the more affected leg during stance in the gait tasks. This is reasonable as the participants used the more affected leg in a passive manner and preferred to keep the knee locked (or even hyper-extended) for greater stability against knee-buckling, resembling the adaptations in hemiparetic gait [Woolley, 2001]. In this posture, very little assistance torque is needed for the knee joint. On the other hand, the knee joint of the less affected leg is more actively involved in the tasks and thereby receives more assistance torque. For example, in stairs ascent, the controller provided a strong knee extension torque to the less affected leg in early stance to aid in driving the center of mass forwards and upwards. Similarly for descent tasks, the controller provided more bracing (extension torque) during stance to the less affected knee to help it absorb potential energy during the eccentric phase; in contrast, the knee of the more impaired side was maintained in a locked state and accordingly received practically no bracing assistance. The swing torques for the MS participant differed from this trend because they could be volitionally controlled using the unaffected hip extensors. Specifically, the MS patient utilized the hip angle based swing basis function to extract more knee flexion assistance for his more impaired (left) side. Finally for sit-stand, both knees received similarly high extension torques as desired.

Overall, the novel bilateral exoskeleton/controller induced marked improvements in all primary metrics we had set forth for both participants. The PPS participant had a drastic improvement in 5xSTS time and a notable improvement in stairs ascent time, and greatly appreciated the exoskeleton's assistance for his weakened quadriceps of his better (left) leg—note his right leg was heavily

atrophied and scored 0 on almost all categories of the MMT. The MS participant on the other hand had intact but spastic quadriceps, weak hamstrings, and highly weakened hip flexors. The exoskeleton provided a substantial benefit to leg clearance (greatly improved peak knee flexion in swing) and mitigated the compensatory circumduction (greatly reduced peak shank abduction angle) exhibited by the MS participant.

In exploratory analyses, we found that the exoskeleton slowed down the participants in level walking (PPS marginally, and MS significantly). This suggests that using the knee module in isolation may not be suitable for highly impaired individuals especially if there exists an additional major impairment at a different joint (the hip for our MS participant). Overall, the selection of the joint modules (ankle/knee/hip, unilateral/bilateral) is critical for holistic benefits with a lower limb exoskeleton. In hindsight, a unilateral knee module on the better leg for the PPS participant and a bilateral hip-knee module for the MS participant would have been ideal choices, which likely would have resulted in more generalized benefits. However, the scope of this chapter was limited to testing the customizability and performance of the knee module through these case studies. Considering this scope, the knee controller demonstrated high versatility and customizability to help these individuals with unique deficits where it could.

In addition to lifting-lowering-carrying in chapter 5, we believe an ideal use case for these bilateral knee modules would be knee osteoarthritis (OA) or general knee pain populations (patellar tendonitis, post-op etc.). See Tab. 6.10 for the pain and difficulty rating (modified WOMAC questionnaire) results of applying a simple quasi-stiffness controller (implemented on Comex 2) on a participant with patelo-femoral joint OA. The pain in this disorder is caused by forces on the patelo-femoral joint, which in turn is related to quadriceps forces. By reducing the quadriceps forces with exoskeleton assistance, the participant reported promising reductions in pain scale ratings for most tasks. However, the exoskeleton/controller combination increased the difficulty level for walking, which is not surprising with a simplistic controller. This further motivates similar research with our latest bilateral knee controller and M-BLUE exoskeleton.

Table 6.10: Modified WOMAC pain and difficulty ratings for patelo-femoral OA participant, 0 = None, 1 = Slight, 2 = Moderate, 3 = Very, 4 = Extremely

Task	Pain rating		Difficult rating	
	Bare	Exo	Bare	Exo
Level Walking	0	0	0	1
Decline	0	0	1.5	2
Incline	0.5	0	1	1
Sit to stand	1	0.5	1	1
Stand to sit	1	0	0	0
Stairs ascent	1	1	1	1
Stairs descent	2	1	2	1

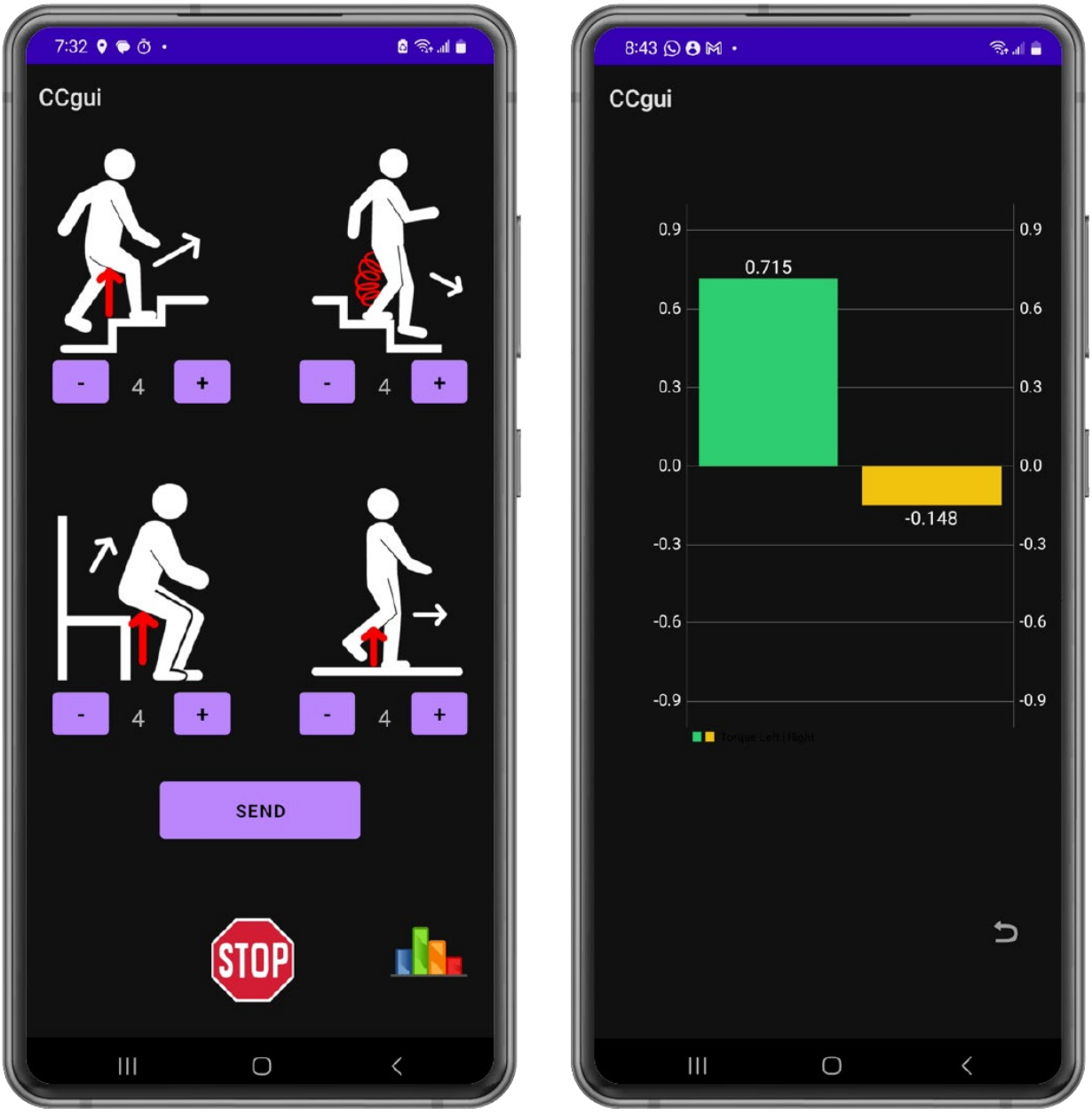

Figure 6.2: Clinician friendly android GUI for controller customization and visual feedback. On the left is the main panel of the GUI which allows the user to update key controller coefficients (assistance levels) for the corresponding tasks depicted with pictures. The main screen can also soft-stop the exo and switch to the next panel shown on the right. On the right is the secondary panel responsible for displaying live commanded torque values from the two (left and right) actuators of the bilateral M-BLUE knee module.

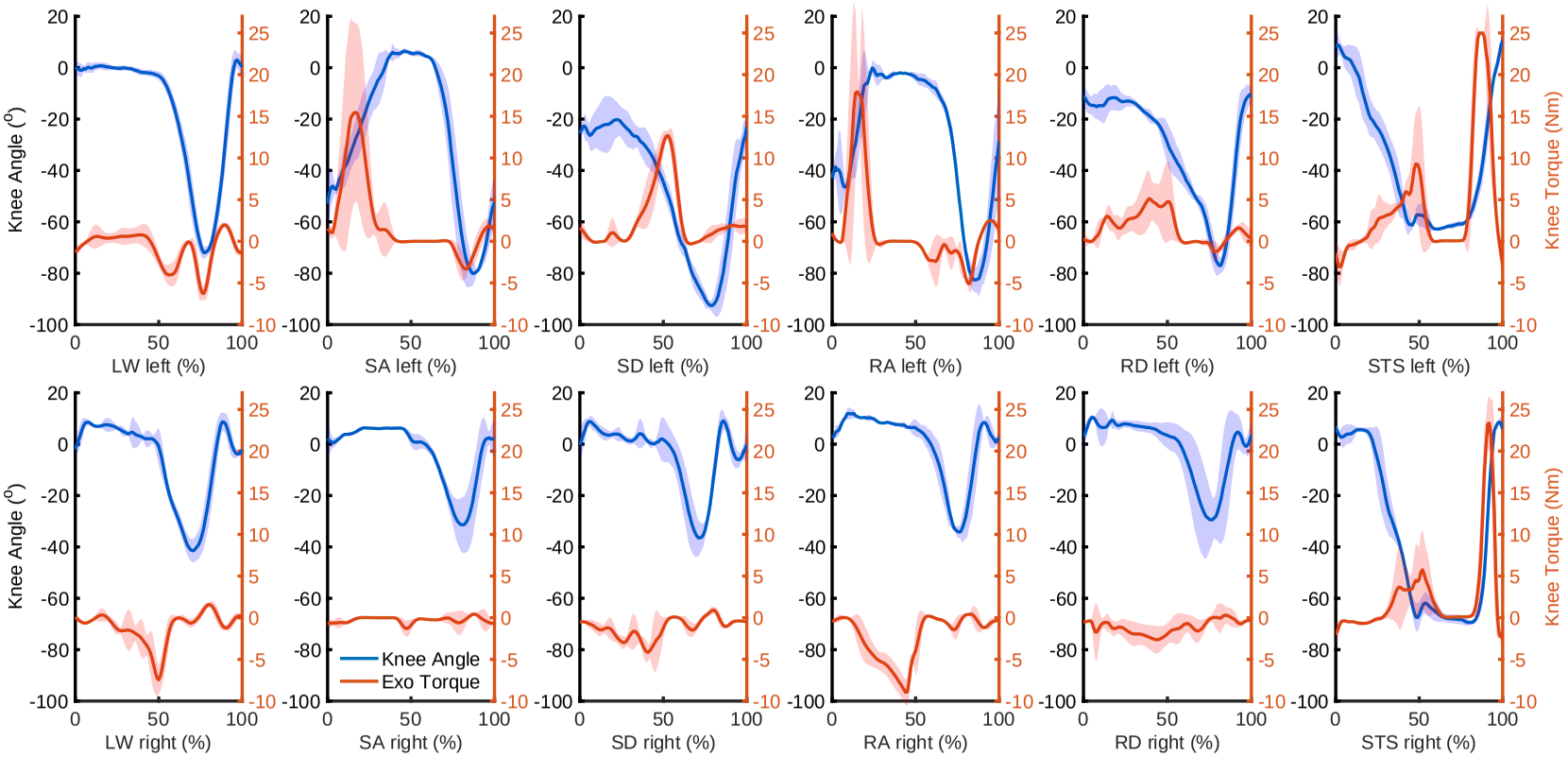

Figure 6.3: Exoskeleton torques and knee angles for all tasks for PPS patient. The figure shows the ensemble averaged knee angles and exoskeleton torques for level walking (LW), stairs ascent (SA), stairs descent (SD), ramp ascent (RA), ramp descent (RD), and sit-stand (STS) normalized to the task cycles of both left (less impaired) and right (severely impaired and atrophied) legs. Positive values represent knee extension angles and knee extension torques.

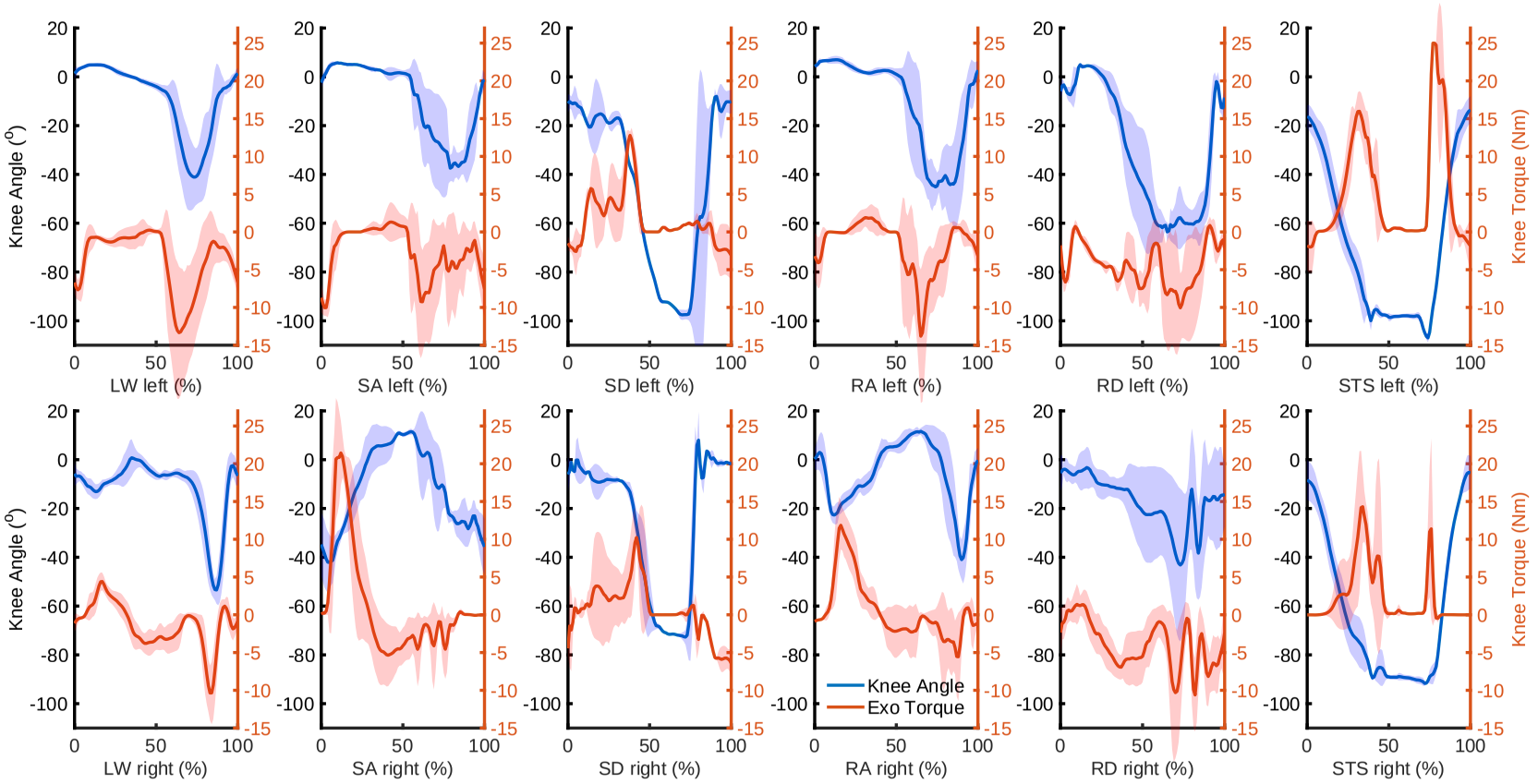

Figure 6.4: Exoskeleton torques and knee angles for all tasks for MS patient. The figure shows the ensemble averaged knee angles and exoskeleton torques for level walking (LW), stairs ascent (SA), stairs descent (SD), ramp ascent (RA), ramp descent (RD), and sit-stand (STS) normalized to the task cycles of both left (highly impaired) and right (less impaired) legs. Positive values represent knee extension angles and knee extension torques.

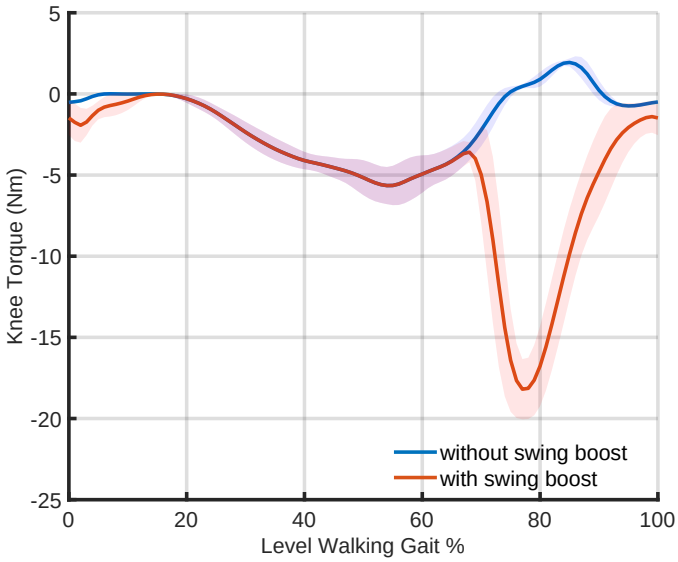

Figure 6.5: Controller simulation with and without swing boost basis. The graph shows the ensemble averaged simulated controller torques based on bare kinematics of MS participant. The blue line shows torque without the swing boost basis, and red curve is with. The shaded regions show the standard deviations about the mean. Positive torques represent extension.

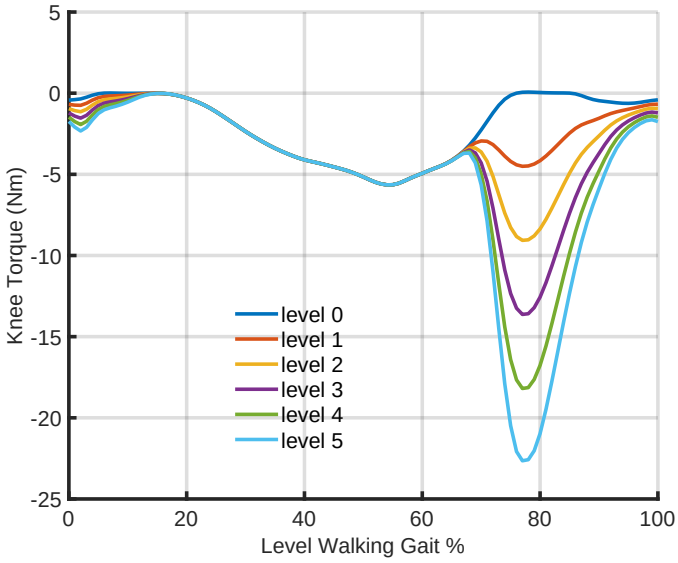

Figure 6.6: Controller simulation with different GUI assistance levels. The graph shows the ensemble averaged simulated controller torques based on bare kinematics of MS participant for various swing assistance levels that can be set by the GUI. The GUI levels range from 0 (no swing assistance) to 5 (maximum swing assistance). Positive torques represent extension.

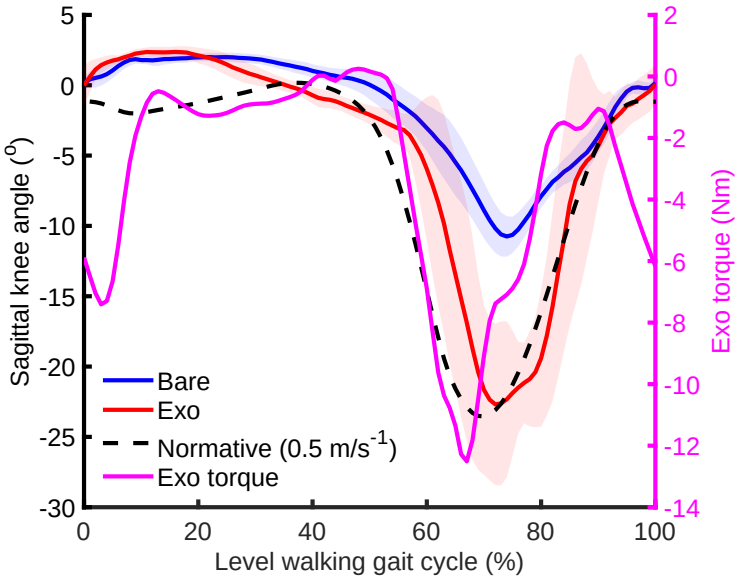

Figure 6.7: MS sagittal knee angles for bare and exo conditions. The figure shows the ensemble averaged sagittal knee angle profiles for bare and exo conditions (extension angles are positive), along with the exoskeleton torque (extension torque is positive) for the left (highly impaired) leg.

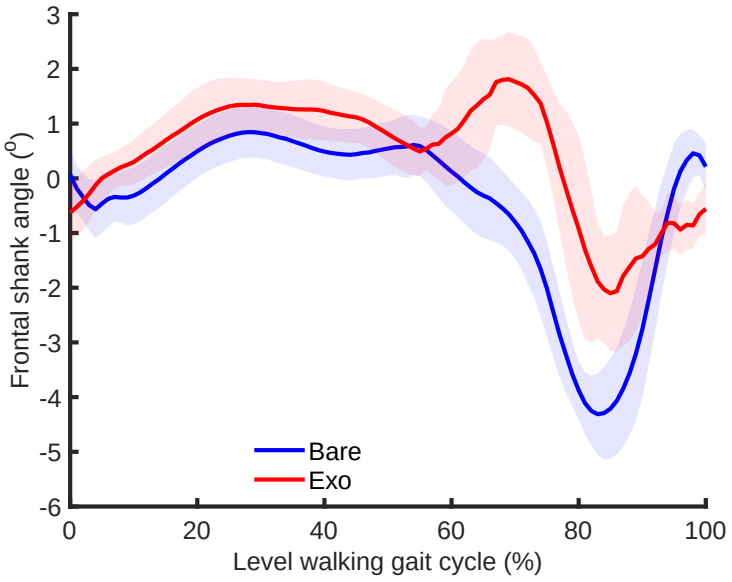

Figure 6.8: MS frontal global shank angles for bare and exo conditions. The figure shows the ensemble averaged frontal plane global shank angle profiles for bare and exo conditions (adduction angles are positive) for the left (highly impaired) leg.

CHAPTER 7

Conclusions and Future Work

The focus of this dissertation is on the control and pre-clinical validation of lower-limb partial assist exoskeletons, i.e., developing and assessing assistance schemes applicable to improving mobility in broad populations that retain a certain level of voluntary motion. More specifically, the dissertation's goal was twofold and constituted: 1) designing an intuitive, and customizable "task-invariant" controller for lower limb backdrivable exoskeletons to assist both healthy and impaired users over multiple terrain in multiple activities; and 2) performing pre-clinical in-vivo experiments designed to investigate the effect of this *partial* assistance scheme on critical, multifaceted human variables.

The primary justification for this goal arose from both mechanical, and controls related gaps in the state-of-the-art lower limb robotic assistance technologies for individuals with remnant voluntary ability. Mainly, this group of individuals requires control schemes that command assistive torques based on live kinematic feedback of their limbs; and thereby require a mechanical actuation system that least impedes this voluntary motion. However, at the start of my dissertation several years ago, partial assistance exoskeleton technology was in an early transition phase from a distinctly different exoskeleton class—bulky, powerful exoskeletons with highly geared (and thereby stiff) actuators for "driving" the limbs of paralyzed individuals with negligible voluntary force production capability [van Kammen et al., 2020]. Accordingly, my research lab progressed through three major versions of exoskeletons (Comex 1, Comex 2, and MBLUE), with each subsequent version being lighter and more backdrivable. In order to address the first part of the goal, it was important to firstly assess the existing partial assist controllers on available hardware (related to the second part of the goal).

My first work in chapter 2 therefore involves mechanical improvements to an existing knee-ankle exoskeleton (Comex 1) and related control improvements to a potential energy shaping controller (a novel "task-invariant" controller developed by my group at the time [Lv et al., 2018]). Specifically, by developing and implementing a custom foot pressure sensor on Comex 1, I addressed a gap preventing the translation of in-silico modeling results to in-vivo usability. Mainly, the unilateral lower-limb potential energy shaping controller was based on two discrete models, 1)

single support stance and 2) swing. For practical implementation purposes this presented a challenge for any double (multiple) support phases., e.g., double support in gait, or multiple support in sitting on a chair. Since the controller inevitably treated these states as single stance, it heavily over-estimated the assistance torques causing problems such as hyper-plantarflexion in late stance, and undesirably high assistance torques while sitting down (a task that ideally needs zero assistance). By scaling the command torques with $sin(vGRF)$, where *vGRF* is the vertical ground reaction force estimate from the foot pressure sensor normalized to body weight, I successfully and smoothly blended the stance and swing models for practical use in multi support phases. The vGRF signal had a high correlation (0.99) and negligible error (0.03 BWs) with respect to the simultaneously recorded "gold-standard" force plate data. Removing this practical hurdle enabled subsequent preliminary validation on a single healthy subject in multiple activities of daily living (level walking, stairs and sit-stand-sit). Meaningful reductions in both ankle and knee joint musculature were found for high torque task phases with relatively slow dynamics (e.g., sit-stand-sit or initial stance in stair ascent). However, the exoskeleton was counterproductive for swifter tasks such as level walking.

In chapter 3, I show and interpret the results from a couple of human subject studies I performed as part of collaborative work to test the efficacy of more advanced, data-driven, *total* energy shaping controllers (M-TOES) implemented on Comex 1 [Lin et al., 2022] and later on the MBLUE. While the earlier study yielded promising results for one subject, the remaining two subjects did not respond consistently to the exoskeleton assistance. The latter study demonstrated the potential of the MBLUE exoskeleton in reducing muscular effort for multiple tasks but this benefit was limited to only the unilateral configurations. Moreover, the bilateral knee and hip configurations demonstrated a non-significant *increase* in muscle effort. Moreover, the M-TOES framework does *not*: 1) provide guarantees on the helpfulness of the assistance torques for feedback kinematics that fall outside the training dataset, and 2) readily allow localized changes to the controller behavior for certain tasks/task phases. These drawbacks (discussed in detail in chapter 3) made the M-TOES controller unsuitable for application to LLC and impaired populations. LLC requires a bilateral knee configuration which the M-TOES was unable to assist with, and impaired populations with pathological (non-normative) kinematics require easily customizable controllers to suit their highly unique needs. These experiences motivated the development of my own clinically intuitive, bilateral knee controller (chapter 4).

In my opinion, the novel bilateral knee controller (chapter 4) and the subsequent multi-terrain LLC study in which it was implemented on MBLUE to perform pre-clinical in-vivo experiments (chapter 5) are the highlights of this dissertation. Experiments with eight healthy participants showed that the novel exoskeleton holistically assisted the quadriceps in multi-terrain LLC in both a non-fatigued state and highly-fatigued state which is critically linked with LBP incidence in

the workplace. Consequently our exoskeleton provided meaningful improvements in performance (significant) and posture (n.s.) in post-fatigue LL, and garnered very satisfactory subjective feedback on its effectiveness in post-fatigue multi-terrain LLC tasks. To my group's knowledge, this combination of multifaceted benefits in multi-terrain LLC tasks by a bilateral knee exoskeleton is unmatched by any current or past research works. Moreover, we tackled three key gaps in LLC literature to date. Firstly, while the highly fatiguing and physically demanding squat lifting technique is recommended for promoting safety in the workplace [NIOSH, 2007; Marilyn Sharp et al., 2006; US ARMY, 2000; Nolan et al., 2018], especially for lifting loads that can be placed between the feet, prior studies did not successfully assist it *in tandem* with the multiple activities (ramps and stair climbing, level walking) encountered in load carrying that further tire the quadriceps (the prime movers in squatting). Secondly, while the connection between quadriceps fatigue and resultant subconscious change in posture from squatting to the riskier stooping has been known since decades [Trafimow et al., 1993], no prior works before ours had shown a corrective restoration of this compensatory change with biomimetic robotic assistance. Thirdly, while research groups biased their focus on directly assisting the affected lower back structures in LBP with back or hip-back exoskeletons that primarily support the muscles for stooping, we presented a complimentary and versatile distal (knee) joint supporting device that supports the muscles for the safer, but *energetically inefficient* squatting (a mainstay justification for *energy injecting* exoskeletons). Note that our work does not support strictly using the squat technique over the stoop: the stoop is helpful for picking up light loads. Further, high moment arms on the low back are inevitable for reaching out for loads that cannot be placed between the feet, thus requiring direct assistance with a hip-back brace or exoskeleton. Therefore, in future work we wish to leverage the modularity of the MBLUE and our recent results with the bilateral knee configuration, to test the efficacy of a bilateral knee-hip configuration in a hybrid squatting and stooping experiment consisting of various load types.

Subsequent to its use in the LLC study, the novel bilateral knee controller was readily customized for participants in the PPS and MS case studies (chapter 6). Some high level customizations which involved mere tweaks to the level of assistance in certain task categories were facilitated by my newly developed, clinician friendly android app (GUI). While we were not able to achieve improvements in the exploratory gait performance metrics (TUG and 6MWT) we demonstrated drastic improvements in the primary metrics for both participants. Moreover, we assisted the weakened left quadriceps and highly atrophied right quadriceps (0/5 MMT result) of the PPS participant to nearly double his 5xSTS speed. Further, after incorporating an additional thigh-angle (pseudo-phase) based torque basis function to assist leg clearance (knee flexion), we were able to restore the MS participant's knee ROM to normative levels for slow walking speeds, and consequently substantially improve his compensatory circumduction motion. To note, the negative

results found for the gait metrics are not unique to our study. and are in line with latest results with a custom knee exoskeleton [Yu et al., 2020] for PPS, and a commercial one studied in a large randomized clinical trial for MS [McGibbon et al., 2018, 2023]. Moreover, our mixed results highlight the importance of carefully matching the modular exo configuration to the primary deficits of the patient. In our case, the primary deficit of our MS patient was his weak hip flexors and hence he would have likely benefited much more from a hip-knee configuration which is left to future work. Lastly, the promising pain scale rating results of a patelo-femoral OA patient assisted with a simple quasi-stiffness controller using Comex 2, motivate a future knee OA study using the more sophisticated bilateral knee controller developed in this dissertation.

BIBLIOGRAPHY

Ali, A., Fontanari, V., Schmoelz, W., and Agrawal, S. K. (2021). Systematic Review of Back-Support Exoskeletons and Soft Robotic Suits. *Frontiers in Bioengineering and Biotechnology*, 9.

Amaro, A., Amado, F., Duarte, J. A., and Appell, H.-J. (2007). Gluteus Medius Muscle Atrophy is Related to Contralateral and Ipsilateral Hip Joint Osteoarthritis. *International Journal of Sports Medicine*, pages 1035–1039. Publisher: © Georg Thieme Verlag KG Stuttgart · New York.

Amin, S., Baker, K., Niu, J., Clancy, M., Goggins, J., Guermazi, A., Grigoryan, M., Hunter, D. J., and Felson, D. T. (2009). Quadriceps strength and the risk of cartilage loss and symptom progression in knee osteoarthritis. *Arthritis & Rheumatism*, 60(1):189–198. _eprint: https://onlinelibrary.wiley.com/doi/pdf/10.1002/art.24182.

Amira, B., France, P., Patrick, D., and Sylvie, N. (2015). Determinants of sit-to-stand tasks in individuals with hemiparesis post stroke: A review. *Annals of Physical and Rehabilitation Medicine*, 58(3):167 – 172.

Antwi-Afari, M. F., Li, H., Edwards, D. J., Pärn, E. A., Seo, J., and Wong, A. Y. L. (2017). Biomechanical analysis of risk factors for work-related musculoskeletal disorders during repetitive lifting task in construction workers. *Automation in Construction*, 83:41–47.

Arefeen, A. and Xiang, Y. (2023). Subject specific optimal control of powered knee exoskeleton to assist human lifting tasks under controlled environment. *Robotica*, pages 1–20. Publisher: Cambridge University Press.

Azadinia, F., Ebrahimi, E., Kamyab, M., Parnianpour, M., Cholewicki, J., and Maroufi, N. (2017). Can lumbosacral orthoses cause trunk muscle weakness? A systematic review of literature. *The Spine Journal*, 17(4):589–602.

Ballantyne, B. T. and Shields, R. K. (2010). Quadriceps fatigue alters human muscle performance during a novel weight bearing task. *Medicine and Science in Sports and Exercise*, 42(9):1712–1722.

Baltrusch, S. J., van Dieën, J. H., Bruijn, S. M., Koopman, A. S., van Bennekom, C. A. M., and Houdijk, H. (2019). The effect of a passive trunk exoskeleton on metabolic costs during lifting and walking. *Ergonomics*, 62(7):903–916.

Bazrgari, B., Shirazi-Adl, A., and Arjmand, N. (2007). Analysis of squat and stoop dynamic liftings: muscle forces and internal spinal loads. *European Spine Journal*, 16(5):687–699.

Bejarano, N. C., Maggioni, S., De Rijcke, L., Cifuentes, C. A., and Reinkensmeyer, D. J. (2016). Robot-assisted rehabilitation therapy: recovery mechanisms and their implications for machine design. In *Emerging Therapies in Neurorehabilitation II*, pages 197–223. Springer.

Beyaert, C., Vasa, R., and Frykberg, G. E. (2015). Gait post-stroke: Pathophysiology and rehabilitation strategies. *Neurophysiologie Clinique/Clinical Neurophysiology*, 45(4):335–355.

Blankenstein, G., Ortega, R., and Van Der Schaft, A. J. (2002). The matching conditions of controlled Lagrangians and IDA-passivity based control. *International Journal of Control*, 75(9):645–665. Publisher: Taylor & Francis.

BLS (2022). Employer-Reported Workplace Injuries and Illnesses - 2021. Technical Report USDL-22-2139, Bureau of labor statistics.

Bone and joint initiative USA (2018). The hidden impact of musculoskeletal disorders on Americans. Technical report, Bone and joint initiative USA.

Bosch, T., van Eck, J., Knitel, K., and de Looze, M. (2016). The effects of a passive exoskeleton on muscle activity, discomfort and endurance time in forward bending work. *Applied Ergonomics*, 54:212–217.

Buesing, C., Fisch, G., O'Donnell, M., Shahidi, I., Thomas, L., Mummidisetty, C. K., Williams, K. J., Takahashi, H., Rymer, W. Z., and Jayaraman, A. (2015). Effects of a wearable exoskeleton stride management assist system (SMA®) on spatiotemporal gait characteristics in individuals after stroke: a randomized controlled trial. *Journal of NeuroEngineering and Rehabilitation*, 12(1):69.

Bureau, U. C. (2014). Mobility is Most Common Disability Among Older Americans, Census Bureau Reports. https://www.census.gov/newsroom/archives/2014-pr/cb14-218.html.

Camargo, J., Ramanathan, A., Flanagan, W., and Young, A. (2021). A comprehensive, open-source dataset of lower limb biomechanics in multiple conditions of stairs, ramps, and level-ground ambulation and transitions. *Journal of Biomechanics*, 119:110320.

CCOHS (2019). CCOHS: Work-related Musculoskeletal Disorders (WMSDs) - Risk Factors. Technical report. URL: https://www.ccohs.ca/oshanswers/diseases/wmsd/risk.pdf.

CDC (2021). Work-Related Musculoskeletal Disorders & Ergonomics | Workplace Health Strategies by Condition | Workplace Health Promotion | CDC. Technical report. https://www.cdc.gov/workplacehealthpromotion/health-strategies/musculoskeletal-disorders/index.html.

Chan, C.-K., Azah, H. N., Yeow, C.-H., Goh, S.-K., Ting, H.-N., and Salmah, K. (2022). Effects of squatting speed and depth on lower extremity kinematics, kinetics and energetics. *Journal of Mechanics in Medicine and Biology*, 22(05):2250032. Publisher: World Scientific Publishing Co.

Chung, M. K., Lee, Y. J., Lee, I., and Choi, K. I. (2005). Physiological workload evaluation of carrying soft drink beverage boxes on the back. *Applied Ergonomics*, 36(5):569–574.

Courtney-Long, E. A., Carroll, D. D., Zhang, Q. C., Stevens, A. C., Griffin-Blake, S., Armour, B. S., and Campbell, V. A. (2015). Prevalence of Disability and Disability Type Among Adults — United States, 2013. *Morbidity and Mortality Weekly Report*, 64(29):777–783.

Damkot, D. K., Pope, M. H., Lord, J., and Frymoyer, J. W. (1984). The Relationship Between Work History, Work Environment and Low-Back Pain in Men. *Spine*, 9(4):395.

de Oliveira Silva, D., Briani, R. V., Pazzinatto, M. F., Ferrari, D., Aragão, F. A., and de Azevedo, F. M. (2015). Reduced knee flexion is a possible cause of increased loading rates in individuals with patellofemoral pain. *Clinical Biomechanics*, 30(9):971–975.

Deasy, M., Leahy, E., and Semciw, A. I. (2016). Hip Strength Deficits in People With Symptomatic Knee Osteoarthritis: A Systematic Review With Meta-analysis. *Journal of Orthopaedic & Sports Physical Therapy*, 46(8):629–639. Publisher: Journal of Orthopaedic & Sports Physical Therapy.

Divekar, N. V., Lin, J., Nesler, C., Borboa, S., and Gregg, R. D. (2020). A Potential Energy Shaping Controller with Ground Reaction Force Feedback for a Multi-Activity Knee-Ankle Exoskeleton. In *2020 8th IEEE RAS/EMBS International Conference for Biomedical Robotics and Biomechatronics (BioRob)*, pages 997–1003. ISSN: 2155-1782.

Dobkin, B. H. and Duncan, P. W. (2012). Should Body Weight–Supported Treadmill Training and Robotic-Assistive Steppers for Locomotor Training Trot Back to the Starting Gate? *Neurorehabilitation and Neural Repair*, 26(4):308–317.

Dobkin, B. H. and others (2003). Methods for a randomized trial of weight-supported treadmill training versus conventional training for walking during inpatient rehabilitation after incomplete traumatic spinal cord injury. *Neurorehab. Neural Repair*, 17(3):153–167.

Embry, K. R., Villarreal, D. J., Macaluso, R. L., and Gregg, R. D. (2018). Modeling the kinematics of human locomotion over continuously varying speeds and inclines. *IEEE transactions on neural systems and rehabilitation engineering*, 26(12):2342–2350. Publisher: IEEE.

Enoka, R. M. and Duchateau, J. (2016). Translating Fatigue to Human Performance. *Medicine & Science in Sports & Exercise*, 48(11):2228.

Gasparri, G. M., Luque, J., and Lerner, Z. F. (2019). Proportional Joint-Moment Control for Instantaneously Adaptive Ankle Exoskeleton Assistance. *IEEE Transactions on Neural Systems and Rehabilitation Engineering*, 27(4):751–759.

Givoni, N. J., Pham, T., Allen, T. J., and Proske, U. (2007). The effect of quadriceps muscle fatigue on position matching at the knee. *The Journal of Physiology*, 584(Pt 1):111–119.

Goršič, M., Song, Y., Dai, B., and Novak, D. (2021). Evaluation of the HeroWear Apex back-assist exosuit during multiple brief tasks. *Journal of Biomechanics*, 126:110620.

Grimmer, M., Riener, R., Walsh, C. J., and Seyfarth, A. (2019). Mobility related physical and functional losses due to aging and disease - a motivation for lower limb exoskeletons. *Journal of NeuroEngineering and Rehabilitation*, 16(1):2.

Hagen, K. B., Hallen, J., and Harms-Ringdahl, K. (1993). Physiological and subjective responses to maximal repetitive lifting employing stoop and squat technique. *European Journal of Applied Physiology and Occupational Physiology*, 67(4):291–297.

Hagen, K. B. and Harms-Ringdahl, K. (1994). Ratings of perceived thigh and back exertion in forest workers during repetitive lifting using squat and stoop techniques. *Spine*, 19(22):2511–2517.

Haight, D. J., Russell Esposito, E., and Wilken, J. M. (2015). Biomechanics of uphill walking using custom ankle-foot orthoses of three different stiffnesses. *Gait & Posture*, 41(3):750–756.

Harib, O., Hereid, A., Agrawal, A., Gurriet, T., Finet, S., Boeris, G., Duburcq, A., Mungai, M. E., Masselin, M., Ames, A. D., Sreenath, K., and Grizzle, J. W. (2018). Feedback Control of an Exoskeleton for Paraplegics: Toward Robustly Stable, Hands-Free Dynamic Walking. *IEEE Control Systems Magazine*, 38(6):61–87.

Harvard International Review (2023). Polio in a Post-Vaccine World: The Consequences of Anti-Vaccination Sentiments. URL: https://hir.harvard.edu/polio-in-a-post-vaccine-world-the-consequences-of-anti-vaccination-sentiments/.

HC Chung and MJJ Wang (2001). The effects of container design and stair climbing on maximal acceptable lift weight, wrist posture, psychophysical, and physiological responses in wafer-handling tasks. *Applied Ergonomics*, 32(6):593–598.

Heo, U., Kim, S. J., and Kim, J. (2020). Backdrivable and Fully-Portable Pneumatic Back Support Exoskeleton for Lifting Assistance. *IEEE Robotics and Automation Letters*, 5(2):2047–2053.

Hidayah, R., Sui, D., Wade, K. A., Chang, B.-C., and Agrawal, S. (2021). Passive knee exoskeletons in functional tasks: Biomechanical effects of a SpringExo coil-spring on squats. *Wearable Technologies*, 2:e7. Publisher: Cambridge University Press.

Hidler, J. M., Carroll, M., and Federovich, E. H. (2007). Strength and coordination in the paretic leg of individuals following acute stroke. *IEEE transactions on neural systems and rehabilitation engineering*, 15(4):526–534. Publisher: IEEE.

Hoang, P. D., Gandevia, S. C., and Herbert, R. D. (2014). Prevalence of joint contractures and muscle weakness in people with multiple sclerosis. *Disability and Rehabilitation*, 36(19):1588–1593. Publisher: Taylor & Francis _eprint: https://doi.org/10.3109/09638288.2013.854841.

Hsiang, S. M., Brogmus, G. E., and Courtney, T. K. (1997). Low back pain (LBP) and lifting technique — A review. *International Journal of Industrial Ergonomics*, 19(1):59–74.

Huysamen, K., de Looze, M., Bosch, T., Ortiz, J., Toxiri, S., and O'Sullivan, L. W. (2018). Assessment of an active industrial exoskeleton to aid dynamic lifting and lowering manual handling tasks. *Applied Ergonomics*, 68:125–131.

Hwang, S., Kim, Y., and Kim, Y. (2009). Lower extremity joint kinetics and lumbar curvature during squat and stoop lifting. *BMC Musculoskeletal Disorders*, 10(1):15.

Jacobs, J. V. (2016). A review of stairway falls and stair negotiation: Lessons learned and future needs to reduce injury. *Gait & posture*, 49:159–167. Publisher: Elsevier.

Jeong, H., Haghighat, P., Kantharaju, P., Jacobson, M., Jeong, H., and Kim, M. (2023). Muscle coordination and recruitment during squat assistance using a robotic ankle–foot exoskeleton. *Scientific Reports*, 13(1):1363. Number: 1 Publisher: Nature Publishing Group.

Kang, I., Molinaro, D. D., Choi, G., Camargo, J., and Young, A. J. (2022). Subject-Independent Continuous Locomotion Mode Classification for Robotic Hip Exoskeleton Applications. *IEEE Transactions on Biomedical Engineering*, 69(10):3234–3242.

Kantharaju, P., Jeong, H., Ramadurai, S., Jacobson, M., Jeong, H., and Kim, M. (2022). Reducing Squat Physical Effort Using Personalized Assistance From an Ankle Exoskeleton. *IEEE Transactions on Neural Systems and Rehabilitation Engineering*, 30:1786–1795. Conference Name: IEEE Transactions on Neural Systems and Rehabilitation Engineering.

Katan, M. and Luft, A. (2018). Global Burden of Stroke. *Seminars in Neurology*, 38(2):208–211. Publisher: Thieme Medical Publishers.

Kermavnar, T., de Vries, A. W., de Looze, M. P., and O'Sullivan, L. W. (2021). Effects of industrial back-support exoskeletons on body loading and user experience: an updated systematic review. *Ergonomics*, 64(6):685–711.

Kim, M.-K. and Yoo, K.-T. (2017). The effects of open and closed kinetic chain exercises on the static and dynamic balance of the ankle joints in young healthy women. *Journal of Physical Therapy Science*, 29(5):845–850.

Kluding, P. M., Dunning, K., O'Dell, M. W., Wu, S. S., Ginosian, J., Feld, J., and McBride, K. (2013). Foot Drop Stimulation Versus Ankle Foot Orthosis After Stroke. *Stroke*, 44(6):1660–1669. Publisher: American Heart Association.

Koopman, A. S., Toxiri, S., Power, V., Kingma, I., van Dieën, J. H., Ortiz, J., and de Looze, M. P. (2019). The effect of control strategies for an active back-support exoskeleton on spine loading and kinematics during lifting. *Journal of Biomechanics*, 91:14–22.

Kumar, S., Zwall, M. R., Bolívar-Nieto, E. A., Gregg, R. D., and Gans, N. (2020). Extremum Seeking Control for Stiffness Auto-Tuning of a Quasi-Passive Ankle Exoskeleton. *IEEE Robotics and Automation Letters*, 5(3):4604–4611. Conference Name: IEEE Robotics and Automation Letters.

Lairamore, C., Garrison, M. K., Bandy, W., and Zabel, R. (2011). Comparison of tibialis anterior muscle electromyography, ankle angle, and velocity when individuals post stroke walk with different orthoses. *Prosthetics and Orthotics International*, 35(4):402–410. Publisher: SAGE Publications Ltd STM.

Lamers, E. P., Soltys, J. C., Scherpereel, K. L., Yang, A. J., and Zelik, K. E. (2020). Low-profile elastic exosuit reduces back muscle fatigue. *Scientific Reports*, 10(1):15958. Number: 1 Publisher: Nature Publishing Group.

Lamers, E. P., Yang, A. J., and Zelik, K. E. (2018). Feasibility of a Biomechanically-Assistive Garment to Reduce Low Back Loading During Leaning and Lifting. *IEEE Transactions on Biomedical Engineering*, 65(8):1674–1680. Conference Name: IEEE Transactions on Biomedical Engineering.

Larson, G. D. J. and Potteiger, J. A. (1997). A Comparison of Three Different Rest Intervals Between Multiple Squat Bouts. *The Journal of Strength & Conditioning Research*, 11(2):115.

Laschowski, B. and McPhee, J. (2023). Energy-Efficient Actuator Design Principles for Robotic Leg Prostheses and Exoskeletons: A Review of Series Elasticity and Backdrivability. *Journal of Computational and Nonlinear Dynamics*, 18(060801).

Laschowski, B., Razavian, R. S., and McPhee, J. (2021). Simulation of Stand-to-Sit Biomechanics for Robotic Exoskeletons and Prostheses With Energy Regeneration. *IEEE Transactions on Medical Robotics and Bionics*, 3(2):455–462. Conference Name: IEEE Transactions on Medical Robotics and Bionics.

Li Hi Shing, S., Chipika, R. H., Finegan, E., Murray, D., Hardiman, O., and Bede, P. (2019). Post-polio Syndrome: More Than Just a Lower Motor Neuron Disease. *Frontiers in Neurology*, 10.

Lin, J., Divekar, N., Lv, G., and Gregg, R. D. (2019). Energy Shaping Control with Virtual Spring and Damper for Powered Exoskeletons. In *2019 IEEE 58th Conference on Decision and Control (CDC)*, pages 3039–3045. ISSN: 2576-2370.

Lin, J., Divekar, N. V., Lv, G., and Gregg, R. D. (2021). Optimal Task-Invariant Energetic Control for a Knee-Ankle Exoskeleton. In *2021 American Control Conference (ACC)*, pages 5029–5034. ISSN: 2378-5861.

Lin, J., Divekar, N. V., Thomas, G. C., and Gregg, R. D. (2022). Optimally Biomimetic Passivity-Based Control of a Lower-Limb Exoskeleton Over the Primary Activities of Daily Life. *IEEE Open Journal of Control Systems*, 1:15–28.

Longpré, H. S., Acker, S. M., and Maly, M. R. (2015). Muscle activation and knee biomechanics during squatting and lunging after lower extremity fatigue in healthy young women. *Journal of Electromyography and Kinesiology*, 25(1):40–46.

Luger, T., Bär, M., Seibt, R., Rieger, M. A., and Steinhilber, B. (2023). Using a Back Exoskeleton During Industrial and Functional Tasks—Effects on Muscle Activity, Posture, Performance, Usability, and Wearer Discomfort in a Laboratory Trial. *Human Factors*, 65(1):5–21. Publisher: SAGE Publications Inc.

Lv, G. and Gregg, R. D. (2018). Underactuated Potential Energy Shaping with Contact Constraints: Application to a Powered Knee-Ankle Orthosis. *IEEE Trans. Control Syst. Technol.*, 26(1):181–193.

Lv, G., Zhu, H., and Gregg, R. D. (2018). On the Design and Control of Highly Backdrivable Lower-Limb Exoskeletons: A Discussion of Past and Ongoing Work. *IEEE Control Systems Magazine*, 38(6):88–113. Conference Name: IEEE Control Systems Magazine.

Ma, V. Y., Chan, L., and Carruthers, K. J. (2014). Incidence, Prevalence, Costs, and Impact on Disability of Common Conditions Requiring Rehabilitation in the United States: Stroke, Spinal Cord Injury, Traumatic Brain Injury, Multiple Sclerosis, Osteoarthritis, Rheumatoid Arthritis, Limb Loss, and Back Pain. *Archives of Physical Medicine and Rehabilitation*, 95(5):986 – 995.

Marigold, D. S. and Eng, J. J. (2006). The relationship of asymmetric weight-bearing with postural sway and visual reliance in stroke. *Gait & posture*, 23(2):249–255. Publisher: Elsevier.

Marilyn Sharp, Mary Rosenberger, and Joseph Knapik (2006). Chapter 5 – COMMON MILITARY TASK: MATERIALS HANDLING. Technical Report RTO-TR-IST-999. URL: https://apps.dtic.mil/sti/pdfs/ADA472464.pdf.

McGibbon, C., Sexton, A., Gryfe, P., Dutta, T., Jayaraman, A., Deems-Dluhy, S., Novak, A., Fabara, E., Adans-Dester, C., and Bonato, P. (2023). Effect of using of a lower-extremity exoskeleton on disability of people with multiple sclerosis. *Disability and Rehabilitation: Assistive Technology*, 18(5):475–482. Publisher: Taylor & Francis _eprint: https://doi.org/10.1080/17483107.2021.1874064.

McGibbon, C. A., Sexton, A., Jayaraman, A., Deems-Dluhy, S., Gryfe, P., Novak, A., Dutta, T., Fabara, E., Adans-Dester, C., and Bonato, P. (2018). Evaluation of the Keeogo exoskeleton for assisting ambulatory activities in people with multiple sclerosis: an open-label, randomized, cross-over trial. *Journal of NeuroEngineering and Rehabilitation*, 15(1):117.

Medrano, R. L., Thomas, G. C., Keais, C. G., Rouse, E. J., and Gregg, R. D. (2023). Real-Time Gait Phase and Task Estimation for Controlling a Powered Ankle Exoskeleton on Extremely Uneven Terrain. *IEEE Transactions on Robotics*, 39(3):2170–2182.

Mentiplay, B. F., Banky, M., Clark, R. A., Kahn, M. B., and Williams, G. (2018). Lower limb angular velocity during walking at various speeds. *Gait & posture*, 65:190–196. Publisher: Elsevier.

Miller, W. C., Deathe, A. B., Speechley, M., and Koval, J. (2001). The influence of falling, fear of falling, and balance confidence on prosthetic mobility and social activity among individuals with a lower extremity amputation. *Archives of Physical Medicine and Rehabilitation*, 82(9):1238–1244.

Millington, P. J., Myklebust, B. M., and Shambes, G. M. (1992). Biomechanical analysis of the sit-to-stand motion in elderly persons. *Archives of Physical Medicine and Rehabilitation*, 73(7):609–617. Publisher: Elsevier.

Molinaro, D. D., Kang, I., Camargo, J., Gombolay, M. C., and Young, A. J. (2022). Subject-Independent, Biological Hip Moment Estimation During Multimodal Overground Ambulation Using Deep Learning. *IEEE Transactions on Medical Robotics and Bionics*, 4(1):219–229.

Morone, G., Matamala-Gomez, M., Sanchez-Vives, M. V., Paolucci, S., and Iosa, M. (2018). Watch your step! Who can recover stair climbing independence after stroke? *European journal of physical and rehabilitation medicine*, 54(6):811–818.

Morone, G., Paolucci, S., Cherubini, A., De Angelis, D., Venturiero, V., Coiro, P., and Iosa, M. (2017). Robot-assisted gait training for stroke patients: current state of the art and perspectives of robotics. *Neuropsychiatric disease and treatment*, 13:1303. Publisher: Dove Press.

Murray, R. M., Li, Z., and Sastry, S. S. (1994). *A mathematical introduction to robotic manipulation*. CRC press.

Murray, S. A., Ha, K. H., Hartigan, C., and Goldfarb, M. (2015). An Assistive Control Approach for a Lower-Limb Exoskeleton to Facilitate Recovery of Walking Following Stroke. *IEEE Transactions on Neural Systems and Rehabilitation Engineering*, 23(3):441–449.

Nadeau, S., McFadyen, B. J., and Malouin, F. (2003). Frontal and sagittal plane analyses of the stair climbing task in healthy adults aged over 40 years: what are the challenges compared to level walking? *Clinical biomechanics*, 18(10):950–959. Publisher: Elsevier.

National Safety Council (2018). Fatigue In Safety-Critical Industries Report - National Safety Council. Technical report. URL: https://www.nsc.org/getmedia/4b5503b3-5e0b-474d-af19-c419cedb4c17/fatigue-in-safety-critical-industries.pdf.aspx.

Nesler, C., Thomas, G., Divekar, N., Rouse, E. J., and Gregg, R. D. (2022). Enhancing Voluntary Motion With Modular, Backdrivable, Powered Hip and Knee Orthoses. *IEEE Robotics and Automation Letters*, 7(3):6155–6162.

Ng, S. S. and Hui-Chan, C. W. (2012). Contribution of ankle dorsiflexor strength to walking endurance in people with spastic hemiplegia after stroke. *Archives of physical medicine and rehabilitation*, 93(6):1046–1051. Publisher: Elsevier.

NIOSH (2007). Ergonomic Guidelines for Manual Material Handling. Technical Report 2007-131.

NIOSH (2020). Back belts: do they prevent injury? URL: https://www.cdc.gov/niosh/docs/94-127/default.html.

Nolan, D., O'Sullivan, K., Stephenson, J., O'Sullivan, P., and Lucock, M. (2018). What do physiotherapists and manual handling advisors consider the safest lifting posture, and do back beliefs influence their choice? *Musculoskeletal Science and Practice*, 33:35–40.

Orr, R., Pope, R., Lopes, T. J. A., Leyk, D., Blacker, S., Bustillo-Aguirre, B. S., and Knapik, J. J. (2021). Soldier Load Carriage, Injuries, Rehabilitation and Physical Conditioning: An International Approach. *International Journal of Environmental Research and Public Health*, 18(8):4010.

O'Reilly, S. C., Jones, A., Muir, K. R., and Doherty, M. (1998). Quadriceps weakness in knee osteoarthritis: the effect on pain and disability. *Annals of the Rheumatic Diseases*, 57(10):588–594. Publisher: BMJ Publishing Group Ltd Section: Extended reports.

Patterson, K. K., Gage, W. H., Brooks, D., Black, S. E., and McIlroy, W. E. (2010). Changes in gait symmetry and velocity after stroke: a cross-sectional study from weeks to years after stroke. *Neurorehabilitation and Neural Repair*, 24(9):783–790. Publisher: SAGE Publications Sage CA: Los Angeles, CA.

Pfusterschmied, J., Stöggl, T., Buchecker, M., Lindinger, S., Wagner, H., and Müller, E. (2013). Effects of 4-week slackline training on lower limb joint motion and muscle activation. *Journal of science and medicine in sport*, 16(6):562–566. Publisher: Elsevier.

Picchiotti, M. T., Weston, E. B., Knapik, G. G., Dufour, J. S., and Marras, W. S. (2019). Impact of two postural assist exoskeletons on biomechanical loading of the lumbar spine. *Applied Ergonomics*, 75:1–7.

Poliero, T., Lazzaroni, M., Toxiri, S., Di Natali, C., Caldwell, D. G., and Ortiz, J. (2020). Applicability of an Active Back-Support Exoskeleton to Carrying Activities. *Frontiers in Robotics and AI*, 7.

Poliero, T., Sposito, M., Toxiri, S., Natali, C. D., Iurato, M., Sanguineti, V., Caldwell, D. G., and Ortiz, J. (2021). Versatile and non-versatile occupational back-support exoskeletons: A comparison in laboratory and field studies. *Wearable Technologies*, 2:e12. Publisher: Cambridge University Press.

Pollo, F. E., Otis, J. C., Backus, S. I., Warren, R. F., and Wickiewicz, T. L. (2002). Reduction of Medial Compartment Loads with Valgus Bracing of the Osteoarthritic Knee. *The American Journal of Sports Medicine*, 30(3):414–421. Publisher: SAGE Publications Inc STM.

Potvin, J. R., McGill, S. M., and Norman, R. W. (1991). Trunk muscle and lumbar ligament contributions to dynamic lifts with varying degrees of trunk flexion. *Spine*, 16(9):1099–1107.

Ranaweera, R., Gopura, R., Jayawardena, T., and Mann, G. (2018). Development of A Passively Powered Knee Exoskeleton for Squat Lifting. *Journal of Robotics, Networking and Artificial Life*, 5(1):45.

Rodzak, K., Slaughter, P., Wolf, D., Ice, C., Fine, S., and Zelik, K. (2023). Can back exosuits simultaneously increase lifting endurance and reduce musculoskeletal disorder risk? URL: https://www.techrxiv.org/articles/preprint/23643633/1.

Sado, F., Yap, H. J., Ghazilla, R. A. R., and Ahmad, N. (2019). Design and control of a wearable lower-body exoskeleton for squatting and walking assistance in manual handling works. *Mechatronics*, 63:102272.

Sasaki, M., Horio, A., Wakasa, M., Uemura, S., and Osawa, Y. (2008). Influence of Quadriceps Femoris Fatigue on Low Back Load during Lifting of Loads at Different Distances from the Toes. *Journal of Physical Therapy Science*, 20(2):81–89.

Shafrin, J., Sullivan, J., Goldman, D. P., and Gill, T. M. (2017). The association between observed mobility and quality of life in the near elderly. *PLOS ONE*, 12(8):e0182920. Publisher: Public Library of Science.

Shakoor, N., Hurwitz, D. E., Block, J. A., Shott, S., and Case, J. P. (2003). Asymmetric knee loading in advanced unilateral hip osteoarthritis. *Arthritis & Rheumatism*, 48(6):1556–1561. _eprint: https://onlinelibrary.wiley.com/doi/pdf/10.1002/art.11034.

Sheila Lennon, David Baxter, A. A. (2001). Physiotherapy based on the Bobath concept in stroke rehabilitation: a survey within the UK. *Disability and Rehabilitation*, 23(6):254–262. Publisher: Taylor & Francis _eprint: https://doi.org/10.1080/096382801750110892.

Slade, P., Kochenderfer, M. J., Delp, S. L., and Collins, S. H. (2022). Personalizing exoskeleton assistance while walking in the real world. *Nature*, 610(7931):277–282. Number: 7931 Publisher: Nature Publishing Group.

Staudenmann, D., Roeleveld, K., Stegeman, D. F., and van Dieën, J. H. (2010). Methodological aspects of SEMG recordings for force estimation – A tutorial and review. *Journal of Electromyography and Kinesiology*, 20(3):375–387.

Straker, L. (2003). Evidence to support using squat, semi-squat and stoop techniques to lift low-lying objects. *International Journal of Industrial Ergonomics*, 31(3):149–160.

Straker, L. and Duncan, P. (2000). Psychophysical and psychosocial comparison of squat and stoop lifting by young females. *The Australian Journal of Physiotherapy*, 46(1):27–32.

Tekscan (2020). FlexiForce A401 Sensor.

Theurel, J. and Desbrosses, K. (2019). Occupational Exoskeletons: Overview of Their Benefits and Limitations in Preventing Work-Related Musculoskeletal Disorders. *IISE Transactions on Occupational Ergonomics and Human Factors*, 7(3-4):264–280.

Trafimow, J. H., Schipplein, O. D., Novak, G. J., and Andersson, G. B. (1993). The effects of quadriceps fatigue on the technique of lifting. *Spine*, 18(3):364–367.

Ulrey, B. L. and Fathallah, F. A. (2013). Effect of a personal weight transfer device on muscle activities and joint flexions in the stooped posture. *Journal of Electromyography and Kinesiology*, 23(1):195–205.

US ARMY (2000). Lifting techniques. Technical report, U.S. ARMY CENTER FOR HEALTH PROMOTION AND PREVENTIVE MEDICINE. URL: https://www.sfdph.org/dph/files/OSH/armylift.pdf.

van der Have, A., Van Rossom, S., and Jonkers, I. (2019). Squat Lifting Imposes Higher Peak Joint and Muscle Loading Compared to Stoop Lifting. *Applied Sciences*, 9(18):3794. Number: 18 Publisher: Multidisciplinary Digital Publishing Institute.

van Kammen, K., Boonstra, A. M., van der Woude, L. H., Reinders-Messelink, H. A., and den Otter, R. (2017). Differences in muscle activity and temporal step parameters between Lokomat guided walking and treadmill walking in post-stroke hemiparetic patients and healthy walkers. *Journal of neuroengineering and rehabilitation*, 14(1):32. Publisher: Springer.

van Kammen, K., Boonstra, A. M., van der Woude, L. H. V., Visscher, C., Reinders-Messelink, H. A., and den Otter, R. (2020). Lokomat guided gait in hemiparetic stroke patients: the effects of training parameters on muscle activity and temporal symmetry. *Disability and Rehabilitation*, 42(21):2977–2985. Publisher: Taylor & Francis _eprint: https://doi.org/10.1080/09638288.2019.1579259.

Verma, R., Arya, K. N., Sharma, P., and Garg, R. (2012). Understanding gait control in post-stroke: implications for management. *Journal of bodywork and movement therapies*, 16(1):14–21. Publisher: Elsevier.

Vicon Motion Systems (1997). BodyBuilder for Biomechanics. URL: https://docs.vicon.com/download/attachments/83296551/BodyBuilderForBiomechanics.pdf.

Vicon Motion Systems (2023). Upper body modeling with Plug-in Gait - Nexus 2.13 Documentation - Vicon Documentation. URL: https://docs.vicon.com/display/Nexus213/Upper+body+modeling+with+Plug-in+Gait.

Villarreal, D. J. and Gregg, R. D. (2014). A survey of phase variable candidates of human locomotion. *Annual International Conference of the IEEE Engineering in Medicine and Biology Society. IEEE Engineering in Medicine and Biology Society. Annual International Conference*, 2014:4017–4021.

Vistamehr, A., Kautz, S. A., and Neptune, R. R. (2014). The influence of solid ankle-foot-orthoses on forward propulsion and dynamic balance in healthy adults during walking. *Clinical Biomechanics*, 29(5):583–589.

Vos, T., Flaxman, A. D., Naghavi, M., and Lozano, R. (2012). Years lived with disability (YLDs) for 1160 sequelae of 289 diseases and injuries 1990–2010: a systematic analysis for the Global Burden of Disease Study 2010. *The Lancet*, 380(9859):2163–2196. Publisher: Elsevier.

Wami, S. D., Abere, G., Dessie, A., and Getachew, D. (2019). Work-related risk factors and the prevalence of low back pain among low wage workers: results from a cross-sectional study. *BMC Public Health*, 19(1):1072.

Wang, D., Dai, F., and Ning, X. (2015). Risk Assessment of Work-Related Musculoskeletal Disorders in Construction: State-of-the-Art Review. *Journal of Construction Engineering and Management*, 141(6):04015008. Publisher: American Society of Civil Engineers.

Wang, J., Li, X., Huang, T.-H., Yu, S., Li, Y., Chen, T., Carriero, A., Oh-Park, M., and Su, H. (2018). Comfort-centered design of a lightweight and backdrivable knee exoskeleton. *IEEE Robotics and Automation Letters*, 3(4):4265–4272. Publisher: IEEE.

Wei, W., Zha, S., Xia, Y., Gu, J., and Lin, X. (2020). A Hip Active Assisted Exoskeleton That Assists the Semi-Squat Lifting. *Applied Sciences*, 10(7):2424. Number: 7 Publisher: Multidisciplinary Digital Publishing Institute.

Welbergen, E., Kemper, H. C., Knibbe, J. J., Toussaint, H. M., and Clysen, L. (1991). Efficiency and effectiveness of stoop and squat lifting at different frequencies. *Ergonomics*, 34(5):613–624.

WIRED (2021). Stress Testing Real-Life Robot Legs | WIRED. URL: https://www.youtube.com/watch?v=CKvEBWaPd2I.

Woolley, S. M. (2001). Characteristics of gait in hemiplegia. *Topics in stroke rehabilitation*, 7(4):1–18. Publisher: Taylor & Francis.

Work Fit (2023). Carrying Up Stairs & Keeping Your Workers Safe on the Job. URL: https://www.work-fit.com/blog/carrying-up-stairs-keeping-your-workers-safe-on-the-job.

Yang, J. and Winter, D. (1984). Electromyographic amplitude normalization methods: improving their sensitivity as diagnostic tools in gait analysis. *Archives of physical medicine and rehabilitation*, 65(9):517–521.

Yeatman, M., Lv, G., and Gregg, R. D. (2019). Decentralized Passivity-Based Control with a Generalized Energy Storage Function for Robust Biped Locomotion. *Journal of Dynamic Systems, Measurement, and Control*, 141(10):101007. Publisher: American Society of Mechanical Engineers.

Yu, K.-P., Yeung, L.-F., Ng, S.-W., and Tong, K.-Y. (2020). Bionic robotics for post polio walking. In Hu, X., editor, *Intelligent Biomechatronics in Neurorehabilitation*, pages 83–109. Academic Press.

Zeilig, G., Weingarden, H., Zwecker, M., Dudkiewicz, I., Bloch, A., and Esquenazi, A. (2012). Safety and tolerance of the ReWalk™ exoskeleton suit for ambulation by people with complete spinal cord injury: A pilot study. *The Journal of Spinal Cord Medicine*, 35(2):96–101.

Zhang, L., Liu, G., Han, B., Wang, Z., Li, H., and Jiao, Y. (2020). Assistive devices of human knee joint: A review. *Robotics and Autonomous Systems*, 125:103394.

Zhang, M., Murphy, L. A., Fang, D., and Caban-Martinez, A. J. (2015). Influence of fatigue on construction workers' physical and cognitive function. *Occupational Medicine (Oxford, England)*, 65(3):245–250.

Zhu, H., Doan, J., Stence, C., Lv, G., Elery, T., and Gregg, R. (2017). Design and validation of a torque dense, highly backdrivable powered knee-ankle orthosis. In *IEEE International Conference on Robotics and Automation*, pages 504–510.

Zhu, H., Nesler, C., Divekar, N., Ahmad, M. T., and Gregg, R. D. (2019). Design and Validation of a Partial-Assist Knee Orthosis with Compact, Backdrivable Actuation. In *2019 IEEE 16th International Conference on Rehabilitation Robotics (ICORR)*, pages 917–924. IEEE.